

**MicroRNAs modulate skeletal
muscle remodelling and
regeneration**

Giorgia Giacomazzi

KU Leuven
Biomedical Sciences Group
Faculty of Medicine
Department of Development and Regeneration
Stem Cell Biology and Embryology



MICRORNAS MODULATE SKELETAL MUSCLE REMODELLING AND REGENERATION

Giorgia GIACOMAZZI

Jury:

Promoter: Prof. Dr. Maurilio Sampaolesi
Co-promoter: Dr. Mattia Quattrocelli
Chair: Prof. Dr. Frederic Lluis
Secretary: Prof. Dr. Liesbeth De Waele
Jury members: Prof. Dr. Stefan Janssens
Prof. Dr. Liesbeth De Waele
Prof. Dr. Marco Sandri
Prof. Dr. Pura Muñoz Cánoves

Dissertation presented in partial
fulfilment of the requirements for
the degree of Doctor in
Biomedical Sciences

“And first he will see the shadows best, next the reflections of men and other objects in the water, and then the objects themselves, then he will gaze upon the light of the moon and the stars and the spangled heaven....

Last of all he will be able to see the sun.”

The Allegory of the Cave,
Book VII, Republic, Plato.

Table of contents

Abbreviations	III
Summary	V
Samenvatting	IX
Chapter 1 - Introduction	1
<u>1 Skeletal muscle: homeostasis and pathological dysregulation</u>	2
1.1 Regulation of skeletal muscle homeostasis	2
1.2 Skeletal muscle disorders	4
1.2.1 Muscular Dystrophies	
1.2.1.1 <i>Treatment</i>	5
1.2.2 <i>Age-related muscle wasting – sarcopenia</i>	6
1.2.2.1 <i>Therapeutic approaches for skeletal muscle wasting</i>	7
<u>2 Stem cell therapy for skeletal muscle disorders</u>	8
2.1 <i>Adult stem cells</i>	8
2.2 <i>Pluripotent stem cells</i>	9
2.3 <i>Ageing and stem cells</i>	11
2.4 <i>Stem cell therapies and epigenetics</i>	13
2.5 <i>Mesodermal iPSC-derived progenitors</i>	14
<u>3 MicroRNAs</u>	16
3.1 <i>Definition, biogenesis and function</i>	16
3.2 <i>MicroRNAs and skeletal muscle regulation – myogenesis</i>	16
3.3 <i>MicroRNAs and skeletal muscle disorders</i>	18
3.4 <i>MicroRNAs, cell fate decision and epigenetic</i>	19
3.5 <i>MicroRNAs as therapeutics- consideration for application</i>	20

Table of contents

<u>4 Extracellular vesicles</u>	22
4.1 <i>Definition and biogenesis</i>	22
4.2 <i>EVs and muscle regeneration</i>	24
Chapter 2 - Aims	26
Chapter 3 - MicroRNAs promote skeletal muscle differentiation of mesodermal iPSC-derived progenitors.	30
1. Abstract	31
2. Introduction	32
3. Materials and methods	34
4. Results	41
5. Discussion	58
6. Supplementary data	63
Chapter 4 – Extracellular vesicles- derived microRNAs improve mesoangioblasts treatment in muscle wasting condition	71
1. Abstract	72
2. Introduction	73
3. Materials and Methods	76
4. Results	81
5. Discussion	92
6. Supplementary data	95
Chapter 5 –General discussion	101
Reference	109
Acknowledgments and conflicts of interest	127
Curriculum vitae	129

Abbreviations

$^{99m}\text{TcO}_4^-$	Pertechnetate
ACTA2	Alpha-actin-2
AMC	Anti-myogenic cocktail
ANXA3	Annexin 3
ANXA7	Annexin 7
ATG10	Autophagy Related 10
AVV	Adeno-associated virus
BF	Bright field
bFGF	Basic fibroblasts growth factor
BLI	Bioluminescence imaging
BMD	Becker muscular dystrophy
BMP6	Bone Morphogenetic Protein 6
BSA	Bovine serum albumin
CK	Creatine kinase
CNN2	Calponin 2
CNN3	Calponin 3
CpGi	CpG islands
CSC	Cardiac stem cells
DGC	Dystrophin glycoprotein complex
DMD	Duchenne muscular dystrophy
DMEM	Dulbecco's Modified Eagle Medium
DNMT	DNA methyltransferases
ESC	Embryonic stem cells
EVs	Extracellular vesicles
FBS	Fetal bovine serum
FGF2	Fibroblasts growth factor 2
f-iPSCs	Fibroblasts derived iPSCs
fLUC	Firefly luciferase
f-MiPs	Fibroblasts derived mesodermal progenitors
GRMD	Golden retriever muscular dystrophy model
HDAC	Histone deacetylases
hDYS	Human dystrophin
HS	Horse serum
iCasp9	Inducible caspase 9
ICM	Inner cell mass
IGF-1	Insulin growth factor 1
IMDM	Iscove's Modified Dulbecco's Medium
iPSC	Induced pluripotent stem cells
ITS	Insulin transferrin selenium
KLF4	Kruppel Like Factor 4
LGMD	Limb girdle muscular dystrophy

Abbreviations

LTBP4	Latent Transforming Growth Factor Beta Binding Protein 4
MAB-iPSCs	Mesoangioblasts derived iPSCs
MAB-MiPs	Mesoangioblasts derived mesodermal progenitors
MABs	Mesoangioblasts
MAGIC-F1	Met activating chimeric engineered factor1
MD	Muscular Dystrophies
MiPs	Mesodermal iPSC derived progenitors
mir	microRNA
miRNAs	microRNAs
MRF	Myogenic regulatory factors
MVE	Multivesicular endosome
MVs	Microvesicles
MYB	Myb proto-oncogene protein
MyHC	Myosin heavy chain
NIS	sodium-iodide symporter
NMJs	Neuromuscular junctions
OCT4	octamer-binding transcription factor 4
OSTN	Osteocrin
PAX7	Paired box protein 7
PET	Positron emission tomography
PMC	Pro myogenic cocktail
PSC	Pluripotent stem cells
RISC	RNA- induced silencing complex
SC	Satellite cells
SMAD4	Mothers against decapentaplegic homolog 4
SMAD5	Mothers against decapentaplegic homolog 5
SMAD6	Mothers against decapentaplegic homolog 6
SMAD7	Mothers against decapentaplegic homolog 7
SOX2	sex determining region Y-box 2
SUV	Standardized uptake value
TALEN	Transcription activator-like effector nucleases
TGF β	Transforming growth factor beta
VEGF	Vascular endothelial growth factor
WT	Wild type

Skeletal muscles constitute about 40% of the body mass in human and is the largest organ of the human body. Muscles provide stability and support, allowing movement and supporting inner organs. Skeletal muscle holds an intrinsic capability of growth and regeneration, in case of injury as well as in physiological conditions, for instance as a consequence of exercise. Some pathological conditions, for example chronic myopathies cause a progressive loss of muscle mass and impaired functionality. Muscle wasting is characterized by atrophy of the skeletal muscle tissue, depletion of myogenic stem cell pools, decay in muscle function. Well known diseases of the skeletal muscle are Muscular Dystrophies (MDs). MDs are marked by a progressive muscular degeneration, which leads patients to physical disability and shortens life expectancy.

No curative treatment is currently available for MDs. A promising approach relies on stem cell therapy. However, issues such as limited availability, control of cell fate and paracrine effects on the host tissue need to be addressed before therapeutic applications may become feasible. Stem cell therapy with donor mesoangioblasts (MABs- vessels associated stem cells) has produced dramatic amelioration in dystrophic mice and dogs. Recently, induced pluripotent stem cells (iPSCs) have been generated from MABs (MAB-iPSCs). MAB-iPSCs reproduce unique features of pluripotent stem cells, still retaining a biased epigenetic memory towards the myogenic lineage. Interestingly, MAB-iPSC-derived mesodermal progenitors (MiPs) can be used for combined treatment of both skeletal and cardiac muscles in dystrophic mice. Human MiPs have also been derived and characterized although questions about their in vivo performance remained unanswered.

Moreover, it is known that the differentiation ability of pluripotent stem cells is regulated by both extrinsic factors, like growth factors, and intrinsic factors including the epigenetic factors. Although still unclear, the retention of progeny-specific epigenetic imprinting in iPSCs, e.g. patterns of DNA methylation, histone marks and ultimately microRNAs (miRNAs) have been often reported and exploited for enhanced differentiation along the parental lineage.

During the first part of the current PhD training we investigated the *in vivo* capacity of human MiPs, mainly focusing our attention on their skeletal myogenic commitment. We assessed the translational potential of human MiPs in dystrophic mice showing that MiPs can successfully engraft dystrophic skeletal muscle, resulting in a functional amelioration of the disease. Next, we compared the transcriptional profiles of human fibroblast-derived - and MAB-MiPs, and the miRNAs profile in order to predict a miRNA cocktail functional for increasing the myogenic commitment of the progenitors. We have tested this cocktail and provide evidence that MiPs contribution to myogenic lineages is increased with specific miRNAs.

In a second part of the project we wished to move forward with a novel therapeutic approach for enhancing muscle regeneration with the ultimate goal of bypassing the use of stem cells. As recently established, muscle fibres secrete extracellular vesicles (EVs), small membranous vesicles derived from late endosomal system. EVs contain lipids, proteins, mRNAs and miRNAs. Scientific interest on EVs has grown since they can be applied in regenerative medicine fields as delivery methods for tissue regeneration. Also, EVs are key players in intercellular cross-talk, horizontally carry messenger-(mRNAs) or miRNAs, and have been shown to act as endocrine signals during myogenesis. However, it is still an open question whether and which role EVs play in regulating the stem cell fate in muscle wasting- specific muscular niche.

We have screened the content of EVs from animal models of muscle hypertrophy and muscle wasting associated with a chronic disease and aging. Analysis of the transcriptome, protein cargo and miRNAs has allowed us to identify a hypertrophic miRNAs signature amenable for targeting muscle wasting. We have tested this signature *in vitro* on mesoangioblasts (MABs), adult vessel associated stem cells, given their relevance for treating muscle loss, and we have observed an increase in myogenic differentiation. Furthermore, injections of miRNA treated MABs in aged mice has resulted in an improvement in skeletal muscle features, such as muscle weight, strength, cross-sectional area and fibrosis. We provided evidence that the

EV-derived miRNA signature we have identified enhance myogenic potential of myogenic stem cells.

Taken together, our results are embedded in the emerging field of combining EV and stem cells for regenerative medicine purposes, as we have employed miRNAs technology and stem cell therapy to target skeletal muscle decay and loss of function.



De skeletspier is het grootste orgaan in ons lichaam, goed voor 40% van ons lichaamsgewicht. Spieren zijn van belang voor stabiliteit, beweging en de ondersteuning van interne organen. Verder heeft de skeletspier de intrinsieke capaciteit om te groeien en regenereren. Deze regeneratie vindt plaats in zowel fysiologische, bijvoorbeeld tijdens fysieke inspanning, en pathologische condities. Desalniettemin veroorzaken sommige pathologische aandoeningen, zoals chronische myopathieën, een progressief verlies van spiermassa wat leidt tot verminderde functionaliteit. Dit verlies van spiermassa is te wijten aan spieratrofie, depletie van de myogene stamcellen en vermindering van de spierfunctie. De meest bekende spierziekten zijn de musculaire dystrofiën (MDs). MDs zijn gekenmerkt door een progressieve spierdegeneratie die leidt tot een fysieke handicap en een verkorte levensverwachting.

Tot nu toe is er nog geen genezing voor MDs. Een veelbelovende strategie hiervoor is het gebruik van stamcellen. Jammer genoeg limiteren bepaalde factoren, zoals de beperkte beschikbaarheid, de ongeschikte paracrine signalen afkomstig van de zieke spier en het gebrek aan controle over de cel status, het gebruik van stamcellen. Stamceltherapie met donor mesoangioblasten (MABs; bloedvat-geassocieerde stamcellen) leidde reeds tot een grote verbetering in zowel dystrofische muizen als honden. Recent werden er MABs gegenereerd uit geïnduceerde pluripotente stamcellen (MAB-iPSCs). MAB-iPSCs bevatten de unieke eigenschappen van pluripotente stamcellen, terwijl ze ook hun bias behouden naar hun myogene afkomst, hun zogenaamd epigenetisch geheugen. Verder kunnen mesodermale progenitoren afkomstig van de MAB-iPSCs (MiPs) gebruikt worden voor de regeneratie van zowel skelet- als hartspier in dystrofische muizen. Hoewel humane MiPs alvast gegenereerd en gekarakteriseerd zijn, is nog niets geweten over hun in vivo capaciteit.

Het is reeds geweten dat de differentiatie van pluripotente stamcellen gereguleerd wordt door zowel extrinsieke, e.g. groeifactoren, als intrinsieke factoren, waaronder epigenetische componenten. Hoewel het mechanisme onduidelijk is, werd de retentie van afkomst-specifieke epigenetische elementen in iPSCs, zoals DNA

methylatie, histon markeringen en microRNAs (miRNAs), reeds vaak gerapporteerd en gebruikt om differentiatie langs de ouderlijke lijn te stimuleren.

In het eerste deel van mijn doctoraatstraining hebben we ons vooral gefocust op de in vivo capaciteit van de humane MiPs om spierweefsel te vormen. Hierbij toonden we aan dat deze MiPs succesvol kunnen integreren in de skeletspier van dystrofische muizen en zo leidde tot een vermindering van de symptomen. Verder hebben we het transcriptoom en miRNA profiel van MAB-MiPs vergeleken met dit van fibroblast-afkomstige MiPs. Hieruit werd een miRNA cocktail voorspeld die mogelijks de myogene commitment van de progenitoren kon verhogen. Deze cocktail werd getest en er werd bevestigd dat deze specifieke miRNAs inderdaad zorgen voor een verhoging van de myogene capaciteit.

In een tweede deel van dit project wilden we focussen op een nieuwe strategie om spiergeneratie te verbeteren waarbij we uiteindelijk het gebruik van stamcellen kunnen omzeilen. Recent werd geconstateerd dat spiervezels extracellulaire vesikels (EVs) secreteren. EVs zijn kleine membraneuze structuren afkomstig van het laat endosomaal systeem, die lipiden, eiwitten, mRNAs en miRNAs bevatten. Deze EVs worden meer en meer gebruikt als transport methode in de regeneratieve geneeskunde, om zo een bepaald cargo aan de weefsels te kunnen leveren. Verder spelen EVs een rol in de intracellulaire communicatie, het overdragen van mRNA en miRNA en worden als endocriene signalen tijdens de myogenese. Desalniettemin is nog niet geweten of en welke rol EVs spelen in het reguleren van het lot van stamcel in een spieratrofie-specifieke omgeving.

Allereerst werden EVs uit zowel diermodellen voor spierhypertrofie en –atrofie gescreend. Voor atrofie werd zowel een chronisch ziektemodel als een ouderdomsmodel gebruikt om te kunnen vergelijken tussen fysiologische en pathologisch condities. Aan de hand van het transcriptoom, proteoom en de miRNAs van deze EVs werd een hypertrofie-specifieke signatuur geïdentificeerd die mogelijks gebruikt kan worden tegen spieratrofie. Deze miRNAs werden in vitro getest op MABs, wat leidden tot een verhoogde spierdifferentiatie. Wanneer MABs, na blootstelling aan de miRNAs, werden geïnjecteerd in oude muizen, werd er een

verbetering gezien in de spier eigenschappen zoals gewicht, sterkte, grootte en hoeveelheid fibrose. Hiermee bewijzen we dat miRNA afkomstig van EVs het myogeen potentieel van stamcellen kunnen verhogen.

In het algemeen kunnen we onze resultaten kaderen in het opkomende veld van regeneratieve geneeskunde waarbij EVs en stamcellen worden gecombineerd. In dit project hebben namelijk gebruik gemaakt van zowel miRNAs als stamcellen om de spierafbraak en het bijhorende functieverlies tegen te gaan.



Parts of this chapter have been published in:

Unconventional players on the striated muscle field: microRNAs, signaling pathways and epigenetic regulators

Giorgia Giacomazzi, Maurilio Sampaolesi, Mattia Quattrocchi. *Curr Stem Cell Res Ther.* 2016;11(7):554-

1 Skeletal muscle: homeostasis and pathological dysregulation

Muscle remodelling is a dynamic process occurring throughout the whole tissue life span. During development, protein synthesis and progenitors activation contribute to new muscle formation¹. Conversely, during adulthood, cellular turnover generally decreases and the muscle mass plasticity is mainly determined by the interplay between anabolism and catabolism. In steady state, these two pathways remain balanced. However, upon injury or excessive activity, several myocytes are damaged and undergo necrosis, and the regeneration process takes place. The necrosis of damaged myocytes elicits an inflammatory response triggering the progenitors to proliferate and regenerate the muscle by engrafting damaged site or by de novo myocyte formation. On the other end, muscle wasting can occur as a physiological age-related condition (sarcopenia). Lastly, chronic illness can also disrupt muscle homeostasis, that is the case of genetic illnesses as for example Muscular Dystrophies, or in other condition of muscle atrophy due to chronic obstructive pulmonary disease, or heart failure (cachexia).

1.1 Regulation of skeletal muscle homeostasis

The dynamic properties of skeletal muscle allow physiological response to changes in load demand². Skeletal muscle can in fact increase or shrink its size by finely regulating anabolic and catabolic pathways via the ubiquitin–proteasome, caspase, and lysosomal degradation systems^{3,4}. Conversely, several factors play a role in muscle growth and regeneration, both at genetic and paracrine levels (Figure 1.1).

At the genetic level, myogenic regulatory factors (MRFs) are transcription factors, including MyoD, Myf5, and Myogenin for the skeletal muscle that together with other key developmental factors, such as Pax7 direct muscle formation and maturation by controlling the expression of crucial genes, e.g. sarcomeric or structural proteins⁵.

At the paracrine level, muscle mass is regulated by secreted factors, such as insulin growth factor 1 (IGF-1) and hepatocyte growth factor (HGF). Although initially mitogenic, IGF-1 displays differentiation properties on the skeletal muscle ⁶, that have been further proven beneficial in sustainment of hypertrophy ⁷. HGF is released from the extracellular matrix in case of injury and promotes quiescent cell activation and proliferation. During development, HGF signalling directs homing of progenitor cells, while during later phases it is mainly involved in cell proliferation ⁸.

Myostatin is one of the most powerful negative regulators of muscle growth ⁹. In skeletal muscle, myostatin negatively regulates muscle mass through interference with Akt signalling pathways. Recent evidence has shown that, together with myostatin, other members of the TGF β family might be involved in regulating skeletal muscle mass and differentiation. In particular, activin-A has been found to be upregulated in skeletal muscle after activation of the tumour necrosis factor alpha/TAK-1 signalling pathway ¹⁰. Furthermore, in the past few years, new signalling players have been unravelled in muscle regeneration. Modulation of G-coupled proteins has been reported to promote skeletal muscle hypertrophy and accelerate skeletal muscle regeneration ¹¹. Additionally, interest in the inflammatory pathways involved in muscular disorders has been growing, because chronic inflammation is a hallmark of many muscle degenerative conditions.

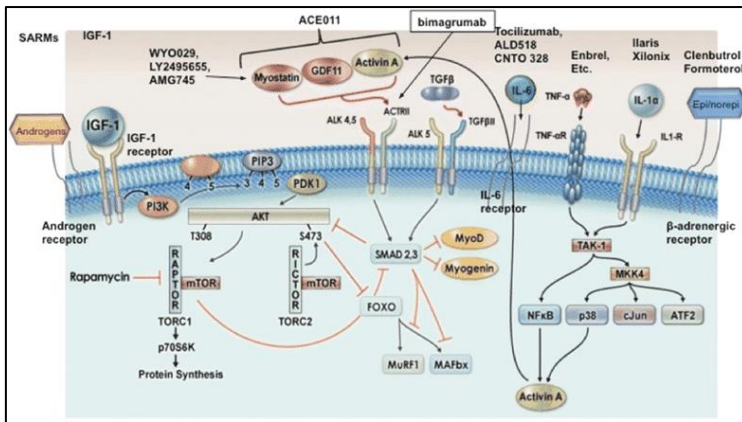


Figure 1.1 Main factors playing a role in muscle growth and regeneration.

Adapted from Matthew N. Et al, 2015

1.2 Skeletal muscle disorders

1.2.1 Muscular dystrophies

Muscular dystrophies (MDs) are a group of diseases characterized by progressive muscular loss and weakness. MDs display clinical heterogeneity, which reflects variety in the underlying molecular mechanisms and clinical features. Also, the age of onset, which spans from early childhood to adulthood and prognosis, is variable^{12, 13}. There are different forms of MDs, classified according to the muscles that are most compromised and to the severity of the damage. The progressive muscle weakness mainly affects limbs, axial and facial muscles, resulting in gradual motility impairment. In addition, respiratory muscles, cardiac muscles and smooth muscles can also be affected, eventually leading to respiratory failure and cardiac decompensation¹².

The most common form of MD is the X-linked Duchenne Muscular Dystrophy (DMD), which has an incidence of 1:3600-6000 male births¹⁴. DMD is a very severe form of MD and features early childhood onset, severe chronic degeneration of locomotory muscles and poor prognosis with death ensuing in the early twenties. Less severe

and acute muscle damage, its use in the clinics is still associated with considerable side effects^{17, 18}. Moreover, treating dystrophy-associated cardiomyopathies and respiratory failure is a compelling challenge.

For decades now, research has been focusing on unravelling the potential therapeutic effects of other promising therapies, such as gene and cell therapies. Gene corrective strategies aim at the integration of the healthy wild type (WT) Dystrophin gene inside the genome of dystrophic myonuclei. Some encouraging results have been achieved by administration of adeno-associated virus carrying a human mini-dystrophin gene in murine animal model of MD, the *mdx* mouse¹⁹. Similarly, adeno-associated virus carrying a human-sarcoglycan gene has been delivered to a hamster model of LGMD type 2F, with some promising results. Finally, exon skipping strategies, aimed at correcting the reading frame have been investigated²⁰.

As comprehensively discussed further, stem cell- therapeutic approaches are of valuable interest in regenerative medicine, given the self-renewal ability, the differentiation potency and the patient-specific application potential that characterized them.

1.2.2 Age-related muscle wasting - sarcopenia

Aging is associated with a progressive decline of muscle mass, muscle quality, and strength, a condition known as sarcopenia²¹. Around 50 years of age, the decrease in muscle mass is approximately 1 to 2 % annual rate and is accompanied by an even stronger decline in functionality reaching an annual rate of 3 % after the age of 60. These rates of decline in strength are even higher in sedentary individuals and twice as high in men as compared to women²². Additionally, it is reported that sarcopenia is not only associated with aging, but also with chronic diseases, malnutrition, loss of mobility due to sedentary lifestyles or prolonged bed rest.

Features of the sarcopenic muscle include atrophy of type 2 (fast-twitch) myofibres and heterogeneity in fibre size, accumulation of intramuscular connective tissue and fat as well as decreased oxidative capacity²³. The decrease in muscle mass that gives rise to sarcopenia involves both a decrease in muscle fibre size (atrophy) and number (hypoplasia), and both slow and fast muscle fibres. Moreover, the loss of muscle tissue is accompanied by fatty infiltration and connective tissue accumulation resulting in a significant decline in contractile capacity of the muscle fibres²⁴. Other features of the sarcopenic muscle include denervation of motor units which are then reinnervated with slow motor units can lead to increased muscle fatigability²⁵. Finally, sarcopenic muscle is marked by defective mitochondrial energy metabolism, increased inflammation and protein catabolism^{26,27}.

1.2.2.1 Therapeutic approaches for skeletal muscle wasting

Currently, therapies to combat sarcopenia are limited. Exercise appears to be an excellent strategy, in elderly people resistance exercise marked increase in skeletal muscle protein synthesis without an increase in whole body muscle breakdown²⁵, thus favouring an hypertrophy of the muscle. However, exercise is often impeded due to lack of motivation and comorbidities, such as osteoarthritis and cardiovascular disease.

Other strategies include hormone replacement, although associated with side effects, and supplementation with β -hydroxy- β -methylbutyrate (HMB), shown to reduce muscle wasting, although effects on muscle strength and performance remain controversial²⁸. It has been reported that addition to the diet with beneficial molecules could provide a potential therapy, given the importance role of nutrition in sarcopenia²⁹. Indeed, elderly patients who received a protein supplementation in the diet showed a moderate increase in muscle strength. Nonetheless, with limited available therapies and sarcopenia being a growing issue, it is important to develop new strategies to combat this syndrome.

2 Stem cell therapy for skeletal muscle disorders

Cell-based therapy to promote muscle regeneration as a potential treatment for MDs and other muscle wasting disorders has been an interest for scientists since the late 80s, when wild type muscle precursor cells were fused with regenerating fibres of the *mdx* mouse model, showing an increment in *Dystrophin*-producing fibres ³⁰. However adult myoblasts still face many hurdles, e.g. low ability to migrate from the site of injection towards damaged fibres, poor survival and potential immune response reactions in the recipient. Stem cells have thus gained increasing attention, for their migratory potential, differentiation capacity and self-renew ability. Figure 1.3 shows a summary of stem cell sources explored for muscle regeneration.

2.1 Adult stem cells

The post-natal skeletal muscle holds the ability to regenerate after injury, attributed to satellite cells (SCs) ³¹. SC are skeletal muscle quiescent progenitors located in a niche beneath the basal lamina that surrounds each myofibre ³². After post-natal development, SCs enter a quiescent phase, and in the adult life they re-enter the mitotic cycle in case of muscle damage. In some myopathies, such as MDs, SCs are activated in the first stages of the disease, however, the genetic lack of *Dystrophin* leads to non-functional newly formed fibres, resulting in a vicious “regeneration-degeneration” cycle that ultimately replenishes SC niche ³³. Several studies have explored the potential of SC for muscle regeneration, and have shown some promising results ^{34, 35}. Nonetheless SCs are associated with a considerable loss of myogenic ability following *in vitro* expansion and the difficulty of cell migration from site of injection to the muscle injury represent a considerable limitation ³⁶.

Mesoangioblasts (MABs) are vessel-associated stem cells that can be isolated from the dorsal aorta during development or from post-natal cardiac and skeletal muscles. MABs were found to be a valid alternative for cell therapy of MDs, as they have been shown to differentiate in most mesodermal cell type including skeletal muscle ³⁷.

Later on, murine and human MABs have been also isolated and characterized from adult skeletal muscles³⁸. When injected intra-arterially in mice, MABs fuse with resident SCs and participate in post-natal muscle recovery. Interestingly, MABs show an intrinsic capacity to spread through the capillary network and reach the damage site, when compared to SCs. To this end, intraarterial delivery of MABs performed in murine and canine models have given encouraging results for clinical application^{39, 40}. More recently mdx-derived MABs transduced with a human artificial chromosome vector containing the entire human dystrophin genetic locus were transplanted into dystrophic mice. The study reported a significant engraftment and differentiation of the MABs, further supported by functional improvement⁴¹. In spite of such promising results in preclinical studies, a phase I/II clinical trial, has shown little to no beneficial effect in the use of HLA-matched allogeneic human MABs to treat paediatric DMD patients⁴². While intra-arterial transplantation of donor MABs in human proved to be feasible and relatively safe, such approach needs further amelioration to reach efficacy⁴².

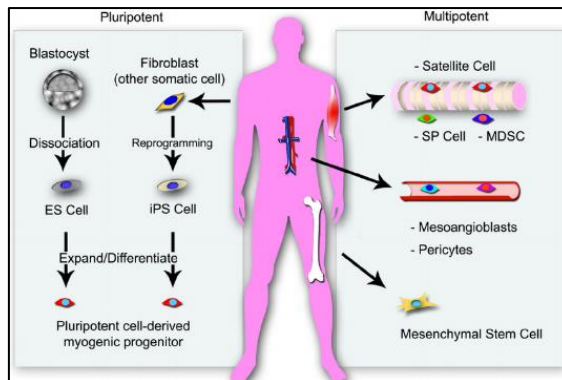


Figure 1.3. stem cell sources explored for muscle regeneration.

Adapted from Hosoyama et al, 2012

2.2 Pluripotent stem cells

Pluripotent stem cells (PSCs) hold the potential to regenerate derivatives of all three embryonic germ layers, endoderm, ectoderm and mesoderm. This property,

together with the strong renewal ability, makes PSCs appealing candidates to target skeletal muscle degenerative disorders, such as MDs and muscle wasting. Nonetheless cell therapy with PSCs has to face the hurdles of ethical issues and immunological concerns, as well as safety. PSCs can, in fact give rise to teratomas when fully or partially undifferentiated. Currently, two PSC types are under investigation for skeletal muscle regeneration: embryonic stem cells (ESCs) and induced pluripotent stem cells (iPSCs).

Embryonic stem cells (ESCs) are derived from the ICM of the blastocyst, they can proliferate maintaining their undifferentiated status, eventually giving origin to differentiated cells. In vitro differentiation of skeletal muscle from ESCs has encountered more obstacles in comparison to differentiation toward other lineages, like blood, endothelial cells and cardiac muscle. Early transplantation studies of human and murine ESC-derived muscle progenies have shown evidence of myoblasts engraftment, as well as contractile function^{43,44}. Nevertheless, ESCs still retain some limitations, such as immunological concerns and, not less importantly, ethical issues.

Major breakthrough in the field of regenerative medicine was achieved in 2006 by Yamanaka and Takahashi with the generation of induced pluripotent stem cells (iPSCs)⁴⁵. iPSCs were created from murine embryonic or adult fibroblasts, by viral transduction with four factors, namely Oct3/4, Sox2, c-Myc, and Klf4, via a process called reprogramming. Similar to ESCs in morphology and behaviour, iPSCs exhibit ESC-specific markers and, when subcutaneously transplanted into nude mice, generate teratomas. Ever since, many studies have focused on reprogramming of a wide range of adult murine and human somatic cells⁴⁶. One way of inducing myogenic differentiation in iPSCs is the overexpression of myogenic genes crucial for differentiation of myogenic progenitors and myoblasts during embryonic myogenesis such as PAX3, PAX7, and MYOD1^{47,48}. Transgene approach methods, often delivering constructs that contain a reporter gene, allow an easier selection of desired progenitors. Nevertheless, concerns regarding the use of these modified cell in patients remain unanswered. Transgene-free methods attain the induction of

myogenesis in iPSCs by means of growth factors and/or signalling molecules that play an important role in muscle development⁴⁹. FGF2, IGF-1 and HGF have been reported in different study as ways to enhance myogenic differentiation, fibre fusion and to sustain myogenic properties *in vitro*⁵⁰⁻⁵². Similarly, the use of small molecules can drive myogenic differentiation. Induction of mesoderm can be accomplished with GSK3 β inhibitors, such as CHIR99021, or supplementation of insulin-transferrin-selenium (ITS) to basal culture medium^{43, 53}. Moreover, Inhibitors of TGF- β type I receptors, such as LDN193189 has been used to increase myogenic differentiation in iPSCs⁵⁴. Notably, overexpression of myogenic factors and small molecules has been applied to generate skeletal muscle progenitors directly from somatic cells without undergoing a pluripotent state in a process known as trans-differentiation^{55, 56}.

2.3 Aging and stem cells

In general, an age-associated decline in stem cells is observed in several organs, and it is considered a major contributor to age-related diseases, such as sarcopenia. Both extrinsic and intrinsic factors drive this stem cell age-associated dysfunction and a summary of the mechanisms are illustrated in Figure 1.4.

Aging muscle is characterized by a concomitant decline in muscle stem cells function and numbers, ultimately contributing to the progressive loss regenerative capacity of the skeletal muscle⁵⁷. During development or upon injury, SCs have to exit the quiescent status and enter the cell cycle to contribute to newly formed myofibres, meanwhile ensuring the maintenance of the stem cell pool. These two functions are coordinated by a rigorous interplay between intrinsic programs and signals such as growth factors cytokines and others, from the stem cell niche and the surrounding environment²³. Adult SCs hold the crucial ability to transit to a reversible quiescent state after providing a source of progeny, reinforcing muscle homeostasis. The decline in functionality and numbers of SCs in the sarcopenic muscle leads to a progressive deterioration of this self-renewing mechanism, the SC pool is exhausted by continuous differentiation as well as apoptosis and senescence. Supporting this

observation, evidence has shown that deletion of Sprouty1 in proliferating SCs leads to persistent activation of the extracellular-signal-regulated kinase/mitogen-activate protein kinase (ERK/MAPK) signalling pathway, which hinders self-renewal. Impaired self-renewal ability causes a subset of SCs unable to re-enter quiescence state to undergo apoptosis^{58, 59}. Aging causes as well a decline in DNA repair mechanisms and an increased accumulation of DNA damage surely weakens stem cells functionality⁶⁰. Other blueprints of aging stem cells are mitochondrial dysfunction, alteration in the metabolism and loss of protein homeostasis⁵⁹. For example, it has been demonstrated that autophagic mechanisms are defective in aged SCs, lysosomes are marked by strongly decreased in proteolytic activity which results in accumulation of indigested products⁶¹. Finally, epigenetic play a role in safeguarding stem cell functionality during adulthood and ageing. The epigenetic network of stem cells comprises define regulators that support gene expressions and activate specific differentiation or pluripotency programs. It is reported that aged stem cells have heritable epigenetic marks, methylation patterns and histone modifications, that can alter stem cell differentiation potential by either restricting or allowing access to key lineage-specific genes^{59, 62}.

With regard to skeletal muscle specific stem cells, a recent study has highlighted how ageing negatively impact the muscle regeneration potential of human MABs: MABs derived from elderly donors displayed a dramatic impairment in the myogenic differentiation ability in vitro and when transplanted in dystrophic mice⁶³.

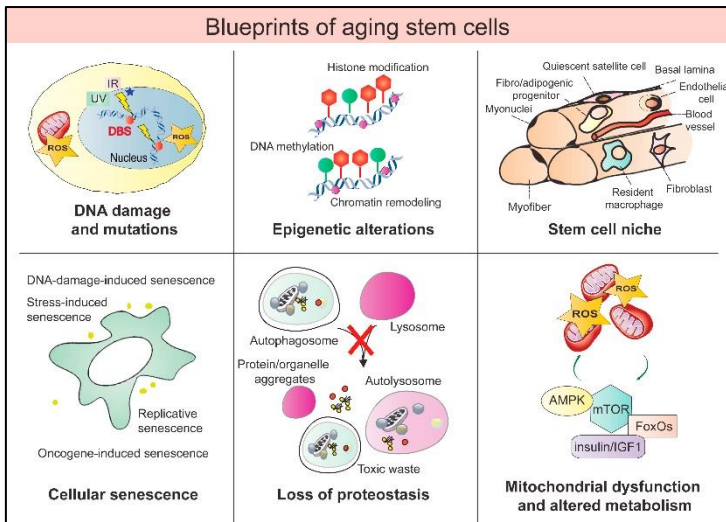


Figure 1.4 Overview of the hallmarks of aging stem cells.

Adapted from Sousa-Victor P et al, 2015

2.4 Stem cell therapies and epigenetics

Reprogramming of somatic cells to pluripotent state encompasses waves of epigenetic remodelling, genome-wide modulation of histones and DNA methylation, that wash out previous epigenetic state and establish new pluripotency circuits⁶⁴ (Figure 1.5). During the reprogramming to a pluripotent state, somatic cells must reshuffle their epigenetic signature, tissue-specific genes and differentiation regulators have to be silenced, whereas pluripotency genes and self-renewal genes must be activated. In addition, early commitment markers have to assume a poised state. Therefore, in principle, to achieve a fully pluripotent state somatic cells must delete any retained memory of the tissue of origin.

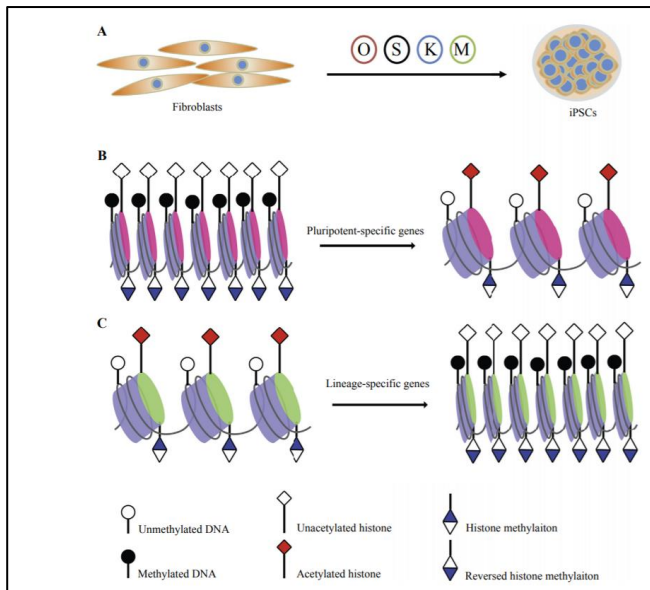


Figure 1.5 Schematic representation of the changes of epigenetic signatures occurring during reprogramming of somatic cells into iPSCs. Adapted from Brix J et al 2015

Several evidence has reported that iPSCs hold epigenetic memory, questioning their real pluripotent state and ultimately their therapeutic applicability^{65,66}. These works have reported that iPSCs derived from different adult murine tissues present an epigenetic signature consisting of inherited biases in DNA methylation or histone deacetylation thus skewing the differentiation. Similar results have been found when using human cells^{67,68}. Undoubtedly, the possibility of retained epigenetic signatures might narrow down the broad therapeutic promises of iPSCs. However, the intrinsic bias of iPSCs differentiation potential might reinforce them towards a specific commitment⁶⁹.

2.5 Mesodermal-iPSC-derived progenitors

Mesoangioblast-derived iPSCs (MAB-iPSCs), generated by our group, show an intrinsic skew towards myogenic commitment, when compared to fibroblast-derived iPSCs (fiPSCs). This commitment bias was quantifiable by both teratoma formation

and gene expression profile ⁶⁹. Upon intramuscular injection in aged *Sgca-null* dystrophic mice, MAB-iPSCs are able to restore up to 50 % of the muscle fibres in area surrounding the injection site, proving the principle of feasibility of generating highly committed myogenic progenitors from myogenically skewed iPSCs. A novel pool of progenitors with myogenic properties was subsequently derived from MAB-iPSCs and fIPSCs, the mesodermal iPSC-derived progenitors (MiPs) ⁷⁰. MiPs are isolated from iPSC pre-induced to mesoderm differentiation as a specific population triple positive for common markers shared by stem cells important for skeletal muscle regeneration, cd140a, cd140b and cd44. Notably, both MAB-MiPs and f-MiPs were able to engraft in the cardiac muscle of dystrophic mice, while only MAB-MiPs were able to functionally regenerate the skeletal muscle when injected intraarterially in dystrophic mice. Interestingly, the boosted differentiation potential toward skeletal muscle correlated with retained signatures of DNA methylation and histone marks from parental progenies ⁷⁰. This study points at MiPs as a new, promising source of skeletal muscle progenitors, while confirming the crucial importance of epigenetic remodelling when iPSCs- based regenerative strategies are desirable. A compelling question regards which factors regulate the differentiative decision that stem cells undertake, namely the stem cell fate. The factors guiding stem cell fate and ultimately its commitment are of main concern in regenerative medicine, as they can yield insights in tuneable mechanisms of differentiation in foetal and adult life.

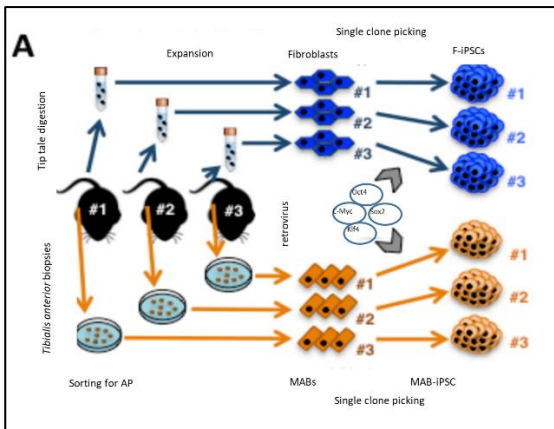


Figure 1.6 Schematic design of iPSC derivation for MiPs production

Adapted from Quattrocelli et al, JCI 2015

3 MicroRNAs

3.1 Definition, biogenesis and function

MicroRNAs (miRNAs) are short non-coding RNAs that regulate gene expression at post-transcriptional level. MiRNAs are encoded in the genome either as individual transcriptional units, or often as intergenic clusters of several miRNAs⁷¹. However, growing evidence has shown that a number of miRNAs are enclosed in the intronic sequences of other genes and are therefore transcribed along with the coding genes^{72, 73}. In the nucleus, miRNAs are generally transcribed by RNA polymerase II in primary transcripts called pri-miRs, subsequently cleaved by the microprocessor complex into shorter precursor molecules called pre-miRs⁷⁴. Pre-miRs are then transported into the cytosol, where they are further cleaved in ~22nt-long double-stranded molecules by a complex that includes another RNase-III, Dicer. MiRNAs are then ready to be loaded on the RNA-induced silencing complex (RISC): the guide strand is loaded while the star strand is generally degraded⁷⁵. However, the modus operandi of miR processing machinery is still largely unknown⁷⁶. The principal RISC components interact with the proteins responsible for RNA remodelling and for the generation of processing bodies (P-bodies), or glycine-tryptophan bodies (GW-bodies), which account for mRNA decapping, deadenylation, and degradation. MiRNAs recognize target sequences at the 3' untranslated region (3'-UTR) and

repress target gene expression either by targeting the mRNA for degradation or by mediating translation inhibition ⁷⁷.

3.2 *MicroRNAs and skeletal muscle regulation – myogenesis*

MiRNAs are active regulators of muscle myogenesis, as shown by several miRNAs enriched at different phase of embryonic and adult myogenesis. Along well-characterized miRNAs important for muscle homeostasis, during the last few years new studies have pointed out at novel players.

MiR-1 and miR-133 are well-established members of the so-called myomiR family and orchestrate skeletal and cardiac muscle regeneration ⁷⁸. Although encoded from the same loci and transcribed together, mir-1 and mir-133 develop into two separate mature miRNAs that hold specific functions. Via the regulation of SRF and MEF2, in fact, they establish distinct negative feedback loops that intrinsically modulate the cellular proliferation and differentiation within muscle cell lineages ⁷⁹. Mir-206 has also been well characterized as a positive regulator of the myogenic commitment, by supporting satellite cell differentiation and repressing many negative modulators of skeletal muscle differentiation ⁸⁰.

Evidence is also accumulating for a set of non-muscle-specific miRNAs that have an effect on muscle remodeling by targeting muscle-specific regulatory factors. An important difference in contrast to mir-1, mir-133 and mir-206, whose expression is muscle specific, is that these miRNAs are broadly expressed in several tissues and yet retain muscle-specific functions ⁸¹. An example is miR-181, a broadly expressed miRNA that has been shown to contribute to myoblast differentiation by targeting a MyoD repressor in mammals ⁸². Mir181 directly binds to HOX11, bringing to an increase in MyoD, a target of HOX11, and therefore to the myogenic differentiation of cells. Similarly, miR-148a has been found crucial for skeletal myogenesis since its main target ROCK1 prevent myoblast fusion. Mir-24, although not a traditional muscle-specific miRNA, plays a role in positively modulating myogenesis via

inhibition of members of the TGF-beta family⁸³. Interestingly, mir-24 is expressed at a later stage of muscle differentiation, suggesting an additional important function in the maintenance of the skeletal and cardiac muscle homeostasis. Other miRNAs are involved in myogenesis, as miR-27b, acting at the onset of myogenesis directly targeting Pax3 proteins ultimately inducing migration and early differentiation of myoblasts⁸⁴. Timely regulators of myogenesis are MiR-26a⁸⁵ and miR-214⁸⁶, whose pattern of expression correlates with myogenic master genes. Once muscle differentiation begins, miR-214 is upregulated via MyoD/MyoG, which promote P21Cip1 and myogenin expression, while miR-26a increases during the later stages of the course of myogenesis.

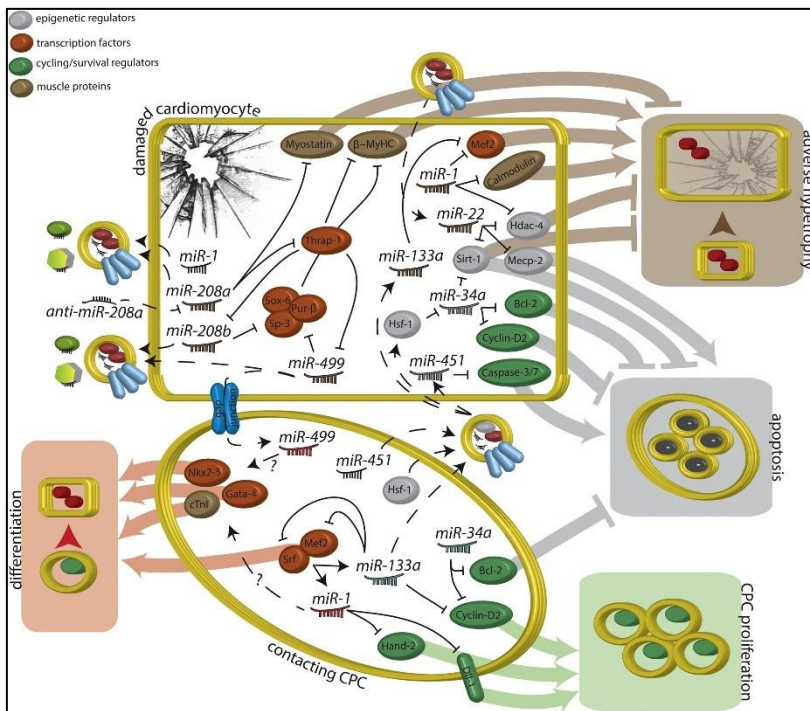


Figure 1.7. Summary of microRNAs involved in myogenesis and muscle wasting.

Adapted from Quattrocelli et al 2014

3.3 MicroRNAs and skeletal muscle disorders

In several muscle disorders, including MDs, miRNAs levels are altered. For instance, regenerative miR-31, miR-206, miR-449 are induced in animal models (*mdx* mouse) and in Duchenne MD patients during the regenerative stage, while other miRNAs, such as miR-1 and miR-29c, are down-modulated during fibre degeneration. These observations suggest that the regenerative miRNAs boost differentiation towards myofibres, while during fibre degeneration other miRNAs negatively regulate apoptotic pathway as a compensatory mechanism for myofibre loss⁸⁷. MiRNA modulation to increase skeletal muscle regeneration in chronic disease and muscle wasting setting has been broadly explored. Myomirs are known to increase muscle progenitors differentiation *in vitro* and *in vivo*⁸⁸. In SCs isolated from *mdx* mice the overexpression of miR-1, miR-133 and miR-206 enhanced their myogenic differentiation and rescued their phenotype when compared to SC isolated from wild-type mice. Other evidence has reported that injection of miR-206 in a rat model of skeletal muscle injury resulted in enhanced muscle regeneration and reduced muscle fibrosis^{89, 90}. Finally, genetic deletion of miR-206 delayed muscle regeneration in cardiotoxin-injured mice and the loss of miR-206 accelerated and exacerbated the dystrophic phenotype in miR-206-KO⁹¹. Other miRNAs have been explored in the field of muscle regeneration. It is the case of miR-486, whose muscle specific overexpression in dystrophic mice resulted in reduced serum creatine kinase levels, and improved performance⁹².

MiRNAs have recently emerged as interesting molecules to target crucial features of skeletal muscle disorders. Fibrosis is a hallmark of many myopathies, intrinsically associated with a dramatic loss of functionality. The delivery of adeno-associated viral vector (AAV) carrying mir-29 into muscles of *mdx:utrn+/-* mice has resulted in a significant decline in fibrotic tissues eventually leading to the development of MRG-201, a synthetic miR mimic (promiR) to miR-29b currently undergoing phase I clinical trial study⁹³. Analogously miR-21 is a known regulator of age-associated muscle fibrosis in *mdx* mice, and to date, the miR-21 fibrogenic pathway is recognized as a

target to treat fibrosis and MDs ⁹⁴. Finally, the properties of other miRNAs have been elucidated with respect to other features of degenerative myopathies, such as inflammatory condition ⁹⁵, and oxidative stress ⁹⁶.

3.4 *MicroRNAs, cell fate decisions and epigenetics*

Given their gene tuning properties, miRNAs are well positioned to contribute to epigenetic signalling and to participate in the control cell fate decision ⁹⁷. Evidence has shown a strong interplay between miRNAs and epigenetics as miRNAs-controlled gene expression also involves targeting of epigenetic regulators ⁹⁸. DNA methyltransferases (DNMT) and histone deacetylases (HDAC) are among known targets of miRNAs. In myoblasts differentiation, for example miR-1 and miR-206 repress HDAC4, allowing expression of MEF2 thus resulting in fusion of newly formed myofibres.

Moreover, miRNAs are core players of the gene network that regulates cell renewal, pluripotency and cell- type specification in pluripotent stem cells. Mice with muscle specific Dicer deletion die at early stages of embryonic development show abnormal morphology of muscle cells and skeletal mass wasting ^{99, 100}. ESCs have a distinct miRNA signature, clusters of miR-290 and miR-302 family are specific for mouse ESC, while human undifferentiated cells express miR-302. They repress several inhibitors of cell cycles to guarantee stem cell self-renewal properties and reinforce the undifferentiated state ¹⁰¹. Moreover, miRNAs can directly orchestrate cell fate decision, promoting for example mesoendoderm lineage specification over neuroectoderm ¹⁰². Later on, miRNAs are largely involved in the refined wiring of the pathways that regulate specific tissue program. In myogenesis myomirs are modulated and transcriptionally activated by MyoD and Myogenin ¹⁰⁰. miR-1 represents an example of a tissue-specific regulator of cell cycle given that its overexpression in developing mouse heart muscle leads to premature cell cycle exit ^{103, 104}. Finally, recent evidence has emerged that miRNAs can control lineage conversion in striated muscle. Cardiac MABs from dystrophic mice can aberrantly

differentiate into skeletal pericytes due to the absence of miR669q, highlighting a direct role of this miRNA in switching between cardiac and skeletal muscle lineages¹⁰⁵.

3.5 *MicroRNAs as therapeutics- consideration for application*

Short, multitargeting different genes and readily deliverable, miRNAs definitely hold appealing therapeutic promises. Several preclinical studies have highlighted the potential of miRNAs-mediated treatment and advances in technologies to deliver RNA molecules in vivo have made miRNA-based therapeutics feasible¹⁰⁶.

An ideal miR delivery system for regenerative medicine should be able to target specific tissue or organ with low cytotoxicity and high efficiency. Synthetic liposomes and viral vectors are extensively used for many applications strategies, however both present major limitations, including immunostimulatory properties, which restrict gene delivery applications¹⁰⁷. Viral-based systems, as adenoviruses or adeno-associated viruses (AAV) hold high efficiency and targeted delivery. As an example, miR-590 and miR-199a were delivered into neonatal mouse heart by an rAAV9 vector, in order to improve cardiac regeneration¹⁰⁸. Nevertheless, immunogenicity and random integration hamper the use of viral vectors for miR gene therapy approaches. Non-viral systems are less toxic and less immunogenic, although therapeutic applications are limited by the low efficiency. Gene gun, electroporation, hydrodynamic, ultrasound, laser-based energy and inorganic carriers have been explored to improve the efficiency of miR delivery. However, in all these procedures damages of cell integrity and apoptosis are frequently observed¹⁰⁹.

Encouraging results in preclinical studies have opened a door for miRNA therapeutics in the clinics. LNA miravirsin, a 15-nucleotide antisense RNA oligo with complementarity to the 5' end of miR-122, has undergone phase I and II clinical trials for the treatment of HCV, eventually advancing in a phase II study with long term follow up¹¹⁰. MRX34, a miR-34 mimic (Mirna Therapeutics) encapsulated in a lipid

carrier called NOV40 entered a multicenter phase I trial in 2013 in patients affected with different type of cancer. However, immune-related adverse events caused termination of the trial¹¹¹. A third example, as previously mentioned, is MRG-201, a synthetic miRmimic to miR-29b, developed by miRagen Therapeutics to reduce fibrotic formation associated to chronic diseases ongoing a phase I clinical trial study. Future challenges calling for improvement in miRNAs therapeutics include identification of the relevant targets amidst the heterogeneity of targets interested by single miRNAs, and delivery techniques¹⁰⁶. The latter point could potentially benefit from the emerging role of novel delivery platforms, such as extracellular vesicles.

4 Extracellular vesicles

Skeletal muscle is a metabolic tissue that has paracrine properties. Along hormones and external regulatory factors, myokines –i.e. cytokines produced, expressed and released from the skeletal muscle- contribute to maintenance of homeostasis and are also involved in the process of myogenesis. Recently interest in secreted extracellular vehicles (EVs) and in their communication network has been increasing, and during the last decades it has emerged that EVs represent key players in intercellular communication¹¹².

4.1 *Definition and biogenesis*

Cells release a number of vesicles from their plasma membrane, both in physiological and pathological conditions. These vesicles are generally referred to as micro vesicles, ectosomes, shedding vesicles, or more generally extracellular vesicles¹¹². It is important to underline the high heterogeneity of EVs, and therefore a lack of a real ground consensus on the terminology. For this reasons EVs are mainly classified based on their size and biogenesis. In more recent years the term exosomes have been commonly used to indicate EVs that are comprised in a size range between 40 and 100 μm shed from cells as a consequence of multivesicular endosome (MVE)

fusion with the plasma membrane ¹¹³. However, it has been reported that circulating vesicles are likely composed of both exosomes and micro vesicles (MVs), undergoing the same release system, thus making it challenging to fully discriminate among the different types of EVs ¹¹⁴. In Figure 1.7 a scheme of the mechanism of EVs shedding is reported as well as the main identified cargos, discussed further on. Although further evidence is still required, it is generally believed that components of the cytoskeleton, associated molecular motors, molecular switches (small GTPases) and the fusion machinery (SNAREs) are all involved in the released of EVs ¹¹².

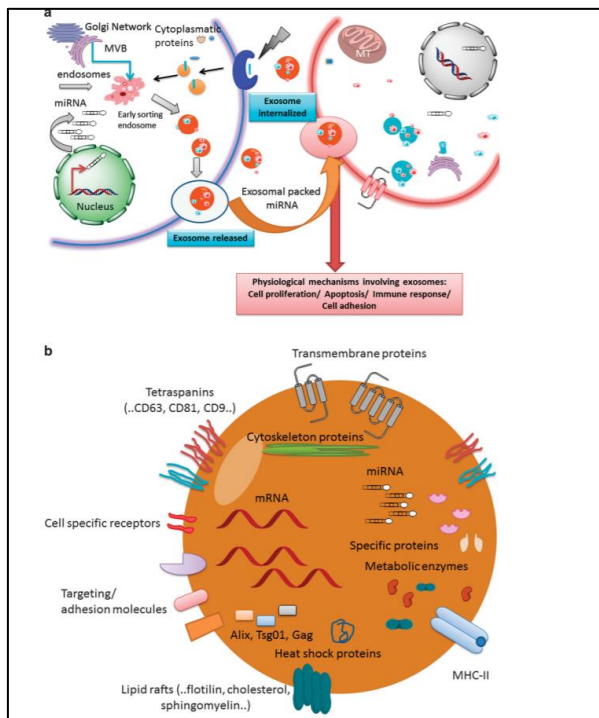


Figure 1.8. Schematic representation of EVs biogenesis and main components of the extracellular membrane and cargo.

This hypothesis is supported by evidence showing that knockdown of Rab27a or Rab27b (members of the Rab GTPase) significantly reduced the amount of secreted EVs in Hela cells ¹¹⁵. EVs carry an heterogenous cargo: miRNAs, long non-coding

RNAs, mRNAs, lipids, proteins have all been identified in EVs derived from different tissues. However, how RNA species and proteins are sorted into mature EVs is still not fully elucidated. For example, RNA might be selectively incorporated in EVs, as suggested by observations that RNAs in secreted EVs might share specific sequence motifs potentially functioning as cis-acting elements for targeting EVs to specific tissues^{112, 116}.

EVs have also been isolated from different body fluids, such as blood, saliva, breast milk, urine, amniotic fluids, hence it appears evident that they represent an important mode of intercellular communication by serving as vehicles for transfer of information and signals between cells. In both physiological and pathological processes, EVs-mediated communication depends on the cells of origin as well as the recipient cells. Albeit still largely unknown, evidence is starting to accumulate regarding cellular and molecular basis for EV targeting. For example, adhesion molecules such as integrins, that are often presents in the surface of EVs, have been implicated in recruitment of MHC class II-containing dendritic cell-derived EVs by T lymphocytes¹¹⁷. Over the years diverse biological functions have been pinned on EVs. Large pieces of evidence are coming from the cancer fields, where the functions of EVs are deeply studied. EVs can, in fact, stimulate antitumoral immune responses, act as antigen-presenting vesicles or even promote angiogenesis and tumour cell migration in metastases¹¹⁸. Additionally, functions of EVs have been unravelled in nervous systems, in the epithelium, in immunological responses and EVs have been implicated to play a role in degenerative conditions and diseases, such as neurodegenerative diseases, immunological diseases and cardiovascular pathologies¹¹⁹.

4.2 EVs and muscle regeneration

Skeletal muscle actively secretes EVs, during differentiation of myoblasts¹²⁰. Several studies have shown that C2C12 as well as primary human SCs release EVs carrying

growth factors, such as basic fibroblast growth factor (bFGF), IGF-1, transforming growth factor-beta1 (TGF-B1), and vascular endothelial growth factor (VEGF), among others ¹²¹. Similarly EVs have been reported to play a role in the crosstalk between proliferating and differentiated muscle progenitors ¹²². As expected, EVs released from skeletal muscle are enriched as well in myomirs and circulating muscle-derived EVs transport these miRNAs ¹²³.

Moreover, paracrine action of EVs secreted by stem cells has been reported, pointing at exosomes as crucial agents in tissue regeneration elicited by cell therapy ¹²⁴. EVs produced by mesenchymal stem cells promote skeletal muscle repair through activation of angiogenesis and myogenesis ¹²⁵. Another study has reported how EVs derived from human skeletal muscle stem cells are able to improve regeneration in injured skeletal muscle and reduce the fibrotic area, by directly triggering myogenesis of stem cells ¹²⁶. Finally, a number of studies has highlighted the promising role of EVs in mediating cardiac regeneration. To this regard, EVs secreted by cardiosphere-derived cells have been identified as pivotal mediators in improvement and regeneration of the infarcted murine heart. Recent evidence has shown the cardio protecting role of anti-apoptotic EVs secreted by a population of mesenchymal stem cells upon injuries, enforcing the importance of micro vesicles in the damaged cardiac muscle niche ¹²⁷. Interestingly, a very recent study reported that EVs from cardiospheres-derived cells injected in the skeletal muscle of dystrophic mice transiently restored partial expression of full-length dystrophin, inducing muscle growth and generally ameliorating pathological features ¹²⁸.

Part 1. MicroRNAs promote skeletal muscle differentiation of mesodermal iPSC-derived progenitors.

The first part of the project resulted in a publication in Nature Communications structured around the following 3 objectives.

Aim 1. In vivo myogenic potential of human MiPs.

In order to assess the in vivo potential of human MiPs we equipped previously derived MiPs of fibroblasts and mesoangioblasts origin with GFP, a sodium-iodide symporter (NIS) tracer for non-invasive PET imaging, as well as an inducible suicidal gene, iCasp9. We injected the cells in immunodeficient dystrophic mice in order to evaluate their muscle regeneration potential.

Aim 2. Whole transcriptome analysis of f-MiPs and MAB-MiPs.

To gain insight in the myogenic difference between MAB- and fibroblast-MiPs, we investigated which genes were differentially expressed between fibroblast- and MAB-MiPs, and whether differentially expressed genes were conserved from the parental cells. We further aimed at perturbing some of these transcripts in order to increase myogenic differentiation of f-MiPs.

Aim 3. MicroRNA profiling of f-MiPs and MAB-MiPs and identification of promyogenic microRNA signature.

In light of a retained genetic signature in MiPs from different origin, we further analysed the miRNA component of the same samples that we previously analysed by RNA-seq. The final goal was to select a pool of microRNAs differentially

expressed in f- MiPs vs MAB-MiPs and modulate the selected microRNA to increase myogenic differentiation potential of MAB-MiPs *in vivo* in dystrophic muscle, and rescue the myogenic commitment of f-MiPs.

Part 2. Extracellular vesicles- derived microRNAs improve mesoangioblasts treatment in muscle wasting condition

Aim 1. Deciphering EVs cargo of healthy mice and mice displaying muscle wasting and identifying a signature amenable for muscle regeneration.

In order to unravel novel secreted targets implicated in muscle regeneration we performed *ex vivo* exosome analysis comparing age-matched wild type, Sgcb-null (dystrophic skeletal muscle), MSTN $-/-$ (hypertrophic skeletal muscle) and elderly mice (> 18 months of age). Through EVs purification and subsequent RNA-sequencing miRNA profiling and protein analysis we have identified key miRNA distinctive signatures of hypertrophic remodelling of muscular tissue.

Aim 2. EV- derived miRNA signature increases myogenic potential of muscle progenitors *in vitro* and *in vivo*.

We identified a set of miRNAs amenable for increasing hypertrophy and modulating muscle regeneration, therefore we next aimed at validating this signature *in vitro* on muscle progenitors of murine and human origin. Furthermore, we aimed at assessing the miRNA signature *in vivo*, injecting MABs in skeletal muscle of elderly mice following a cardiotoxin injury. We show that the identified EV- derived miRNA signature is able to increase MABs efficiency and increase muscle features in elderly mice.



MicroRNAs promote skeletal muscle differentiation of mesodermal iPSC-derived progenitors.

The results described in this are published:

Giorgia Giacomazzi, Bryan Holvoet, Sander Trenson, Ellen Caluwé, Bojana Kravic, Hanne Grosemans, Álvaro Cortés-Calabuig, Christophe M. Deroose, Danny Huylebroeck, Said Hashemolhosseini, Stefan Janssens, Elizabeth McNally, Mattia Quattrocchi & Maurilio Sampaolesi.

Nat Commun. 2017 Nov 1;8(1):1249. doi: 10.1038/s41467-017-01359-w.

1. Abstract

Muscular dystrophies (MDs) are often characterized by impairment of both skeletal and cardiac muscle. Regenerative strategies for both compartments therefore constitute a therapeutic avenue. Mesodermal iPSC-derived progenitors (MiPs) can regenerate both striated muscle types simultaneously in mice. Importantly, MiP myogenic propensity is influenced by somatic lineage retention. However, it is still unknown whether human MiPs have *in vivo* potential. Furthermore, methods to enhance the intrinsic myogenic properties of MiPs are likely needed given the scope and need to correct large amounts of muscle in the MDs. Here, we document that human MiPs can successfully engraft into the skeletal muscle and hearts of dystrophic mice. Utilizing non-invasive live imaging and selectively induced apoptosis, we report evidence of striated muscle regeneration *in vivo* in mice by human MiPs. Finally, combining RNA-seq and miRNA-seq data, we define miRNA cocktails that promote or inhibit the myogenic potential of human MiPs.

3.2 Introduction

Stem cells hold potential for understanding the regeneration mechanisms with possible applications to degenerative disorders ¹²⁹. In particular, the recent advancements in the field of induced pluripotent stem cells (iPSCs) are paving the way to multi-tissue differentiation in patient-matched, isogenic settings ¹³⁰. This is particularly compelling for multi-tissue degenerative diseases, such as muscular dystrophies (MDs) ^{131, 132}. MDs encompass a heterogeneous group of inherited myopathies that affect skeletal muscle but in some subgroups also cardiac muscle ¹³³. At present, no regenerative treatments are available to counteract myofibre and myocyte wastage and functional loss.

The differentiation ability of iPSCs is under the influence of both extrinsic and intrinsic factors ¹³⁴. Extrinsic factors that direct differentiation include the addition and withdrawal of specific growth factors. Cell-intrinsic factors include the epigenetic factors that influence the propensity of iPSCs towards the intended lineage ¹³⁵. Albeit still unclear, the retention of progeny-specific epigenetic imprinting in iPSCs, e.g. patterns of DNA methylation and histone marks, has been often reported and exploited for enhanced differentiation along the parental lineage ¹³⁶. However, it is not yet possible to manipulate the aforementioned epigenetic layers in specific loci. Therefore, the research involving the so-called “epigenetic memory” is still mainly descriptive and the main interventional path resides in the choice of the source cells for iPSC generation ⁶⁷. Thus, the search for epigenetic signatures that can be modulated to specifically alter the differentiation propensity of iPSCs, or their derivatives, is still on.

MicroRNAs (miRNAs) are well positioned to contribute to epigenetic regulation of differentiation of stem cells ¹³⁷. The potential of miRNA-based orchestration of cell fate is evident along the striated muscle lineages and, recently, miRNAs have been described as part of the epigenetic signature retained after cell reprogramming ¹³⁸. MiRs are of particular interest because they and their anti-miRNAs are small and

readily deliverable to manipulate differentiation potential. Better definition of transcriptional and miRNAs profiles will assist in the goal of designing cocktails for skewing the differentiation propensity.

Recently, we described a novel pool of mesodermal, iPSC-derived progenitors (MiPs) for striated muscle regeneration^{139, 140}. MiPs were sorted as CD140a⁺/CD140b⁺/CD44⁺ cells from differentiating iPSCs of murine, canine, and human origins. Importantly, murine MiPs were able to functionally regenerate both cardiac and skeletal muscles in murine models. Furthermore, the propensity of MiPs toward the skeletal muscle lineage appeared augmented when derived from skeletal muscle mesoangioblasts (MAB-MiPs), as compared to isogenic fibroblast-derived MiPs. The boosted differentiation potential toward skeletal muscle correlated with retained signatures of DNA methylation and histone marks from parental progenies¹³⁹. In this study we investigated the *in vivo* capacity of human MiPs, mainly focusing our attention on their skeletal myogenic commitment. First, we assessed the translational potential of human MiPs in xenograft-permissive dystrophic mice showing evidence of striated muscle regeneration. Next, we compared the transcriptional profiles of human fibroblast-derived - and MAB-MiPs, and finally we compared their miRNAs profiles in order to predict a miRNA cocktail amenable for modulating the intrinsic propensity and for overcoming the parental lineage retention. We showed that the treatment of MiPs with a selected promyogenic miRNA cocktail further improved MiPs contribution to skeletal muscle regeneration.

3.3 Materials and Methods

Injection of MiPs and animal models

Human fibroblast- and MAB-MiPs derived from fetal fibroblasts and MABs¹³⁹ were transduced with GFP-iCasp9-¹⁴¹ and NIS-Puro^R-bearing¹⁴² viral vectors. GIN⁺ cells were then sorted for GFP and cultured in the presence of 1µg/ml puromycin (Sigma-Aldrich), following reported conditions¹³⁹. All protocols on live mice were performed in compliance with the Belgian law and the Ethical Approval of KU Leuven (P095/2012).

Rag2-null/γc-null/Sgcb-null male mice¹³⁹ were divided in randomized groups at 3 months of age (n=6, sham; n=6, fibroblast-MiPs; n=6, MAB-MiPs) and injected with GIN⁺ MiPs (passage 7-10). MiPs were exposed to RPMI20%10% medium for 48hours, then injected in parallel in the left ventricle myocardium and in both femoral arteries under isoflurane anaesthesia into each animal (5x10⁵ cells/5x2.5µl in the myocardium; 5x10⁵ cells/100µl per femoral artery, dose of cell injected was previously established by our group as optimal dose for intraarterial injections). Sham-treated controls received equal treatment and amounts of cell-free saline solution. Engraftment, regeneration and functional outcome were investigated at 4 and 8 weeks post-injection. One day after the mid-term analyses, 3 mice from each cohort were injected with AP20187 (5x2mg/body-kg every other day, i.p.), whereas the other mice of each cohort received vehicle injections.

High-resolution digital ultrasound images were obtained by an experienced echocardiographer using Vevo 2100 Imaging System (Visualsonics) with a 30 MHz probe. Mice were anaesthetized using 1 % isoflurane in oxygen, and positioned on the heating pad of the system, in order to maintain normothermia under continuous monitoring. Pre-warmed ultrasound gel was applied on the shaved thorax. B-mode-based 3D reconstruction was carried using the VisualSonics rail system with fixed probe, with ECG- and respiratory gating. FS was calculated based on LVIDD/s values,

whereas EDV and CO were calculated based on 3D analysis. Raw data were collected in blind.

Treadmill analysis was conducted on a 10°-uphill oriented treadmill belt with 1m/min² acceleration on a starting speed of 10m/min. Mice run was stopped after ≥5 consecutive seconds on the pulsed grill.

Muscle force assessment was performed on freshly isolated EDL muscles upon sacrifice, using a 1200A *in vitro* muscle test system (Aurora Scientific). Muscle force was probed upon 20 iterated bouts of isometric contractions (200hz, 80V, 0.5msec stimulation, 0.5sec tetanus, 10sec interval; 30°C) in dedicated buffer (1.2mM KH₂PO₄, 0.57mM MgSO₄*7H₂O, 2mM CaCl₂*2H₂O, 10mM HEPES, 0.5mM MgCl₂*6H₂O, 0.5mM MgCl₂*6H₂O, 4.5mM KCl, 120mM NaCl, 0.7mM Na₂HPO₄, 1.5mM NaH₂PO₄, 10mM D-Glucose, 15mM NaHCO₃; pH 7.3; Sigma-Aldrich). Data were analysed as % of max absolute force of input sham muscles.

CK levels were measured in resting conditions (>24hours after last treadmill exercise) from serum obtained from >50ul blood (withdrawn from the tail vein). CK level quantitation was performed using the Creatine Kinase Activity Colorimetric Assay kit (BioVision), following manufacturer's instructions for both sample preparation and standard curve assessment.

Cell differentiation

MiP differentiation with C2C12 myoblasts was conducted as previously reported¹³⁹. Briefly cells were seeded 1:10 MiP/myoblast ratio in RPMI 20%/10% medium on collagen-coated vessels for 24 hours, then differentiated in DMEM 2% Horse serum medium for 96 to 120 hours in 5% O₂/5% CO₂ at 37°C. MiPs and C2C12 were seeded and AP20187 (10nmol) was added 48 hours prior to immunostaining analysis. Myogenic differentiation of human MiPs was conducted seeding 5,000 cells/cm² on gelatin(Millipore)-coated plastic (NUNC) in DMEM-F12 supplemented with 20% FBS and 1%ITS (all reagents from Thermo Fisher Scientific). After 24 hours, medium was

changed to DMEM-F12 supplemented with 20% FBS, 2nM SB431542 hyclate and 2nM LDN193189 hydrochloride (Sigma-Aldrich). After 48 hours, medium was changed to DMEM-F12 supplemented with 2% horse serum, 2nM SB431542 hyclate and 2nM LDN193189 hydrochloride for additional 48 hours, prior to immunostaining analysis.

Gene-targeting cocktails were composed as follows: AMC, esiRNAs anti-ANXA3/-ANXA7/-PAX7/-SMAD7 (Sigma-Aldrich); PMC, esiRNAs anti-OSTN/-MYB/-LHX2/-BMP6/-SMAD5/-LTBP4 (Sigma-Aldrich). Cells were transfected with a total of 1mg esiRNAs and 1ml lipofectamine 2000 (Thermo Fisher Scientific) per mw24 well. AMC-treated cells were then kept in medium supplemented with 100ng/ml BMP6 (Peprotech), whereas PMC-treated cells in medium supplemented with 100ng/ml Noggin (Thermo Fisher Scientific). Gene expression and differentiation assays were conducted 48 hours after transfection. miRNA-targeting cocktails were composed as follows: AMC, miR-mimics for miR-34c-5p/-34c-3p/-362/-210/-590, anti-miRs anti-miR-132/-146b/-424/-212/-181a; PMC, miR-mimics for miR-132/-146b/-424/-212/-181a, anti-miRs anti-miR-34c-5p/-34c-3p/-362/-210/-590 (all oligonucleotides from Sigma-Aldrich). Cells were transfected with 100nmol of each miR-mimic and 20nmol of each anti-miR per mw12 well, with 2 μ l lipofectamine 2000. Gene/miRNA expression and differentiation assays were conducted 48 hours after transfection.

Non-invasive imaging

Wild type and GIN⁺ MiPs were plated in quadruplet and incubated with pertechnetate (^{99m}TcO₄⁻) tracer solution (0.74 MBq/ml in DMEM) for 1 hr. afterwards, cells were rinsed with ice-cold PBS and supernatant was collected. The cells were lysed and collected. The radioactivity of the pellet and supernatant was measured by 2480 Wizard² Automatic Gamma Counter (PerkinElmer, Waltham, MA, USA). The results were adjusted for tracer decay. Uptake values were corrected for cell amounts in the according samples as measured via the NucleoCounter NC-100 system (ChemoMetec, Allerod, Denmark). The mice received an intravenous

injection of 3.7-5.55 MBq ^{124}I (PerkinElmer) on day 3 and an intramuscular injection of 100 μl LASIX (20 mg/ml, Sanofi, Paris, France) as diuretic. At 3 hrs later, a 20 min static scan was acquired with the Focus 220 small-animal PET system (Siemens Medical Solutions, Malvern, PA, USA). A transmission scan was acquired using a ^{57}Co source (185 MBq, Eckert and Ziegler, Berlin, Germany). PET images were reconstructed using a maximum a posteriori (MAP) image reconstruction algorithm and were then analysed with PMOD 3.0 (PMOD technologies, Zurich, Switzerland) Data were averaged on both legs per animal to keep the intra-injection variability in account. SUV was calculated according to the following formula: $\text{SUV} = \text{activity concentration in volume of interest} / (\text{injected activity} / \text{weight of animal})$. Volumes of interest were manually positioned around the graft regions.

Molecular and immunostaining assays

Validation of RNA-seq and miRNA-seq data was carried out by means of qPCR, using SybrGreen for gene levels and Taqman for miRNA levels. Gene qPCR was performed on 1:5 diluted cDNA obtained from 1 μg total RNA (SybrGreen mix, SSIII cDNA production kit and RNA extraction kit from Thermo Fisher Scientific), using Vii7 384-plate reader (Thermo Fisher Scientific; final primer concentration, 100nM; final volume, 10 μl ; *PGK*, internal reference; thermal profile, 95°C 15sec, 60°C 60sec, 40x). miRNA qPCR was performed on 1:15 diluted cDNA obtained from 20ng total miRNA preparation (miRNA isolation kit, Thermo Fisher Scientific). Reagents and probes for reverse transcription and Taqman-based qPCR are from Thermo Fisher Scientific, and manufacturer's protocols were applied.

Methylation patterns were assayed by means of bisulphate sequencing of CpG islands in the promoter regions of target genes (as reported in UCSC genome browser (hg19); primers by MethPrimer). Genomic DNA was isolated through genomic DNA mini kit (Thermo Fisher Scientific), then 1 μg /20 μl was bisulphate-converted using EpiTect Bisulfate kit (Qiagen). Single CpG island amplicons were amplified by PCR (final primer concentration, 330nM; final volume, 20 μl ; thermal

profile: 95°C 30sec, 55°C 60sec, 72°C 60sec, 40x, primers are listed in Supplementary Table 2) at T3000 thermocycler (Biometra) using Taq polymerase (Thermo Fisher Scientific), then gel-extracted by means of Gel Extraction kit (Thermo Fisher Scientific) and ligated into pGEM plasmids via TA cloning (Promega). Single bacterial clones were bulk-sequenced (GATC Biotech) and analysed by means of QUMA online software. Statistical analysis was performed on average methylation values of 5 sequences per cell clone (3 clones per cell type, from independent donors).

Histone mark levels were assayed by means of chromatin immunoprecipitation (ChIP) on the same CpG islands assayed by bisulphate sequencing, adapting previously reported conditions¹⁴³ to 5×10^6 cell pellets. $1 \mu\text{g}/10 \mu\text{gDNA}$ polyclonal antibodies anti-K9me3 (repressive mark), anti-K4me2 (permissive mark) and anti-K27ac (active mark; all antibodies from Active Motif #39142/39133/39765) was used in the ChIP, and protein-A-coated sepharose beads (GE Healthcare) were used for the subsequent pull-down. IgG isotype (eBioscience) was used as negative ChIP control. 5% out of 100% initial sonicated genomic DNA fragment suspension was used as reference input. Purification of ChIP and input DNA was performed by means of MinElute kit (Qiagen) and quantification as % of input was performed through SybrGreen qPCR, following conditions reported above. Statistical analysis was performed using 3 qPCR replicates per cell clone (3 clones per cell type, from independent donors).

Western Blot (WB) analyses were performed on $50 \mu\text{g}$ cell/tissue lysate ($100 \mu\text{g}$ for DYS analysis) according to commonly used procedures in 10% acrylamide (6% for DYS analysis) hand-cast gels. Here follows the list of antibodies and relative dilutions: mouse anti-sarcomeric α actinin (Abcam #ab72592), 1:500; rabbit anti-GFP (Thermo Fisher Scientific, #A11122), 1:500; mouse anti-DYS3 (interacting with canine and human isoforms, Novocastra #DYS3-CE-S), 1:500. Bands were detected and pictured at Bio-Rad GelDoc by means of Pico substrate (Thermo Fisher Scientific; Dura substrate for DYS analysis). Densitometric analyses were carried on gels loaded, blotted and detected in parallel by means of QuantityOne software (Bio-Rad).

Whole fluorescence imaging of injected tissues was performed at Olympus SZX12 stereomicroscope by means of SISgetIT software (2" exposition for GFP, 0.2" for brightfield, semirefringent bottom) murine MiP *in vivo* experiments, and with Zeiss SteREO Discovery V12 microscope by means of AxioImaging software (2" exposition for GFP, 0.2" for brightfield, semirefringent bottom). For NMJ imaging and quantitation, mouse soleus and extensor digitorum longus muscles were dissected and fixed in 4% PFA. Muscle fibres were prepared and stained with rhodamine-coupled bungarotoxin using 1:2.500 dilution (rhodamine-BTX, Invitrogen) for 1 h at room temperature. Stained bundles were washed three times and embedded in Mowiol. Z-stacks of individual NMJs were taken with 40x oil objective (Zeiss Examiner Z1). Images were deconvoluted and analysed using 3D deconvolution and 3D measurement modules in AxioVision Software. Data are presented as the mean values, and the error bars indicate \pm s.e.m. The number of biological replicates per experimental variable (n) is usually n>5 or as indicated in the figure legends. The significance is calculated by unpaired two-tailed t test and provided as real p-values that are believed to be categorized for different significance levels, like, *** p <0.001, ** p <0.01, or * p <0.05. Immunofluorescence staining was performed following the commonly used steps of Triton-based (Sigma-Aldrich) permeabilization, donkey serum-(Sigma-Aldrich) background blocking, overnight incubation with primary antibody at 4°C, 1hour incubation with 1:500 AlexaFluor-conjugated donkey secondary antibodies (Thermo Fisher Scientific), and final counterstain with Hoechst. Here follows the list of primary antibodies and relative dilutions: rabbit anti-laminin (Sigma #L9393), 1:300; goat anti-GFP (Abcam #ab5450), 1:500; mouse anti-MyHC (DSHB #MF20), 1:3; mouse anti-sarcomeric α actinin (Abcam #ab72592), 1:300; rabbit anti-Myocd (SantaCruz #sc-33766), 1:100; mouse anti-DYS3 (canine- and human-specific, Novocastra #DYS3-CE-S), 1:100; mouse anti-Pax3 (R&D #MAB2457), 1:300; rabbit anti-lamin A/C (#Epitomics 2966-1), 1:600. Imaging was performed at Eclipse Ti microscope (Nikon) by means of Image-Pro Plus 6.0 software (Nikon). Quantitation of engraftment, satellite cell and fibre counts were performed by means of ImageJ software (NIH, USA) on at least 10 fields across heart and muscle

samples. SCs and MABs were sorted as CD56⁺ and AP⁺ populations at passage 0. Antibodies: mouse anti-CD56 (R&D, FAB7820A), 2 μ l/10⁵cells; mouse anti-AP (R&D, #FAB1448P), 2 μ l/10⁵cells.

RNA-seq and miRNA-seq

A 10x10⁶ cell pool per clone was divided in two 5x10⁶ pools for RNA (Total RNA isolation kit and post-isolation DNase, Thermo Fisher Scientific) and miRNA (miRNA isolation kit, Thermo Fisher Scientific) extraction, respectively. RNA (>10 μ g) and miRNA (approximately 1 μ g) samples were then verified and processed by the Genomics Core (KU Leuven – UZ Leuven, Belgium). RNA sequencing libraries were constructed with the TruSeq RNA Sample Prep Kits v2 (Illumina). RNA-sequencing after miRNA treatment was performed 48 hours after treatment (n=3 per conditions). Three RNA samples per group (one per clone) were indexed with unique adapters and pooled for single read (50bp) sequencing in Illumina HiSeq2000. RNA-seq reads were aligned with TopHat v2.0.2 to the human genome version hg9¹⁴⁴. Transcripts were assessed and quantities were determined by Cufflinks¹⁴⁴. Differential expression levels were assessed using DESeq¹⁴⁵. GO analysis was performed by means of BinGO (biological process; within Cytoscape 3.2.1) on DE genes in fibroblast- vs MAB-iPSCs, and in fibroblast- vs MAB-MiPs comparisons. GO terms with P<0.05 were subsequently compared between iPSC and MiP stages. Variance, count and fold change analyses, as well as charts and z.test matrices were conducted by means of Excel software (Microsoft). Heat maps were obtained analyzing the z.test value matrices with GITools 2.2.2¹⁴⁶ (hierarchical clustering, Manhattan distance, average linkage). Data about 3'UTR binding prediction and related mirsvr scores were obtained from microRNA.org^{147, 148} (Aug 2010 release; conserved, good-score matrix).

Statistical analyses

Sample size for *in vitro/in vivo* experiments was calculated by means of Sample Size Calculator (<http://www.stat.ubc.ca/~rollin/stats/ssize/index.html>; parameters: power, .80; alpha, .05). When applicable, sample size analysis was based on average values obtained from preliminary optimization/validation trials. When comparing multiple data pools, Kruskal-Wallis test followed by Mann-Whitney U test between two target populations were applied and significance was scored when $P < 0.05$ for both tests. When comparing two data pools, Mann-Whitney U test was applied and significance scored when $P < 0.05$. All statistical analyses were conducted using Prism v5.0 (GraphPad).

Study approval

All protocols and experiments on mice and murine samples were performed in compliance with the Belgian law and the Ethical Approval of KU Leuven.

3.4 Results

***In vivo* relevance of human MiPs**

To gain further translational evidence of MiP application, we investigated the regenerative potential of human MiPs *in vivo*. Importantly, we asked whether the myogenic propensity of human MAB-MiPs, previously shown *in vitro*¹³⁹, was durable *in vivo*. In addition, we sought to determine whether the human MiPs are necessary for the putative regenerative effect. To address these questions, we equipped previously characterized human, isogenic fibroblast-derived MiPs and MAB-MiPs with GFP, a sodium-iodide symporter (NIS) tracer for non-invasive PET imaging¹⁴², as well as an inducible suicidal gene, iCasp9. This iCasp9 gene triggers apoptosis of cells when exposed to the synthetic inducer AP20187¹⁴⁹. We first validated the engineered GFP⁺/iCasp9⁺/NIS⁺ (GIN⁺) MiPs *in vitro*. Suitability for PET imaging was determined by ^{99m}TcO₄ uptake assay (Figure. 3.1 A). Also, cell death was specifically activated within 48 hours in GIN⁺ cells only after exposure to the inducer, whereas

the inducer alone had negligible effect on control cells lacking iCasp9 (Figure 3.1 B). We then injected GIN⁺ MiPs in *Rag2*^{-/-};*γC*^{-/-};*Sgcb*^{-/-} mice, which bear skeletal and cardiac muscle degeneration on a xenograft-permissive genetic background¹³⁹. The *Sgcb* model of limb girdle muscular dystrophy was used because it displays a more severe phenotype than the *mdx* mouse. Each animal received 5x10⁵ cells as an intramyocardial injection in the left ventricle and during the same procedure 5x10⁵ cells in each femoral artery (bilateral). One-week post-injection, GIN⁺ cells were traceable in the heart and in the hindlimb muscles of cell-treated animals, but not of sham-treated, by PET imaging, although we observed some variability in the detection method. (H and HL fields, Figure 3.1C). Semi-quantitative analysis of the standardized uptake value (SUV) showed no engraftment difference between fibroblast-derived MiPs and MAB-MiPs in the heart, whereas hindlimb muscle engraftment was higher (+38.32%) in MAB-MiP-treated animals (Figure 3.1 D). Four weeks post-injection, half of each cohort received intraperitoneal injection of AP20187, while the other half received a vehicle control. The effect of AP20187 was then investigated 8 weeks after the cell injections. Stereo- and immunofluorescence analyses showed that MAB-MiPs engrafted the heart similarly to fibroblast-derived MiPs. Conversely, MAB-MiPs engrafted the hindlimb muscles more efficiently than fibroblast-derived MiPs. Moreover, detection of engrafted fibres was dramatically reduced after AP20187 administration (Figure 3.2 B). We quantitated MiP-specific contribution to hindlimb stem cells by cytometry-based sorting of the GFP⁺ subfraction of resident CD56⁺ satellite cells and AP⁺ MABs. In both pools, MAB-MiP-treated animals displayed larger GFP⁺ subfractions than fibroblast-MiP-treated ones and GFP⁺ cells were undetectable after AP20187 administration (Figure 3.1 F).

Differentiation of engrafted MiPs was evaluated using antibodies that detect human but not mouse dystrophin protein (hDYS). hDYS was evident at the sarcolemma following engraftment, and this same pattern was ablated after AP20187 administration (Figure 3.2 A, B). Four weeks post-injection, GFP⁺/hDYS⁺ areas accounted for 34.23±5.96% and 32.68±6.83% of the left ventricular wall in fibroblast-

derived-MiP and MAB-MiP-injected mice, respectively ($P=0.62$, $n=5$, Mann-Whitney U-test). In the *gastrocnemius* muscles of the same mice, GFP⁺/hDYS⁺ myofibres accounted for $7.25\pm 0.95\%$ and $22.201\pm 5.99\%$ respectively ($P<0.05$). Myofibre measurement at 8 weeks showed that GFP⁺/hDYS⁺ myofibres accounted for $4,23\pm 1.95\%$ and $14,89\pm 3.73\%$ in fibroblast-MiP- and MAB-MiP-injected mice respectively ($P<0.05$).

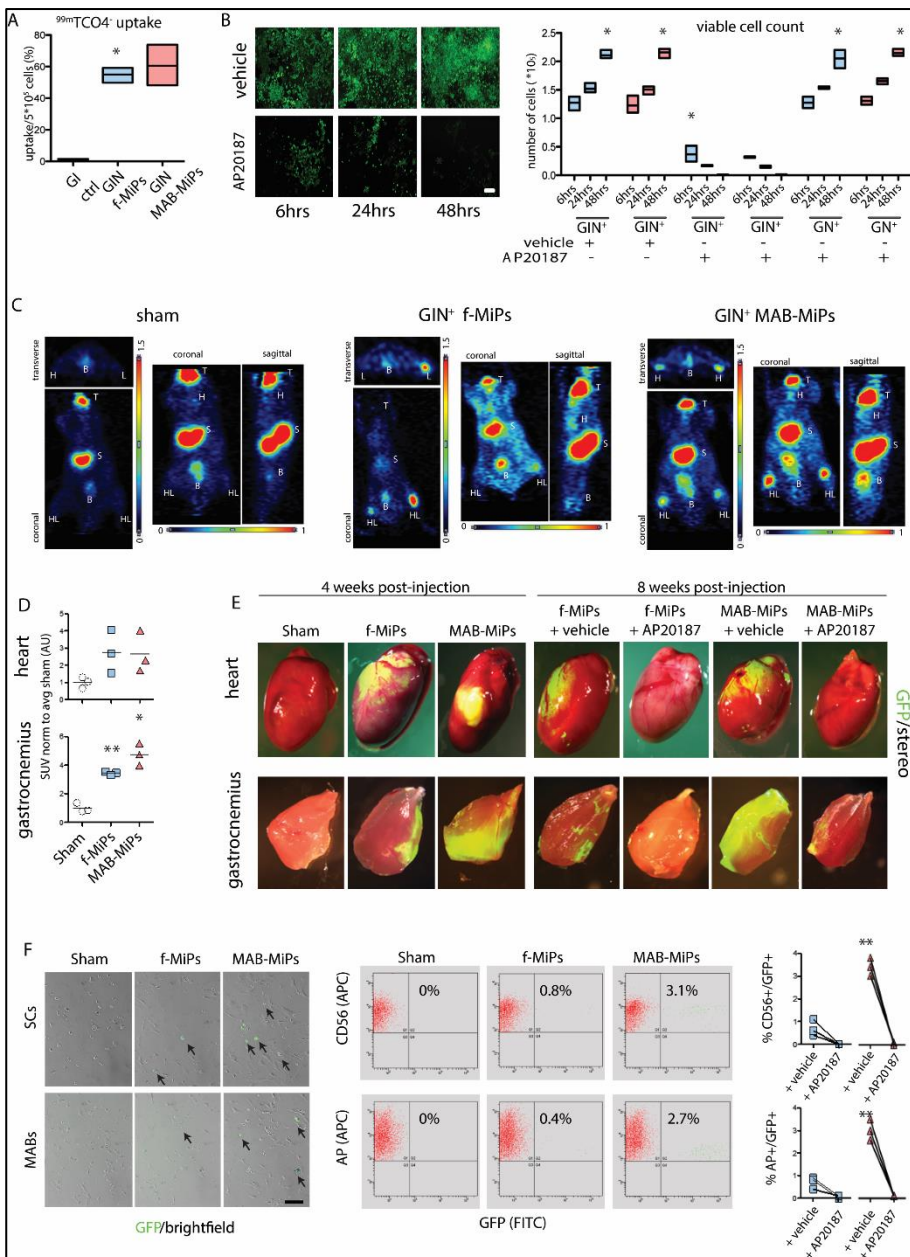


Figure 3.1 Human MiPs display differential myogenic propensity *in vivo*. (A) Validation of NIS transgene functionality for PET imaging by quantitation of $^{99m}\text{TcO}_4^-$ uptake *in vitro*. *, Kruskal-Wallis test and Mann-Whitney U-test vs ctrl, $P < 0.05$, $n = 3/\text{cohort}$. Scale bar approximately $100\ \mu\text{m}$ (B) Validation of iCasp9 transgene by viable cell count after AP20187 administration *in vitro*. Only iCasp9+ MiPs did significantly

undergo progressive cell death, which appeared virtually complete after 48h. *, 2-way ANOVA with Bonferroni correction, $P < 0.05$ (interaction), $n = 3$ /cohort. Data points depict average and min-to-max span for each sample. (C) One week after injection, PET scan of live animals shows engraftment of GIN+ MiPs in heart (H) and hindlimbs (HL) muscles of only MiP-treated mice. T, thymus; S, stomach; B, bladder; endogenous positive PET signals. (D) SUV levels in heart and hindlimb regions of PET-scanned mice. *, $P < 0.05$ vs sham; **, $P < 0.05$ vs sham and fibroblast-MiPs; Kruskal Wallis and Mann-Whitney U test; $n = 3$ /cohort. (E) Stereofluorescence analysis of heart and hindlimb (*gastrocnemius*) muscles of recipient mice before (4 weeks p.i.) and after (8 weeks p.i.) AP20187 administration. (F) Live fluorescence and cytometry analyses of CD56-isolated SCs and AP-isolated MABs from recipient mice at end-point. both SCs and Mabs MAB-MiP-treated animals displayed larger GFP⁺ subfractions than fibroblast-MiP-treated ones and GFP⁺ cells were undetectable after AP20187 administration **, $P < 0.05$ vs fibroblast-MiP-treated mice; Kruskal Wallis and Mann-Whitney U test; $n = 3$ /cohort at end-point, scale bar approximately 100 μm .

Regeneration of engrafted striated muscles was quantitated by means of tetanic force measurement, treadmill assay, echocardiography and serum creatine kinase (CK) level monitoring. Four and eight weeks post-injection, *extensor digitorum longus* (EDL) tetanic force and run time values on the treadmill showed that MAB-MiP-treated animals performed better than fibroblast-derived-MiP-treated animals (Figure 3.2 C). Left ventricle fractional shortening was similarly improved by fibroblast-derived-MiPs as well as MAB-derived-MiPs (Figure 3.2 D). Serum CK levels were decreased in MiP-treated animals, with lower levels in MAB-MiPs animals (9.7 ± 0.32 U/l; mean \pm s.e.m.-) than in fibroblast-derived-MiP-treated ($10, 8 \pm 0.21$ U/l) (Figure 2d). Notably, all functional parameters were reverted to baseline-like levels after AP20187 administration (Figure 3.2 C). In addition, we evaluated the morphology of neuromuscular junctions (NMJs) in the skeletal muscles of injected animals. When stained with fluorescent bungarotoxin, NMJs in sham animals appeared fragmented, unlike the normal, contiguous structures found in WT muscles. Fibroblast-MiP- or MAB-MiP-engrafted fibres (discriminated from the non-engrafted according to GFP expression) displayed NMJs with similar morphology to WT and strongly reduced fragmentation (Figure 3.2 E). Finally, we evaluated the extent of fibrotic scarring in the skeletal muscle of injected animals.

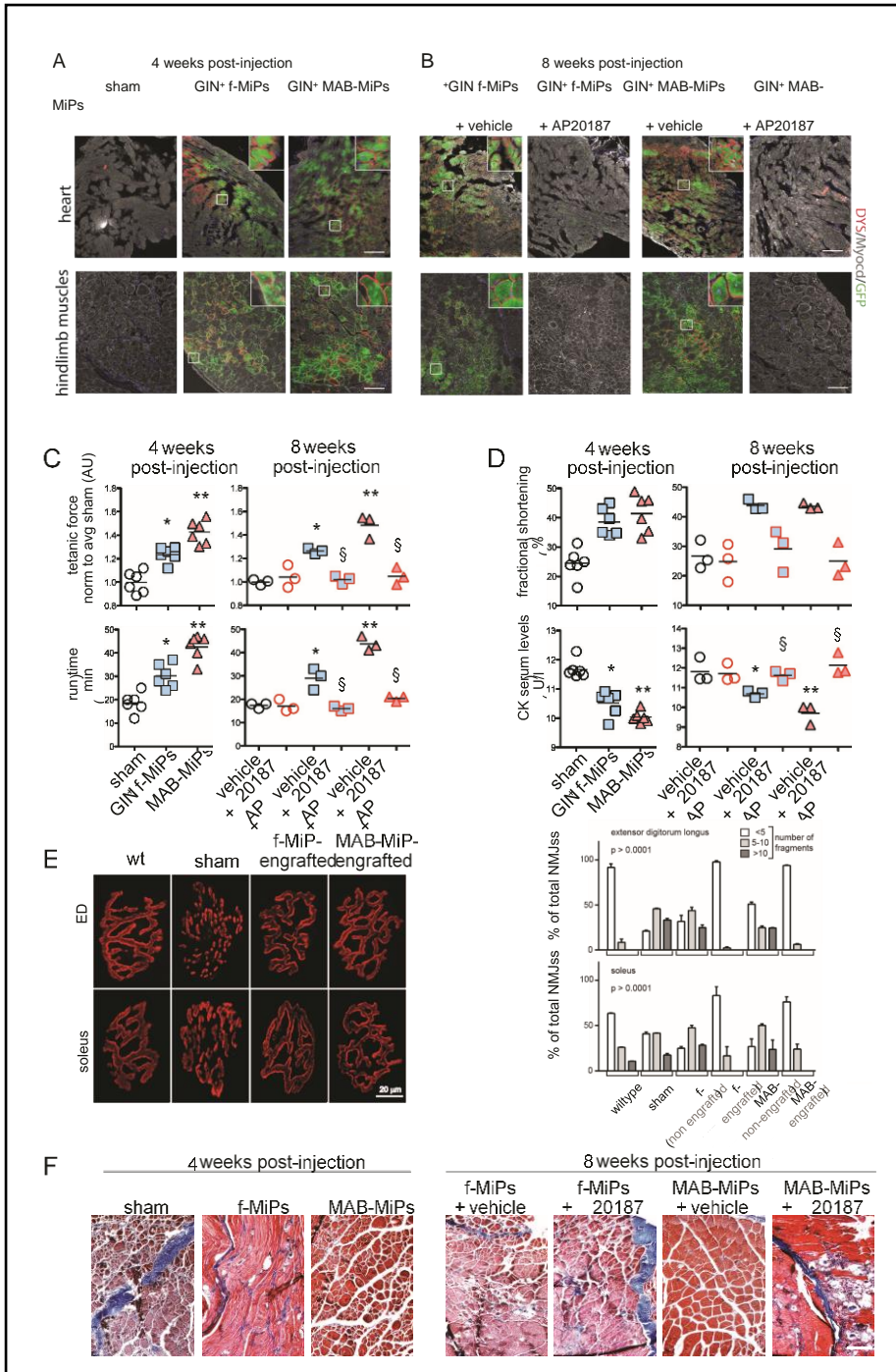


Figure 3. 2. Human MiPs engraft and are able to functionally regenerate dystrophic muscles. A-B) Four weeks after delivery, immunostaining shows that fibroblast- and MAB-MiPs engraft and express hDYS to a similar extent in the heart, but differently in the hindlimb muscles (*gastrocnemius*). After AP20187 administration and at the end of treatment (eight weeks post-delivery), the trend remains in vehicle-treated mice, whereas GFP and hDYS signals are ablated from AP20187-treated mice. Scale bars, approximately 100µm; insets, 20X magnification of indicated field. **(C)** Tetanic force of EDL muscles and treadmill assay showed that skeletal muscle performance was increased in fibroblast-MiP-treated vs mice, and increased in MAB-MiP- vs fibroblast-MiP-treated mice. Also, the functional gain was lost after AP20187 injection. **(D)** Functional assessment of the heart, by means of fractional shortening quantitation, shows comparable amelioration in both MiP-treated cohorts, but not after induced MiP death. Furthermore, CK serum levels followed a trend similar to functional assessment of the skeletal muscles. Data points depict the average value of each animal. In E-F: *, P<0.05 vs sham; **, P<0.05 vs sham and fibroblast-MiPs; §, P<0.05 vs own vehicle-control; Kruskal Wallis and Mann-Whitney U test; n=6/cohort before AP20187, n=3/cohort at end-point. **(E)** Bungarotoxin-based staining of NMJs throughout whole EDL and *soleus* muscles (n=3/cohort) reveals that dystrophic mice (sham) present highly fragmented NMJs, while MiP-engrafted fibres present NMJs with a morphology similar to WT fibres. Quantitation of non-, mildly and highly fragmented NMJs displays that only MiP-engrafted, but not non-engrafted, fibres in treated animals have a WT-like quantitative pattern (n=3/cohort). Depicted are average±st.dev bars. f-, fibroblast-derived. **(F)** Masson's trichromic staining of hindlimb (*quadriceps*) muscles of recipient mice. Scale bar approximately 50 µm. Blue scars denote fibrosis, while myocytes are stained in red. Fibrosis is significantly reduced in MAB-MiPs recipient muscles at 4 weeks p.i, while the difference is ablated after AP20187 administration at 8 weeks p.i.

Masson's trichromic staining revealed that fibrosis was reduced to a higher extent in MAB-MiP- than in fibroblast-MiP-treated animals, while it appeared partially reconstituted after AP20187 administration (Figure 3.2 F). Together, these data suggest that human MiPs have regenerative potential for dystrophic skeletal muscles *in vivo*. Importantly, the reversal of the beneficial effects after AP20187-induced cell death indicates that MiPs are necessary for exerting the observed regenerative effects. Furthermore, the intrinsic *in vivo* propensity towards the skeletal muscle lineage was more evident and durable from MAB-MiPs than those derived from fibroblasts.

Genetic determinants control myogenic potential of MAB-MiPs

To gain insight in the myogenic difference between MAB- and fibroblast-MiPs, we proceeded to investigate which genes were differentially expressed between fibroblast- and MAB-MiPs, and whether differentially expressed genes were conserved from the parental cells. To this goal, we used RNA-seq to analyse the transcriptional profiles of fibroblast- and MAB-MiPs and the iPSC lines from which the MiPs were derived. For this analysis we used iPSC at the first stage of our differentiation, namely already primed to mesodermal lineages in order to increase the chance of identifying changes in lineage determination genes. The transcriptional profile of both fibroblast-derived- and MAB-derived MiPs was enriched (count >100 FPKM) in genes associated with myogenic mesoderm formation, including the epigenetic regulators *TET1/2/3*, *DNMT1/3a*, *HDAC4*, *SMARCE1/2/3*, the mesodermal markers *MEF2C*, *GATA4*, *TBX3*, *PAX3*, *SIX1*, *ISL1* and the markers of striated muscle *MYOM2/3*, *DMD*, *SGCB*. Conversely, pluripotency-related genes such as *POU5F1*, *NANOG*, *ZFP42*, *DPPA4*, *LIN28a*, *GDF3* were poorly detectable or absent (count <10 CPM; $P < 0.05$ vs all three categories of enriched genes) (Figure 3.3 A). Moreover, mRNAs of *AGRIN* and *UTROPHIN* were highly enriched in MiPs (FPKM (avg \pm s.d.), 1257.15 \pm 191.58 and 1560.39 \pm 329.15 in fibroblast- and MAB-MiPs respectively). Unbiased sample clustering and principal component analysis showed that samples clustered primarily according to stage (iPSCs vs MiPs), and secondarily according to progeny (Figure 3.3 A, B). Intriguingly, gene ontology (GO) comparison of differentially expressed genes at iPSC stage (fibroblast- vs MAB-iPSCs) and MiP stage (fibroblast- vs MAB-MiPs) showed high overlap (79.53%) of Biological Process terms. Overlapping GO terms mainly pertained to developmental program, signalling and cellular metabolism (Figure 3.3 D). When clustered on a heat map, patterns of gene expression emerged reflecting stage-specific (differing iPSCs from MiPs, regardless of progeny) or progeny-specific (differing fibroblast- vs MAB-derived cells, regardless of stage) (Supplementary Figure 3.1 A).

We found 905 genes differentially expressed between fibroblast-derived-MiPs and MAB-MiPs (Figure 3.3 E). Among the significantly differentially expressed genes (P_{adj}

<0.05), several myogenic inhibitors were upregulated in fibroblast-derived-MiPs, whereas several muscle proteins and myogenesis-associated genes were upregulated in MAB-MiPs. Agonists of BMP signalling such as *BMP6*, *SMAD5* and *LTBP4* were upregulated in fibroblast-MiPs, whereas the BMP signalling inhibitor *SMAD7* was upregulated in MAB-MiPs (Figure 3f). Plotting the fold change of significantly differentially expressed genes in MiPs compared to iPSCs, we found that 56.17% of differentially expressed genes conserved the progeny-specific trend across stages, including many identified with the previous analysis (Figure 3.3 G). We validated a subset of genes important for myogenesis using qPCR. We first compared the expression levels by qPCR between fibroblast- and MAB-progenies at somatic, iPSC and MiP stages. *OSTN*, *MYB*, *LHX2*, *BMP6* and *SMAD5* were consistently upregulated in fibroblasts, fibroblast-iPSCs and fibroblast-MiPs, while *ANXA3*, *SMAD7* and *PAX7* were upregulated in MABs, MAB-iPSCs and MAB-MiPs. *LTBP4* was upregulated in fibroblasts and fibroblast-MiPs, but not in fibroblast-iPSCs, and similarly *ANXA7* was upregulated in MABs and MAB-MiPs, but not in MAB-iPSCs (Supplementary Figure 3.1 B).

We then examined CpG methylation and histone mark enrichment in the promoters of these same genes. Bisulphite sequencing analyses revealed that CpG methylation for *OSTN*, *MYB*, *LHX2*, *BMP6* and *SMAD5* was increased in the MAB progeny, while CpG methylation for *ANXA3*, *SMAD7* and *PAX7* was increased in the fibroblast progeny (Figure 3.3 H). The CpG methylation patterns appeared less discriminative for *LTBP4* and *ANXA7* (Figure 3.3 H). Chromatin immunoprecipitation analyses revealed that the non-permissive marker H3K9me3 was correlated with the methylation patterns and, conversely, the permissive markers K4me2 and K27ac correlated with the transcriptional upregulation trends (Figure 3.3 I). Notably, *LTBP4* showed enrichment of K9me3 in the MAB progeny, of K4me2 in fibroblasts and fibroblast-MiPs, and of K27ac in fibroblast-iPSCs, MAB-iPSCs and MAB-MiPs. Conversely, *ANXA7* showed enrichment in K9me3 in the fibroblast progeny and in permissive marks in the MAB progeny, with a spike of K27ac in fibroblast-iPSCs

(Figure 3.3 I). In association with the myogenic propensity shown by MiPs *in vivo*, we defined *OSTN*, *MYB*, *LHX2*, *LTBP4*, *BMP6* and *SMAD5* as an anti-myogenic gene pool, and *ANXA3/7*, *SMAD7* and *PAX7* as a pro-myogenic gene pool.

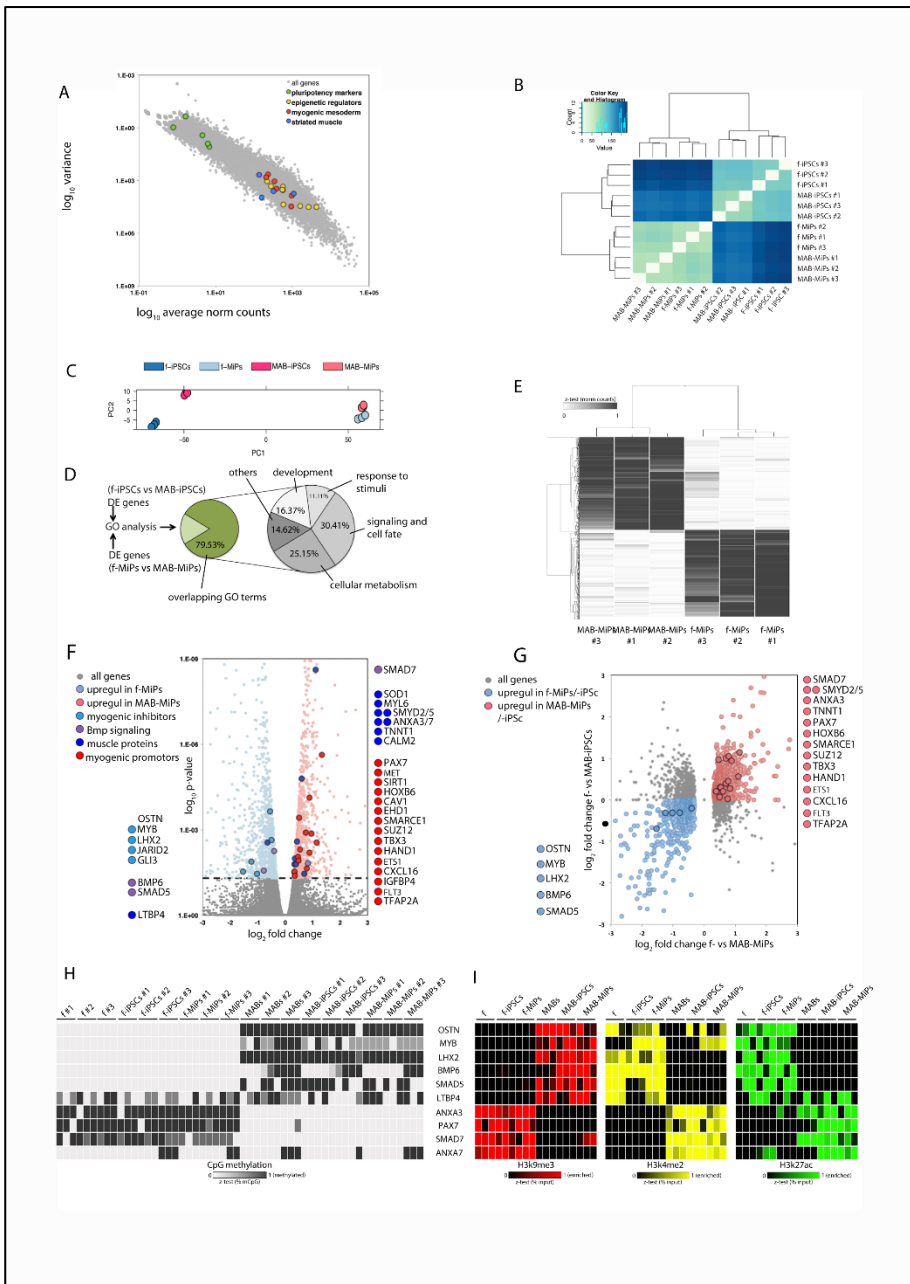


Figure 3.3 RNA-seq shows progeny-specific retention of part of transcriptional profile. (A) \log_{10} plot of variance vs normalized (norm) count for all genes detected in fibroblast- and MAB-MiPs. Data points depict average values of detected genes. Genes associated with pluripotency and with epigenetic/genetic

control on muscle mesoderm are highlighted. **(B)** Unbiased clustering of all MiP and parental iPSC samples analyzed by RNA-seq. **(C)** PC analysis of all samples reveals stage-specific, progeny-specific clustering. **(D)** GO analysis (Biological Process) of DE genes between fibroblast- and MAB-derived cells reveals that >79% GO terms are overlapping between MiP and iPSC stages. Sub-categorization of overlapping GO terms is charted at the right. **(E)** Heatmap (z-test) of DE genes (threshold, >10 norm counts) discriminating fibroblast- and MAB-MiPs. **(F)** Volcano plot of fold change vs p-value of all DE genes at MiP stage (threshold, $P=0.05$, dashed line). Left side of the chart, all genes and highlighted candidates enriched in fibroblast-MiPs; right side, genes and candidates enriched in MAB-MiPs. **(G)** Log₂ chart of fold change at MiP stage vs at iPSC stage of significantly DE genes (threshold, $P>0.05$ at MiP stage). Light blue dots depict genes upregulated in fibroblast-iPSCs and fibroblast-MiPs, while light red dots depict upregulated genes in MAB-iPSCs and MAB-MiPs. Circled dots represent the candidates, as identified in **(F)**, with conserved DE trend. **(H)** Quantitation of results obtained from bisulfate sequencing of upstream CpG islands of selected gene shortlists in fibroblast- and MAB-MiPs, and their parental iPSC and somatic cells. Data is depicted as heatmap (z-test) of average percentages of methylated CpGs ($n=3$ replicates/cell clone). **(I)** Quantitation of results obtained from CHIP-qPCR experiments analyzing fibroblast- and MAB-MiPs, and their parental iPSC and somatic cells. H3k9me3, repressive mark; H3k4me2, H3k27ac, permissive marks. Data is depicted as heatmap (z-test) of average percentages of IP-enriched vs total input DNA ($n=3$ replicates/cell clone). f, fibroblast-derived; DE, differentially expressed.

We then asked whether perturbation of these pools could shift the myogenic propensity of fibroblast- and MAB-MiPs. To this end, we combined the endoribonuclease-prepared small interfering RNAs (esiRNAs) targeting the anti-myogenic pool in a pro-myogenic cocktail. Conversely, the esiRNAs targeting the pro-myogenic pool were combined in the anti-myogenic cocktail. Scramble esiRNAs were used as control conditions. Since several key components of the BMP cascade were involved in both gene pools, we enhanced the anti-myogenic cocktail with soluble BMP6 and the pro-myogenic cocktail with soluble Noggin. We first validated the effects of anti-myogenic and pro-myogenic cocktails on target gene expression. Anti-myogenic pool genes, *LHX2*, *LTBP4*, *MYB*, *OSTN*, and *SMAD5*, were downregulated in the presence of pro-myogenic cocktail. Similarly, the pro-myogenic pool genes, including *ANXA3*, *ANXA7*, *PAX7*, and *SMAD7*, were downregulated in the presence of anti-myogenic cocktail (Supplementary Figure 3.1 C). We then tested the effect of these cocktails on *in vitro* myogenic propensity of MiPs in co-culture with C2C12 myoblasts and we proceeded to stain with lamin A/C human nuclei in chimeric

myotubes (Supplementary Figure 3.1 D and E). We observed a significant increase ($P < 0.05$ vs own ctrl (scramble), 2-way ANOVA) in the number of myofibres with 3 human nuclei after PMC treatment compared to cells that received the AMC treatment or to controls. We additionally performed the co-cultures also in presence of the suicidal gene in the MiPs, GIN⁺ MiPs (Supplementary Figure 3.4 A). A higher myogenic propensity would result in higher contribution to chimeric myotubes and hence a higher loss of myotubes after exposure to AP20187. Myogenic propensity was significantly reduced ($P < 0.05$ vs own ctrl (scramble), 2-way ANOVA) in fibroblast-derived MiPs and MAB-MiPs after treatment with anti-myogenic cocktail, whereas it was increased in pro-myogenic cocktail treated cells (Supplementary Figure 3.4 A). Importantly, pro-myogenic cocktail-treated fibroblast derived-MiPs showed comparable myogenic differentiation to control MAB-MiPs. Thus, perturbation of gene subsets by means of defined factor cocktails enabled perturbation of MiP myogenic propensity. Particularly, reduction of anti-myogenic genes in fibroblast-derived- MiPs resulted in a myogenic potential that is comparable to MAB-MiPs.

Cell type specific miRNAs regulate myogenic potency of MiPs

In light of retained miRNA signatures after reprogramming¹³⁸, we asked whether miRNAs also influenced the myogenic potential of MiPs. We analyzed the miRNA component of the same samples that we previously analyzed by RNA-seq. The miRNA profile of both fibroblast derived and MAB MiPs was enriched (count >30 FPKM) in miRNAs associated with mesodermal progression and myogenesis including *let-7a*, *miR-1/-590/-497/-34a/-27b/-101/-133a/-138/-15a/-15b/-16/-199a/-21/-22/-221/-23a/-24*. In contrast, miRNAs associated with pluripotency including *miR-372/-302a/-302b/-302c/-302d/-367/106a/-363* were barely detectable or absent in these cells (count <2 FPKM; Figure 3.4 A). Similar to the observations in the RNA-seq dataset, unbiased sample clustering and principal component analysis showed stage-specific clustering (iPSCs vs MiPs), with cell type-specific segregation (fibroblast-derived vs- MAB-derived) among each stage (Figure 3.4 B and C). At the MiP stage, we found 611 differentially expressed miRNAs

discriminating fibroblast derived-MiPs versus MAB-MiPs (Figure 3.4 D). Among the significantly upregulated miRNAs in fibroblast-MiPs, we selected those with predicted targets among the upregulated genes previously identified by RNA-seq. However, we did not experimentally confirm that selected miRNAs are directly targeting the selected differentially expressed genes. Data on the 3'UTR binding prediction and related mirsvr scores were obtained from microRNA.org (Supplementary Figure 3.2). Following this RNA-seq-based filter, we identified *miR-34c-5p/34c-3p/-362/-210/-590* for fibroblast derived-MiPs, and *miR-212/-132/-424/-146b/-181a* for MAB-MiPs (Figure 4e and Supplementary Figure 3.2). Among those, *miR-34c-5p/-34c-3p/-362* and *miR-132/-424/-146b* followed the same differential expression trend seen at the iPSC stage, together with 44.84% of total differentially expressed miRNAs (Figure 3.4 F). We validated the expression profile of all these miRNAs across somatic, iPSC and MiP stages using qPCR (Supplementary Figure 3.3 A). As in the previous experiments, we sought to define oligonucleotide cocktails to simultaneously perturb these miRNAs. We combined synthetic inhibitors of fibroblast-MiP-associated miRNAs and synthetic mimics of MAB-MiP-associated miRNAs and tested whether this had pro-myogenic potential. Conversely, inhibitors of MAB-MiP-associated miRNAs and mimics of fibroblast-MiP-associated miRNAs were tested for anti-myogenic potential. These inhibitor and mimics were tested for their effect on target miRNA level expression (Supplementary Figure 3.3 B). Notably, MiPs treated with this miRNA-based anti-myogenic cocktail showed downregulation of pro-myogenic genes. Those MiPs treated with a miRNA-based pro-myogenic cocktail had decreased levels of anti-myogenic genes (Supplementary Figure 3.3 C). Consequently, we asked whether the miRNA-targeting cocktails could shift the myogenic propensity of MiPs when co-cultured with C2C12. We found that miRNA based anti-myogenic cocktail decreased myotube formation while the miRNA-based pro-myogenic cocktail increased the myogenic differentiation.

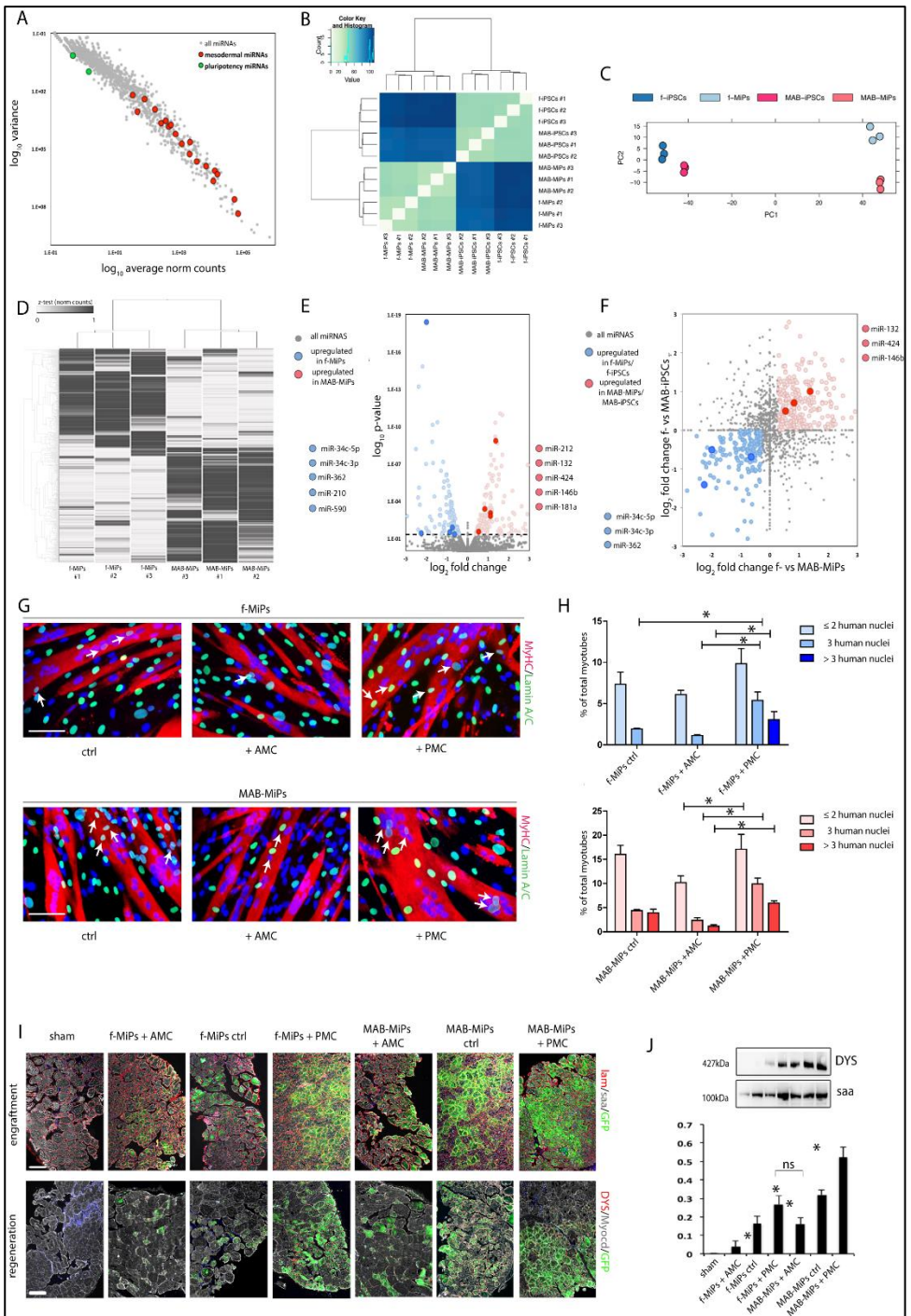


Figure 3. 4 miRNA-seq analysis allows identification of progeny-specific miRNA cocktails for propensity perturbation. (A) Variance vs norm count plot of all detected miRNAs in fibroblast- and MAB-MiPs. Data points depict average values of detected miRNAs. miRNAs associated with pluripotency and with muscle mesoderm are highlighted. **(B)** Unbiased clustering of all MiP and parental iPSC samples analyzed by RNA-seq. **(C)** PC analysis of all samples reveals stage-specific, progeny-specific clustering. **(D)** Heatmap (z-test) of DE miRNAs (threshold, >10 norm counts) discriminating fibroblast- and MAB-MiPs. **(E)** Volcano plot of fold change vs p-value of all DE miRNAs at MiP stage (threshold, $P=0.05$, dashed line). Left side of the chart, all genes and highlighted candidates (miRNAs predicted to bind 3'UTR of MAB-MiP-upregulated genes) enriched in fibroblast-MiPs; right side, genes and candidates (miRNAs predicted to bind 3'UTR of fibroblast-MiP-upregulated genes) enriched in MAB-MiPs. **(F)** Log_2 chart of fold change at MiP stage vs at iPSC stage of significantly DE miRNAs (threshold, $P>0.05$ at MiP stage). Light blue dots depict miRNAs upregulated in fibroblast-iPSCs and fibroblast-MiPs, while light red dots depict upregulated miRNAs in MAB-iPSCs and MAB-MiPs. Circled dots represent the candidates, as identified in **(E)**, with conserved DE trend. **(G-H)** Quantification of MiP myogenic propensity in co-culture with C2C12 myoblasts after seven days of differentiation. Myotubes with three or more nuclei were counted as well as human nuclei contributing to chimeric myotubes. Representative fields and quantitation of chimeric myotubes are presented. $P<0.05$ vs treated and non treated. Kruskal Wallis and Mann-Whitney U test; $n=3$ replicates per clone. f-, fibroblast-derived; AMC, anti-myogenic cocktail (gene-based), PMC, pro-myogenic cocktail (gene-based), scale bar approximately $100\mu\text{m}$ **(I)** Immunostaining analysis of hindlimb (gastrocnemius) muscles of dystrophic, immunodeficient mice injected with AMC- or PMC-treated MiPs. Upper panels show engraftment, lower panels show appearance of human-specific DYS subsarcolemmal pattern in engrafted fibres. Scale bars, approximately $100\mu\text{m}$. **(J)** DYS quantitation by protein analysis is reported on the right. In G-I: ns, non significant difference; *, $P<0.05$; Kruskal-Wallis test and Mann-Whitney U-test vs own ctrl (scramble oligos), $n=3$ /cohort. Depicted are average \pm st.dev bars. f-, fibroblast-derived; DE, differentially expressed; AMC, anti-myogenic cocktail (miRNA-based), PMC, pro-myogenic cocktail (miRNA-based).

We tested the cocktails in presence and in absence of the apoptotic drug (Figure 3.4 G and H and Supplementary Figure 3.4 B). Similarly to what we reported in Supplementary Figure 3.1 D and E we observed a significant ($P<0.05$ vs own ctrl (scramble), Kruskal Wallis) upregulation of chimeric fibres containing 3 or more human nuclei in co-cultures that received pro-myogenic treatment compared to cells that received the anti-myogenic treatment or to controls. Finally, we tested the translational relevance of such approach by injecting cocktail-pretreated cells in the femoral artery of *Rag2^{-/-};iC^{-/-};Sgcb^{-/-}* mice. Four weeks post-injection, MiP-specific

engraftment and hDYS expression appeared significantly decreased ($P < 0.05$ vs own ctrl (scramble), Kruskal Wallis) for anti-myogenic-treated cells and increased for pro-myogenic-treated cells, when compared to relative controls (Figure 3.4 I). Quantitating the regeneration levels by means of hDYS protein levels, we found that pro-myogenic-treated fibroblast-MiPs performed as control MAB-MiPs (Figure 3.4 J). Thus, we have shown that a defined combination of microRNAs and soluble ligands contributes to somatic lineage determination in MiPs. Furthermore, perturbation of defined subsets of miRNAs by means of oligonucleotide cocktails was able to rescue the myogenic potential gap observed in fibroblast-MiPs compared to MAB-MiPs.

Next, in order to unravel additional potential targets of the microRNAs we performed RNA-seq analysis after the treatment with the selective miRNA cocktails. As shown in Figure 3.5 A cells clustered according to the treatment that was conducted. We found over 6000 genes differentially regulated between MAB-MiPs treated with pro-myogenic cocktails and untreated, and 3736 genes differentially expressed between MAB-MiPs treated with anti-myogenic vs untreated. For the fibroblast-MiPs we detected 1194 differentially expressed genes between pro-myogenic treated cells and untreated, and 829 between anti-myogenic treated cells and untreated ($P_{\text{adj}} < 0.05$, Figure 3.5). Consistent with previous analysis *ANXA3* was upregulated in MAB-MiPs upon pro-myogenic treatment, while component of the BMP cascade, such as *SMAD9* and *BMP6* were downregulated in MAB-MiPs treated with pro-myogenic and upregulated in MiPs treated with anti-myogenic cocktails (Figure 3.5 C and E). *LTBP4* was also upregulated in cells treated with anti-myogenic cocktail, whereas *MYB* was downregulated upon pro-myogenic treatment (Figure 3.5 D and E). In addition, genes encoding for muscle proteins, including *MYL6*, *ACTA2*, *TNNT1*, were upregulated in pro-myogenic-cocktail treated MiPs, and conversely downregulated in anti-myogenic treated. In these cells myogenic promoters and gene critical for muscle regeneration such as *HAND1*, *CXCL16*, *MET* and *DLL* were found downregulated (Figure 3.5 D). Interestingly, we observed genes involved in smooth muscle differentiation, including *CNN2* and *CNN3* and other genes relevant for

skeletal muscle functionality like *MAST1* significantly downregulated in cells that received an anti-myogenic treatment (Figure 3.5 D and F). Epigenetic regulators, including *TET1*, *CBX6* and *HDAC6* were found differentially regulated following the miRNA treatment. Furthermore in cells treated with anti-myogenic cocktails we detected upregulation of several genes that could be involved in muscle homeostasis, TGF β ligand *GDF15* and autophagy related genes *ATG10* and *ATG14*. (Figure 3.5 E and F).

Finally, we investigated the CpG methylation and the histone markers enrichment in the promoters of the putative pro-myogenic gene pools and anti-myogenic gene pools (Figure 3.5 G and H). In accordance to the RNA-seq data anti-myogenic genes *BMP6*, *SMAD5* and *MYB* showed a decrease in methylation in MAB-MiPs treated with anti-myogenic cocktail (Figure 3.5 G). Furthermore in these cells *MYB* displayed an increase in permissive histone markers H3k4me2, H3k27ac. When treated with pro-myogenic cocktails, MAB-MiPs showed a decrease of the non permissive marker H3k9me3 in *ANXA3* as well as an enrichment of permissive histone marker H3k4me2 in the promoters of pro-myogenic genes *PAX7*, *ANXA3* and *SMAD7* (Figure 3.5 H).

In fibroblast-MiPs methylation was increased in the promoters of *SMAD7* and *ANXA7* upon anti-myogenic treatment and this correlates with an increase in H3k9me3 in the promoters of these genes. Conversely anti-myogenic genes such as *MYB* and *BMP6* were found partially methylated and decreased in permissive markers H3k4me2 and H3k27ac after treatment with pro-myogenic cocktail in accordance to what we observed in the RNA-seq data. Taken together our results provide more insight in the anti-myogenic and pro-myogenic miRNA cocktails that we have previously defined, adding additional interesting targets that could be responsible for the differential *in vivo* performance of MiPs.

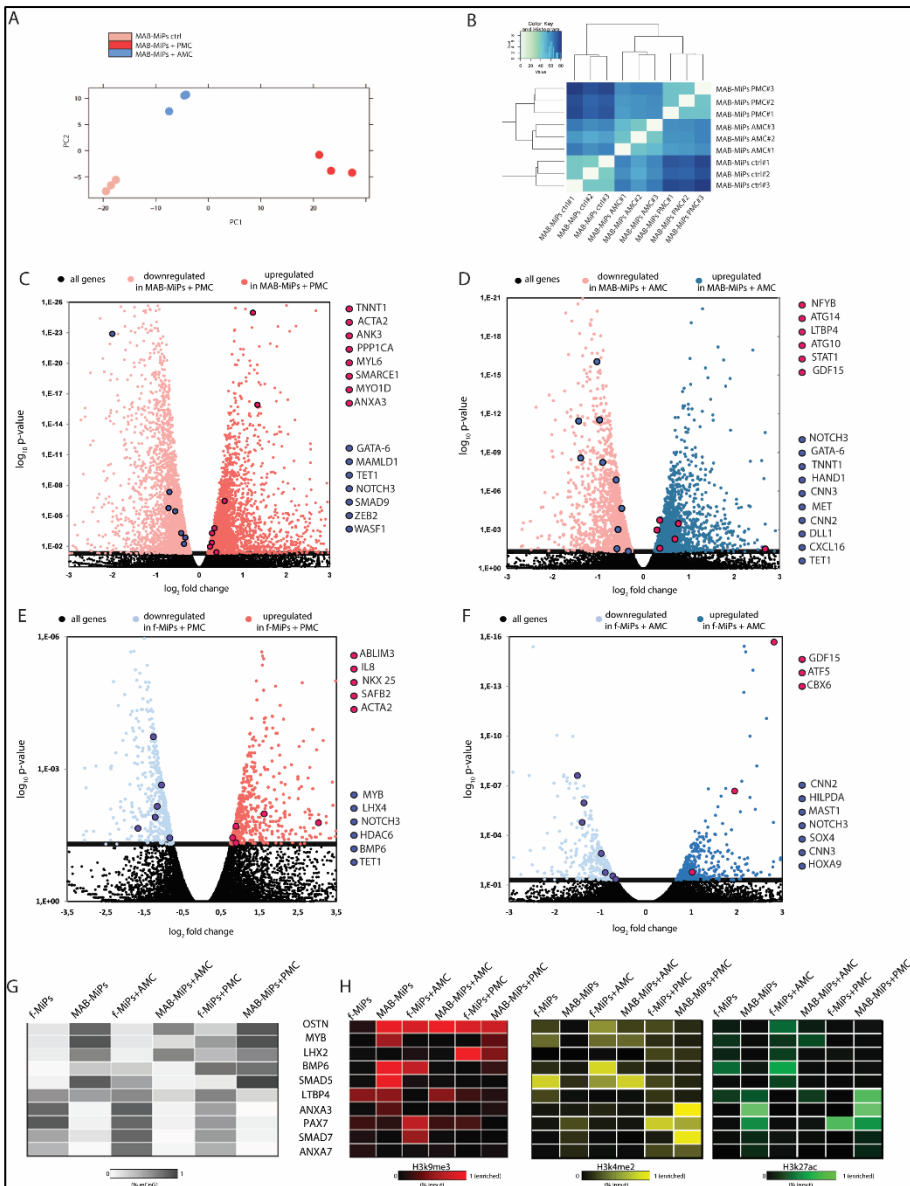


Figure 5. RNA-seq after miRNA cocktail exposures shows myogenic-specific commitment enhancement of transcriptional profile. (A) PC analysis of a MAB-MiPs samples reveals stage-specific, progeny-specific clustering **(B)** Unbiased clustering of MAB-MiPs analyzed by RNA-seq. **(C-F)** Volcano plots of fold change vs p-value of all DE genes in different conditions (threshold, $P=0.05$, dashed line). MAB-MiPs untreated vs MAB-MiPs+AMC **(C)**, MAB-MiPs untreated vs MAB-MiPs+PMC **(D)**, fibroblast-MiPs untreated vs fibroblasts-MiPs+AMC **(E)**, fibroblast-MiPs untreated vs fibroblasts-MiPs+PMC **(F)**. Left side of all charts,

all genes and highlighted candidates enriched in untreated-MiPs; right side, genes and candidates enriched in treated-MiPs. Blue dots depict genes that were found downregulated while red dots depict genes that were found upregulated upon treatments. **(G)** Quantitation of results obtained from bisulfate sequencing of upstream CpG islands of selected anti-myogenic and pro-myogenic gene pools in treated and untreated cells. Data is depicted as heatmap of average percentages of methylated CpGs. **(H)** Quantitation of results obtained from ChIP-qPCR experiments analyzing fibroblast- and MAB-MiPs treated and untreated. H3k9me3, repressive marker; H3k4me2, H3k27ac, permissive markers. Data is depicted as heatmap of average percentages of IP-enriched vs total input DNA (n=3). f-, fibroblast-derived. AMC, anti-myogenic cocktail (miRNA-based), PMC, pro-myogenic cocktail (miRNA-based).

3.5 Discussion

Simultaneous regeneration of skeletal and cardiac muscle in dystrophic subjects is compelling, considering that effective repair of skeletal muscle would likely worsen heart conditions¹⁵⁰. In this regard, MiPs may represent a valid cell tool, as they can be injected in the circulation and efficiently regenerate both striated muscle types¹³⁹. However, two main questions remained unaddressed with respect to the actual translational potential of this iPSC-based strategy: *in vivo* behaviour of human MiPs and whether the myogenic differentiation potential of human MiPs is influenced by reprogrammed cell types or origins, and if external modulators could improve the performance.

To this end we explored the *in vivo* potential of human MiPs in immunodeficient dystrophic mice in order to determine whether the source of MiPs alters the outcome after engraftment. Taking histological, molecular and functional data together, the capacity to regenerate skeletal muscle of MAB-MiPs appears greater than fibroblast-derived-MiPs. Interestingly, the cardiomyogenic potential seems comparable between the two MiP types. These features recapitulate the *in vitro* behaviour previously shown for those cells¹³⁹. In order to document that improvement after engraftment was due to cell intrinsic effects, we used induced apoptosis in engrafted MiPs and found that this associated with reversal of the beneficial effects at both molecular and functional levels. We cannot exclude the

detrimental effects were partially linked to the drug that induced apoptosis, AP20187. However, this seems unlikely considering that the compound has negligible toxic effects *in vivo* below 10mg/kg¹⁵¹. Intriguingly, MiP engrafted fibres showed improved NMJ morphology to levels comparable to WT fibres. The mRNAs for AGRIN and UTROPHIN, reported agonists of NMJ formation^{152, 153}, were highly enriched in MiPs. More refined studies are still needed to address the mechanism by which MiPs regenerate the fragmented NMJs in engrafted skeletal muscle fibres.

In this study, we used dual delivery by injecting into both the heart and femoral arteries to remain consistent with previously reported conditions in mice¹³⁹. However, we decided to further explore only the mechanisms to enhance the myogenic potential of MiPs, given the different performance *in vitro* and *in vivo* of MiPs towards skeletal muscle, dependent on their cell type or origin, while the cardiac commitment *in vivo* did not show differences between human f- and MAB-MiPs, consistently with murine and canine MiPs⁷⁰. Analysis of transcriptional profiles in MiPs confirms that MiPs retain much of the identity of their original cell source. We selected genes to be manipulated to enhance myogenic potential based on their known involvement in MD or in muscle biology. Both *LTBP4*, which was upregulated in fibroblast-MiPs, and *ANXA7* which was upregulated in MAB-MiPs, showed progeny-specific differential expression in somatic cells, but not in iPSCs. Considering the epigenetic data, it appears that both genes presented a rather permissive histone signature in our iPSCs. This probably contributed to restoring similar expression levels of *LTBP4* and *ANXA7* in fibroblast- and MAB-iPSCs. Therefore, it may be possible that the progeny-related trends of differential expression for these genes are linked to a non-pluripotent state. *LTBP4* is a TGF β regulator in the skeletal muscle, and can modify muscular dystrophy¹⁵⁴. Intriguingly, annexins are also being investigated as genetic modifiers of dystrophic progression¹⁵⁵. In our experiments, *LTBP4* appeared associated with decreased myogenic potential, while *ANXA7*, together with *ANXA3*, associated with increased propensity.

Thus, more focused efforts should be directed on how these factors possibly modify the lineage potential of human MiPs.

Use of miRNAs for enhancing myogenic fate *in vivo* is particularly compelling and may have high translational potential¹⁵⁶. To address whether we could identify miRNAs that could be used to promote myogenesis, we overlaid RNA-seq and miRNA-seq data with the aim of defining key components that could be used to enhance myogenic potential. In both RNA- and miRNA-seq, the samples cluster primarily according to cell type and this is reflected in the iPSCs and their resulting MiPs. However, MiPs, whether derived from fibroblast or MABs, share many differentially expressed genes but fewer miRNAs. This observation suggests that MiPs may require a more complex body of miRNAs to tightly control a smaller transcriptional divergence. Based on parental cell progeny, we defined combinations of miRNAs to modulate MiP myogenic propensity. Myogenic differentiation *in vitro* and *in vivo* was respectively decreased or increased using cocktails of miRs. Notably, a cocktail of pro-myogenic miRs was able to rescue fibroblast-derived MiPs to the degree that they performed similarly to MAB-MiPs. Intriguingly, among the miRNAs we filtered into the anti-myogenic pools, *miR-34c/-362/-210* have been previously associated with pathological state of muscles¹⁵⁷⁻¹⁵⁹ and *miR-590* has been recently associated with differentiation inhibition and the TGF β pathway¹⁶⁰. Conversely, within the pro-myogenic pool, *miR-424/-146b/-181a* are associated with myogenesis and muscle development¹⁶¹⁻¹⁶³. *miR-212/-132* have been shown to inhibit *MECP2*¹⁶⁴, which in turn regulates muscle maturation¹⁶⁵. The miRNAs tested in the cocktails were selected based on their known functions as well as their differential expression.

RNA-sequencing analysis after anti-myogenic and pro-myogenic miRNA treatment allowed identifying target genes involved in miRNA regulation of MiPs. We found a high number of genes differentially expressed upon miRNA cocktail exposures. Among those, *ANXA3*, *SMAD5*, *BMP6*, *MYB*, *LTBP4* were predicted targets of miRNAs included in the cocktails. In particular exposure to pro-myogenic cocktail determined a consistent downregulation of elements of the BMP/TGF β signalling pathway, and

conversely anti-myogenic exposure resulted in an increased of *GDF15*, that has been interestingly associated with muscle wasting *in vivo* and whose receptor *GFRAL* has been implicated in ERK signalling¹⁶⁶. Upon pro-myogenic treatment we detected upregulation of genes coding for proteins important for skeletal (*ACTA2*, *ABLIM3*) and smooth (*CNN2*, *CNN3*) muscle homeostasis. These findings suggest potential contributions of the pro-myogenic miRNAs we selected in enhancing smooth muscle differentiation as well thus opening the research of MiPs for appealing new strategies for muscle degenerating disease like MDs, where smooth muscles are highly affected. Consistent with the *modus operandi* of miRNAs many epigenetic modulators were found differentially regulated in treated cells. Interestingly we detected an upregulation of *SAFB2* in pro-myogenic treated cells. It has been shown that its paralog *SAFB1* facilitates the transition of myogenic gene chromatin from a repressed to an activated state¹⁶⁷; our results suggest that *SAFB2* could be involved in similar processes. Finally, we have detected upregulation of autophagic markers such as *ATG10* following anti-myogenic treatment, whose aberrant expression has previously been implicated in disease associated with atrophy of the skeletal muscle¹⁶⁸.

Moreover, CpG island methylation and histone markers enrichment analysis after miRNA treatment shed more light on the set of anti-myogenic and pro-myogenic genes that we have put forward. Although CpG island methylation analysis was conducted on the most proximal CpG islands to the transcription start site, this does not indicate that they are directly implicated in gene regulation, nor that they are the only CpG islands responsible for it. Nevertheless, our data suggests that these genes might be epigenetically regulated at the same time by miRNAs, DNA methylation and histone modifications.

In particular anti-myogenic *BMP6*, *SMAD5* and *MYB* displayed a consistent pattern of DNA methylation and histone markers enrichment, suggesting a simultaneous multifactorial regulation. Other genes, such as *ANXA3* and *LTBP4* did not show univocal signature at epigenetic level upon treatment. Finally, *ANXA7*, *PAX7* and

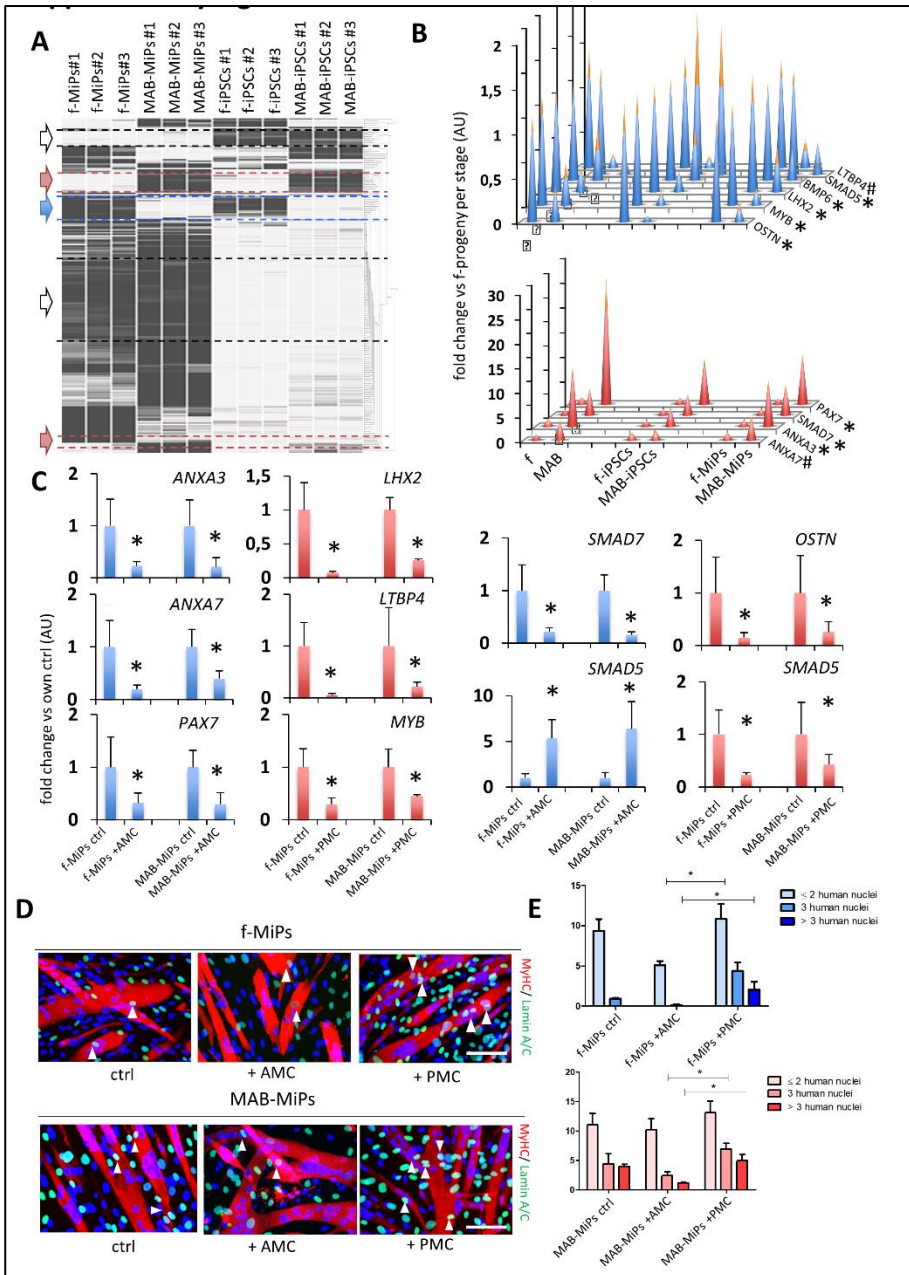
SMAD7 promoters' methylation and histone markers enrichment was modulated upon treatment, although we did not detect them among the differentially expressed genes, suggesting once again the multifactorial mechanisms of actions of epigenetic regulators.

We acknowledge that multiple strategies remain to refine and optimize miRNAs useful for promoting myogenesis. In the future, these miRNA-based strategies might benefit muscle regeneration not only based on cell delivery, but also mobilizing and modulating resident stem cells.

This growing knowledge will be fundamental to improve precision and efficiency of miRNA modulation and, ultimately, MiP fate. Moreover, it will be primarily important to test our approach in large animal models, as proof of principle of a potential scale up. To this end the Golden Retriever Muscular Dystrophy model (GRMD) would provide the ideal fit to investigate cell engraftment, dystrophin restoration, and functional rescue of both striated muscle types.

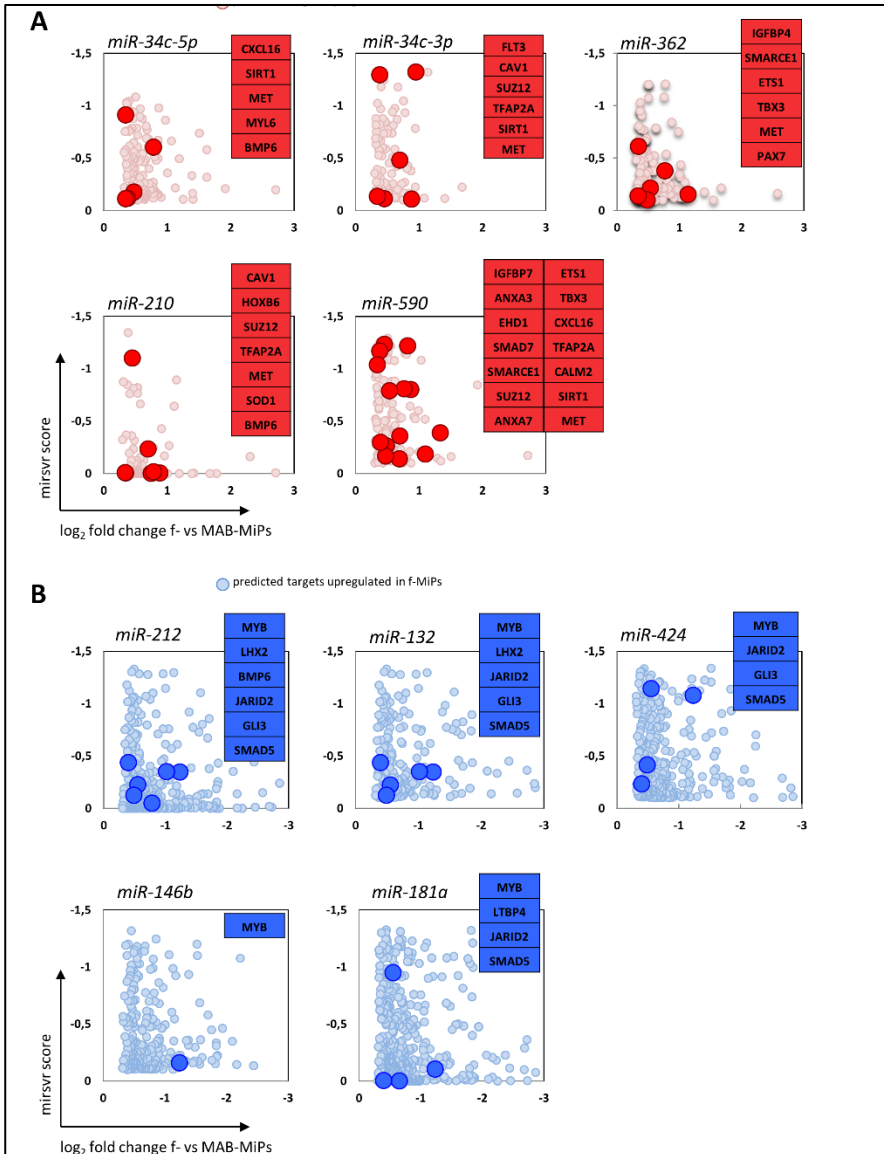
3.6 Supplementary Data

Supplementary Figure 3.1. Gene shortlist for propensity perturbation in MiPs.



(A) Heatmap (z-test) of DE genes (threshold, >10 norm counts) discriminating fibroblast- and MAB-MiPs, and fibroblast- and MAB-iPSCs. Emerging patterns of stage-associated (white arrow), fibroblast-progeny-associated (blue arrow) and MAB-progeny-associated (red arrows) are highlighted. (B) Histograms depicting qPCR-assessed expression levels of shortlisted genes, comparing MAB- vs fibroblast-derived cells across stages (somatic, iPSCs, MiPs). Blue bars depict average values of genes enriched in fibroblast-MiPs, red bars relate to genes enriched in MAB-MiPs, yellow spikes depict st.dev values. *, $P < 0.05$ MAB- vs fibroblast- at all stages; #, $P < 0.05$ at somatic and MiP, but not at iPSC stage; Kruskal Wallis and Mann-Whitney U test; $n=3$ replicates/clone. (C) Expression levels in MiPs and AMC- or PMC-treated MiPs (gene targeting cocktails) of targeted genes. *, $P < 0.05$ vs own ctrl (scramble), Kruskal Wallis and Mann-Whitney U test; $n=3$ replicates/clone. (D-E) Quantification of MiP myogenic propensity in co-culture with C2C12 myoblasts after seven days of differentiation. Myotubes with three or more nuclei were counted as well as human nuclei contributing to chimeric myotubes. Representative fields and quantitation of chimeric myotubes are presented. $P < 0.05$ vs treated and non-treated. Kruskal Wallis and Mann-Whitney U test; $n=3$ replicates/clone. f-, fibroblast-derived; AMC, anti-myogenic cocktail (gene-based), PMC, pro-myogenic cocktail (gene-based), scale bar approximately $100\mu\text{m}$.

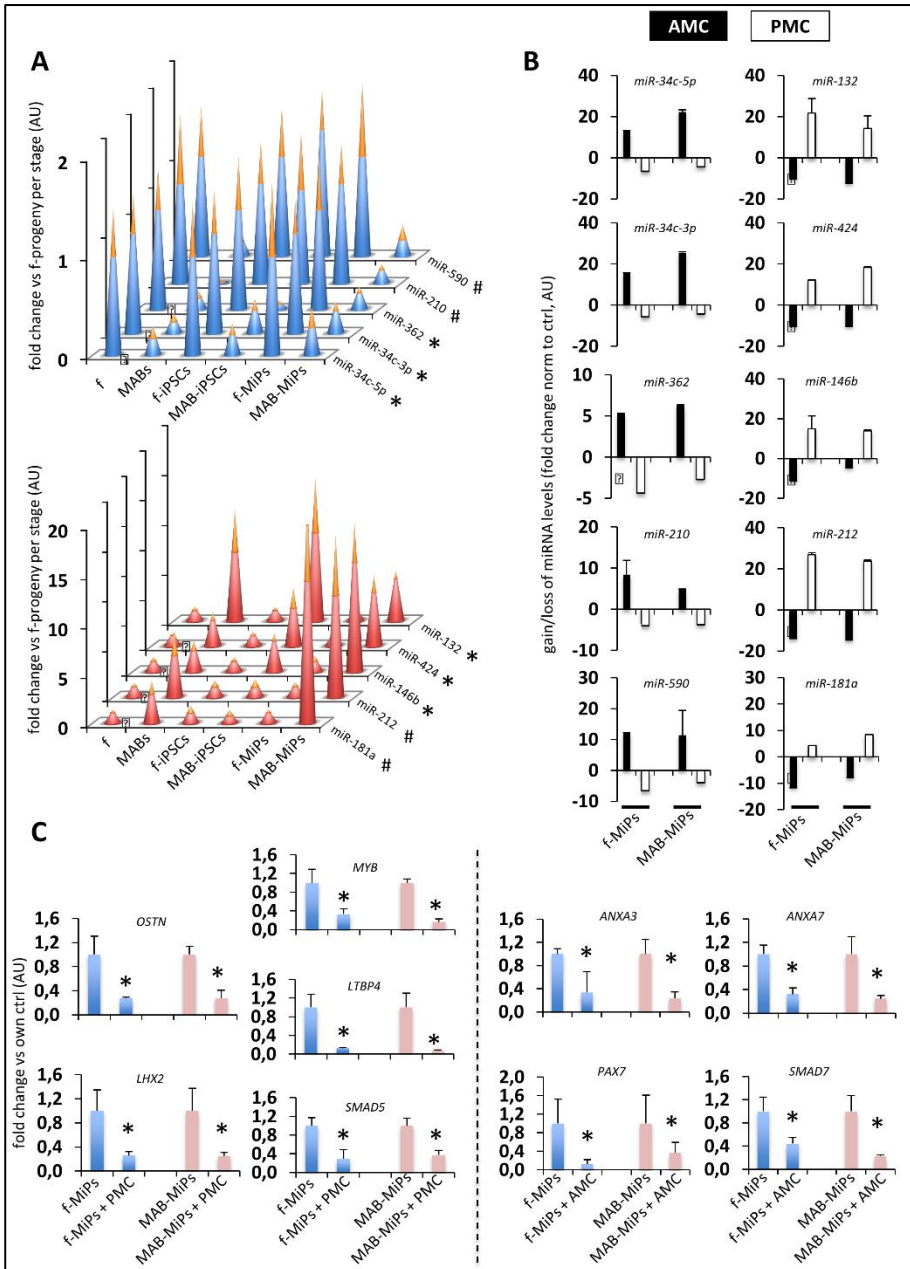
Supplementary Figure 3.2. Filtering the candidates from miRNA-seq comparison by means of RNA-seq-based indications.



The mirsvr score vs fold change plots in this Figure illustrate the predicted targets of miRNA-seq-based candidates among RNA-seq-based interesting hits. Specifically, charts in (A) depict the predicted targets

(interesting hits are highlighted) of fibroblast-MiP-enriched miRNAs among genes upregulated in MAB-MiPs. Conversely, charts in **(B)** depict the predicted targets (interesting hits are highlighted) of MAB-MiP-enriched miRNAs among genes upregulated in fibroblast-MiPs. f, fibroblast-derived.

Supplementary Figure 3.3 Perturbing miRNAs and predicted targets with AMC and PMC containing miR-mimics and anti-miRs.



(A) qPCR-based validation miRNA-seq-based hits across stages. Blue bars depict average values of genes enriched in fibroblast-MiPs, red bars relate to genes enriched in MAB-MiPs, yellow spikes depict st.dev values. *, $P < 0.05$ MAB- vs fibroblast- at all stages; #, $P < 0.05$ at somatic and MiP, but not at iPSC stage; Kruskal Wallis and Mann-Whitney U test; $n=3$ replicates/clone. **(B)** qPCR-based evaluation of target

miRNA levels after AMC or PMC administration to MiPs *in vitro*. N=3 replicates/clone; depicted are average \pm st.dev bars. **(C)** qPCR-based assay of expression levels of predicted targets of perturbed miRNAs in presence of AMC or PMC. *, P<0.05 vs own ctrl (scramble), Kruskal Wallis and Mann-Whitney U test; n=3replicates/clone. f-, fibroblast-derived; AMC, anti-myogenic cocktail (miRNA-based), PMC, pro-myogenic cocktail (miRNA-based).

differentiation. AP20187 induces death of MiP-chimeric myotubes, therefore high propensity associates with high mortality (as depicted in the scheme on the left). Representative fields and quantitation of MyHC signal are presented, scale bar approximately 100 μ m (C) Application of AMC and PMC mixes to induced MiP differentiation toward skeletal muscle lineage *in vitro*. Quantitation of differentiation efficiency is reported on the right. f-, fibroblast-derived; AMC, anti-myogenic cocktail, PMC, pro-myogenic cocktail, scale bar approximately 100 μ m.

Extracellular vesicles- derived microRNAs improve mesoangioblasts treatment in muscle wasting condition

Giorgia Giacomazzi, Ester Martinez Sarrà, Silvia Querceti, Hanne Grosemans, Rik Gijssberg, Mattia Quattrocchi & Maurilio Sampaolesi.

Manuscript in preparation

4.1 Abstract

Skeletal muscle holds an intrinsic capability of growth and regeneration both in physiological conditions, as well as in case of injury. Chronic muscle illnesses, generally caused by genetic and acquired factors, lead to deconditioning of the skeletal muscle structure and function, and are associated with a significant loss in muscle mass. At the same time, progressive muscle wasting is a hallmark of aging. Given the paracrine properties of myogenic stem cells, extracellular vesicles (EVs) - derived signals have been implicated both in the pathogenesis of degenerative neuromuscular diseases and as a possible therapeutic target. In our work we have screened the content of EVs from animal models of muscle hypertrophy and muscle wasting associated with a chronic disease and aging. Analysis of the transcriptome, protein cargo and miRNAs has allowed us to identify a hypertrophic miRNAs signature amenable for targeting muscle wasting. We have tested this signature *in vitro* on mesoangioblasts (MABs), adult vessel associated stem cells, given their relevance for treating muscle loss, and we have observed an increase in myogenic differentiation. Furthermore, injections of miRNA treated MABs in aged mice has resulted in an improvement in skeletal muscle features, such as muscle weight, strength, cross-sectional area and fibrosis. We provided evidence that the EV-derived miRNA signature we have identified enhance myogenic potential of myogenic stem cells.

4.2 Introduction

Muscle remodeling is a dynamic process occurring throughout the whole tissue life span. In physiological conditions and during development and growth, skeletal muscle is finely regulated by homeostatic processes that maintain a balance between anabolic and catabolic pathways¹. During development, protein synthesis and progenitor's activation contribute to new muscle formation. Conversely, during adulthood, cellular turnover generally decreases and the muscle mass plasticity is mainly determined by the interplay between anabolism and catabolism¹⁶⁹. In steady state, these two pathways remain balanced. However, skeletal muscle homeostasis might be disrupted when damages occur, or more severely, in presence of degenerative diseases that induce acute chronic damage, such as Muscular Dystrophies (MD)¹². At the same time, a negative equilibrium between anabolic and catabolic factors, as well as between apoptosis and regeneration processes is naturally associated with progressing muscle loss that occurs during aging²⁸. Aging is, in fact, marked by decreased function and mass across all organs. Skeletal muscle loss in aging is referred to as sarcopenia and it is correlated with also a progressive decline in functionality and depletion of resident stem cell pools⁵⁷. Albeit still controversial, evidence has shown that the gradual decline in satellite stem cells number observed in aging, is associated to a correspondent decrease in their ability to sustain muscle regeneration upon injury^{170, 171}. Skeletal muscle wasting is therefore a critical condition that can be linked to degenerative diseases, or be a consequence of chronic illness as for cancer cachexia, or rather be an intrinsic property of the aging process.

Concurrently, the research on the application of stem cells in muscle wasting conditions has been broad and has shown partial beneficial effects in counteracting dystrophy-induced muscle damage or other chronic muscle injuries¹⁷². In particular the use of mesoangioblasts (MABs), interstitial, vessel-associated adult stem cells, has given promising results when MABs were transplanted intraarterially in murine

and canine models of MD ^{39, 173}. More recent evidence has shown that MABs are able to functionally fuse with resident fibres and give rise to higher number of donor fibres when injected intramuscularly in dystrophic muscle or following acute injuries ¹⁷⁴. Additionally, the aging effects on the potential of progenitors cells has been highlighted, as MABs derived from younger donor held greater intrinsic myogenic ability compared to MABs derived from elderly donors ⁶³. This data strongly suggests that the potential of stem cells in contributing to muscle regeneration is decisively influenced by their aging stage.

Considering recent evidence establishing the secretory ability of skeletal muscle, growing interest has been dedicated to the investigation of paracrine modulators, as myokines and more recently extracellular vesicles, involved in muscle regenerative processes ^{175, 176}. Recent studies on extracellular vesicles (EVs) and exosomes have pointed out that secreted vesicles play a role both in muscle physiological growth and development ¹⁷⁷, in muscle regeneration following injury or chronic illness ^{128, 178} and ultimately in muscle wasting and aging ¹⁷⁹. microRNAs (miRNAs) are among the selected cargos secreted into EVs and exosomes. miRNAs involvement in skeletal muscle homeostasis, regeneration and wasting is rather well described ¹⁸⁰. Interestingly, it has been reported that EVs carry members of the myomirs family of miRNAs, such as mir1, mir133a and mir206, and thus might contribute directly to convey regenerative signaling to the skeletal muscle ¹²³. Nonetheless, there is still a lack of consensus on the characterization of EVs as such and although studies have shown the contribution to muscle regeneration by both EVs and cells transplantation, the field is still open for further approaches, especially with the use of EVs and MABs. Furthermore, much less evidence is available on the other components of EVs load cargo, such as RNAs and proteins, and on their possible reciprocal interaction. Finally, an exciting features of EVs is the possibility to custom load them for specific delivery as shown by a number of studies that have paved the way for the use of EVs as delivery machine for targeted therapeutics ¹⁸¹⁻¹⁸⁴.

In the current study, we performed in depth analysis the content of plasma-derived EVs from mouse models of muscle hypertrophy, dystrophy and age-induced atrophy in order pinpoint the secreted key players orchestrating muscle homeostasis in physiological and pathological conditions, further amenable for enhancing muscle regeneration.

4.3 Materials and Methods

Cell culture and differentiation.

The majority of human MAB lines employed in this study were already present in the laboratory and some new lines were isolated as previously described (ref). MABs were cultured in IMDM supplemented with 15% FBS, 1% Pen-Strep, 1% L-glutamine, 1% sodium pyruvate, 1% non-essential amino acids, 1% insulin- transferrin-selenium and 0.2% b-mercaptoethanol, (all reagents from GIBCO,USA) in 5% O₂ /5% CO₂ at 37°C. C2C12 were cultured in DMEM supplemented with 10% FBS, 1% Pen-Strep, 1% L-glutamine, 1% sodium pyruvate, 1% non-essential amino acids, and 0.2% b-mercaptoethanol, (all reagents from GIBCO,USA). Myogenic differentiation of MABs and C2C12 was induced incubating the cells with DMEM high glucose, supplemented with 2% of HS, 1% penicillin/streptomycin solution, 2 mM glutamine, and 1 mM sodium pyruvate (all reagents from GIBCO) for 5 days (C2C12) and 12 days (MABs).

Viral infection

To enable tracking of human MABs after injection in vivo and in real time, and to prove cell viability, human MABs were transduced with a MLV-derived lentiviral vector -eGFP-T2A-fLuc constructed by the Leuven Viral Vector Core at 1:200 concentration for 72 hours (virus titer 2.34e+08 TU/ml).

Animal procedures

All protocols on live mice were performed in compliance with the Belgian law and the Ethical Approval of KU Leuven (P202/2016, P175/2016 with expansion). For plasma collection 10 *Mstn-null*, 10 *Sgcb-null*, 10 C57/bl6(adult) and 10 C57/bl6 (aged) mice were euthanized with ketamin (dose) to preserve the rib cage and blood was drawn by a single heart puncture. For cells injections 10 Rag2-null/c-null/C57/bl6 mice were divided in 2 groups, 5 animals received intramuscular injections of 2.5×10^5 miRNA-treated MABs and 5 animals received intramuscular injections of 2.5×10^5 untreated MABs into right limbs. Left hindlimb muscles were

injected with physiological solution as control. At day 21 mice were euthanized by cervical dislocation and hindlimb muscle were harvested in OCT at -80°C until further analysis. EDL muscle was immediately processed for functional analysis (Aurora). The samples were then cut transversally in 7- μm sections using a cryostat machine (Leica, Wetzlar, Germany). Histological and morphometric analysis was investigated at 21 days after injections.

Distribution and viability of human MABs eGFP/fLUC in vivo

For in vivo bioluminescence (BLI), mice were first anesthetized with 1.5% of isoflurane in 100% of oxygen and then given a single injection containing d-luciferin potassium salt dissolved in phosphate-buffered saline (PBS) (126 mg/kg). Ten minutes after luciferin injection, mice were placed in the imaging chamber (IVIS Spectrum, Perkin Elmer, X). Next, consecutive frames were acquired for 60 seconds until the maximum signal intensity was reached. After drawing a region of interest (ROI) around the hindlimb muscles the maximal radiance (p/s/cm²/sr) was measured within this region and subsequently images were analyzed using Living Image version 4.5. BLI data were obtained 1h, 1,3,7,14 and 21 days post injections. Mice were euthanized by cervical dislocation immediately after in vivo BLI and the hindlimb muscles were collected in OCT.

Muscle function by an intact muscle test system (Aurora Scientific Instruments)

EDL functionality was evaluated as previously described¹⁸⁵. Briefly, the EDL was immediately excised from each mouse, maintain in a storage solution in a temperature controlled (30 °C) chamber containing the buffer solution and continuously gassed with a mixture of 95% O₂ and 5% CO₂. The muscle was initially held for isometric and was stimulated with 0.5 ms single pulse to measure the isometric twitch force and contraction time. A second pulse was applied to check the consistency of the values obtained and to better balance muscle equilibration before applying tetanic stimulation.

The muscle was then subjected to a first train (0.6 s at 120 Hz) to induce unfused tetanus, and to a second train (0.6 s at 180 Hz) to evoke the maximal tetanic force.

EVs isolation and characterization

EVs were extracted from mouse plasma following established protocols of ultracentrifugation¹⁸⁶. This protocol allowed isolation of EVs with a size comprised within 100 and 250 nm. TEM analysis was performed in collaboration with Nanosight analysis was performed with Nanosight NS300 in collaboration with the laboratory of Laboratory of Lipid Metabolism and Cancer, KU Leuven.

MicroRNA modulation

microRNAs cocktails were composed as follows: mimics for mir1, mir 208a, mir133a (hypertrophic cocktail) mimic for mir 206 and antimir for mir1, mir133a and mir208a (dystrophic cocktail). Human MABs were transfected with 30nmol of each miR-mimic and 10nmol of each anti-miR per mw12 well, with 2ul lipofectamine 2000. miRNA expression analysis, injections *in vivo* and differentiation assays were conducted 48 hours after transfection.

Molecular analysis

MicroRNA content in EVs was analyzed by mmu miRNome micro-RNA profiling kit (Systems Bioscience) following manufacturer's instruction (n=4). Validation of this findings was performed by Taqman analysis for miRNA levels (Taqman q-PCR using 1:15 diluted cDNA obtained from 20ng total miRNA preparation).

Western blotting (WB) analysis was performed on lysates from cells in RIPA buffer (Sigma-Aldrich) supplemented with 10 mM Sodium Fluoride, 0.5 mM Sodium Orthovanadate, 1:100 Protease Inhibitor Cocktail, and 1 mM Phenylmethylsulfonyl Fluoride (PMSF). Equal amounts of protein (30 mg) were denaturated in sample-loading buffer (50 mM Tris-HCl, pH 6.8, 100 mM DTT, 2% SDS, 0.1% bromophenol blue, 10% glycerol for 10 minutes at 95°C), run on SDS-polyacrylamide gel, and transferred to nitrocellulose membranes (Protran, Nitrocellulose membrane, Sigma-

Aldrich). After Tris-buffered saline (TBS) containing 0.05% Tween and 5% non-fat dry milk (Sigma-Aldrich)- backgroundblocking membranes were incubated overnight with primary antibody ¹⁷⁴. Following secondary antibody incubation (1:5000) in TBS-Tween and 2.5% non-fat dry milk (Sigma-Aldrich) membranes were incubated with Super signal Femto or Pico (Thermo Fischer) and bands were detected with GelDoc chemiluminescence detection system (BioRad).

Mass Spectrometry analysis

Mass spectrometry analysis was performed as previously described ¹⁸⁷. Briefly, Liquid Chromatography (nanoLCCULTURA-EKSIGENT) followed by MS (nanoLC-MS/MS) was performed on a LTQ Orbitrap Velos (Thermo Fisher, Waltham, MA, USA). Vesicles were stored in PBS and concentrated with 10 mM dithiothreitol, alkylated with 55 mM iodoacetamide, precipitated by 10% TCA, washed with 100% acetone and reconstituted in 2 μ L of 8 M urea. Digestion was performed overnight and blocked with 1% formic acid. The amount of sample submitted to MS analyses was based on particle quantity and ranged from 9.9×10^8 to 5×10^9 , among all samples analysed. The eluate was applied to the nanospray source of the Orbitrap spectrometer and a full scan was acquired for all spectra within the 400–1,500 m/z range with a 30,000 resolution and a maximum injection time of 500 ms. The MS/MS was performed using data-dependent dynamic exclusion of the top 20 most intense peptides using repeat count=1, repeat duration=30 s, exclusion list size of 500 and exclusion list duration=30 s as parameters.

RNA-sequencing

RNA samples extracted from EVs were verified and processed by the Genomics Core (KU Leuven – UZ Leuven, Belgium). Due to very low concentration of RNA (< 5 μ g/ μ l) a preamplification step was required before sequencing. RNA sequencing libraries were constructed with the TruSeq RNA Sample Prep Kits v2 (Illumina). Samples were indexed with unique adapters and pooled for single read (50bp) sequencing in Illumina HiSeq2000. RNA-seq reads were aligned with TopHat v2.0.2 to the mouse

genome version mm10. Differential expression levels were assessed using DESeq (n=6 *Mstn*-null derived samples, n=5 *Sgcb*-null derived, n=3 wild type). Since we failed to detect any differentially expressed genes we further selected a cut of of ≥ 50 reads and performed GO analysis by means of BinGO.

Immunofluorescence, Immunohistochemistry and microscopy.

Immunofluorescence staining was performed following the commonly used steps of Triton-based permeabilization, donkey serum- background blocking, overnight incubation with primary antibody at 4°C (Myhc in house hybridoma 1:20, hLAMN 1:200, laminin 1:100) 1hour incubation with 1:500 AlexaFluor-conjugated donkey secondary antibodies and final counterstain with Hoechst.

Pictures were acquired on a on a Nikon Eclipse Ti microscope (Nikon). Pictures of human MABs in vitro differentiation assay were acquired on Nikon Ti2 automated fluorescent image scanner, pre-specified 4 x 4 fields per well centered on a 24-well format were captured using an automated x-y motorized stage. Afterwards images acquired per well were electronically stitched NIS-Element software (Nikon) for full well image reconstitution.

Haematoxylin and eosin staining was performed as previously described. Briefly Cryosections were fixed with 4% paraformaldehyde for 15 minutes. Slides were then soaked in distilled water for 5 minutes, Harris haematoxylin for 4 minutes and washed afterwards in running water for 2 minutes. Afterwards the sections were immersed for 1 minute each in acid alcohol, running water, bluing reagent, running water, eosin, 95% ethanol, 100% ethanol and histoclear and were finally mounted with DPX and left on a slide heater overnight. Pictures from cryosections were taken with a Nikon Eclipse Ti microscope (Nikon). Cross-sectional area was determined using ImageJ software (NIH). Masson's trichrome was performed as previously reported (ref). Briefly, after 15 minutes in 4% paraformaldehyde of fixing, cryosections were incubated for 15 min at 57 °C in Bouin solution and subsequently stained in Working Weigert's Iron Hematoxylin Solution for 5 minutes, washed in running tap water for 5 minutes and stained in Biebrich Scarlet-Acid Fucsin for 5

minutes. Afterwards slides were soaked in de-ionised water and in Working Phosphotungstic\Phosphomolybdic acid solution for 5 minutes and stained in Aniline Blue solution for 5 minutes and acid acetic 1% for 2 minutes. After mounting pictures were taken on a Nikon Eclipse Ti microscope (Nikon). Fibrotic area was quantified using ImageJ software (NIH).

Statistical analysis

Statistical analysis and graphing of the results was performed on GraphPad Prism 7.0 (GraphPad Software, San Diego, CA, USA). Two-tailed *t* test or one-way ANOVA were used to compare interrelated samples, while two-way ANOVA was used to analyse multiple factors. Confidence intervals were fixed at 95% ($p < 0.05$), 99% ($p < 0.01$) and 99.9% ($p < 0.001$). Data is reported as as mean \pm standard error of the mean (s.e.m.). Refer to figure legends for specific information regarding the statistical test used and the number of independent experiments or biological replicates.

4.4 Results

Characterization of extracellular vesicles from wild type, hypertrophic, dystrophic and aged mice.

We started our analysis isolating EVs from the plasma of aged-matched control C57/bl6 mice, *Mstn-null* mice (hypertrophic), *Sgcb-null* mice (dystrophic) and aged mice (C57/bl6 \geq 18 months- Figure 4.1). EVs were characterized by Nanosight analysis which revealed an average size of 100 nm for WT, dystrophic and aged-derived EVs populations, further confirmed by electron microscopy analysis (Figure 4.1 A-D). We observed that hypertrophic- derived EVs had significantly lower concentration and this correlated with significantly higher average size (Figure 4.1 B-D). We further characterized EVs for known extracellular vesicles/ exosomes markers, reporting that EVs from all conditions were positive for CD81, CD9, CD63 (Figure 4.1 C).

Extracellular vesicles from hypertrophic mice enhance differentiation in myogenic progenitors *in vitro*.

We next tested the functional effect of EVs on murine myoblasts (C2C12 cells), and later to confirm our results in human mesoangioblasts (MABs) (Figure 4.2). First, we established the ability of the myoblasts to uptake RFP marked EVs. After 4 hours of EVs treatment we could successfully detect EVs in the cytoplasm of the treated cells (Figure 4.2 A). After 48 hours of EV exposure we induced myogenic differentiation in C2C12 cells. Our results showed that C2C12 cells treated with hypertrophic- derived exosomes differentiated more efficiently, as reported by the increase of fusion index and myosin heavy chain protein content (Figure 4.2 B, C and D). In order to confirm our observation, we next tested the effects of EVs on human MABs (Figure 4.2 E,F and G). In accordance to our previous findings human MABs treated with hypertrophic-derived EVs 48 hours before differentiation displayed an increased myogenic differentiation as shown by immunofluorescence, fusion index analysis and wester blot. Additionally, the exposure to dystrophic and aged-mice- derived Evs resulted in a detrimental effect on human MAB myogenic differentiation compared to controls and Evs hypertrophic-derived treated cells (Figure 4.2 E,F and G). Our results show that hypertrophic-derived EVs significantly enhance differentiation of myogenic progenitors *in vitro*.

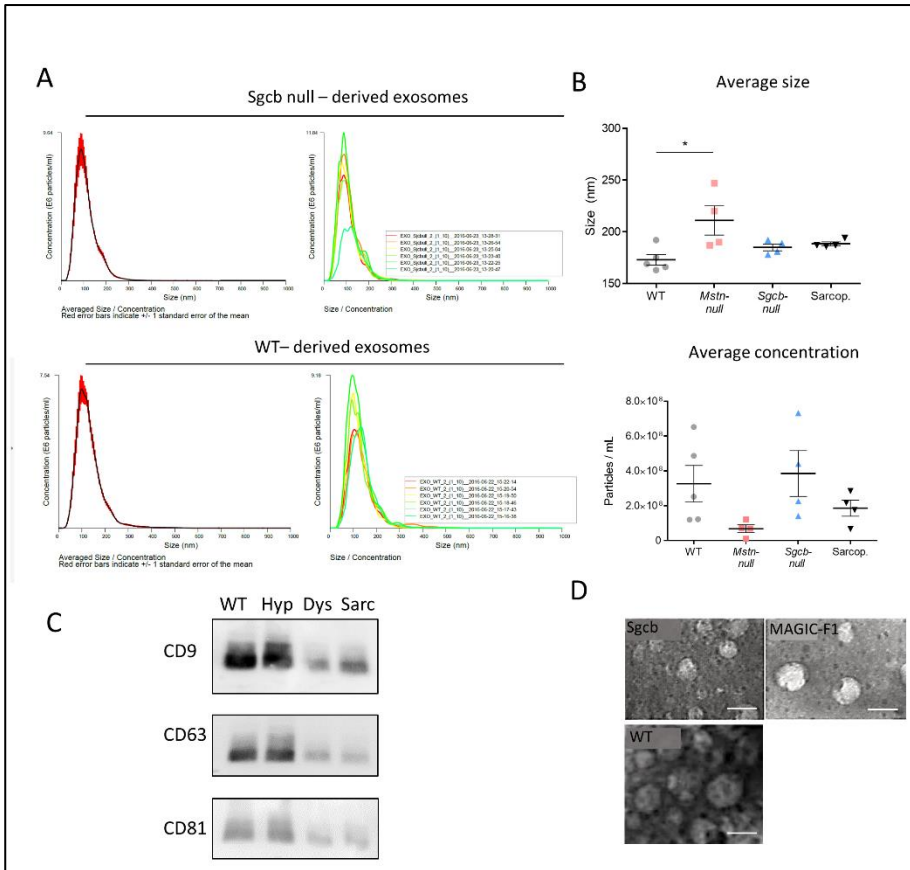


Figure 4.1 Characterization of EVs derived from serum of different mouse models.

A) Nanosight analysis of EVs, representative graphs of *Sgcb-null* and wt derived EVs are shown. **B)** Average size (top) and concentration (bottom) of EVs. **C)** TEM analysis of EVs. **D)** Western blotting of common markers of EVs/Exosomes. N=4, P<0.05.

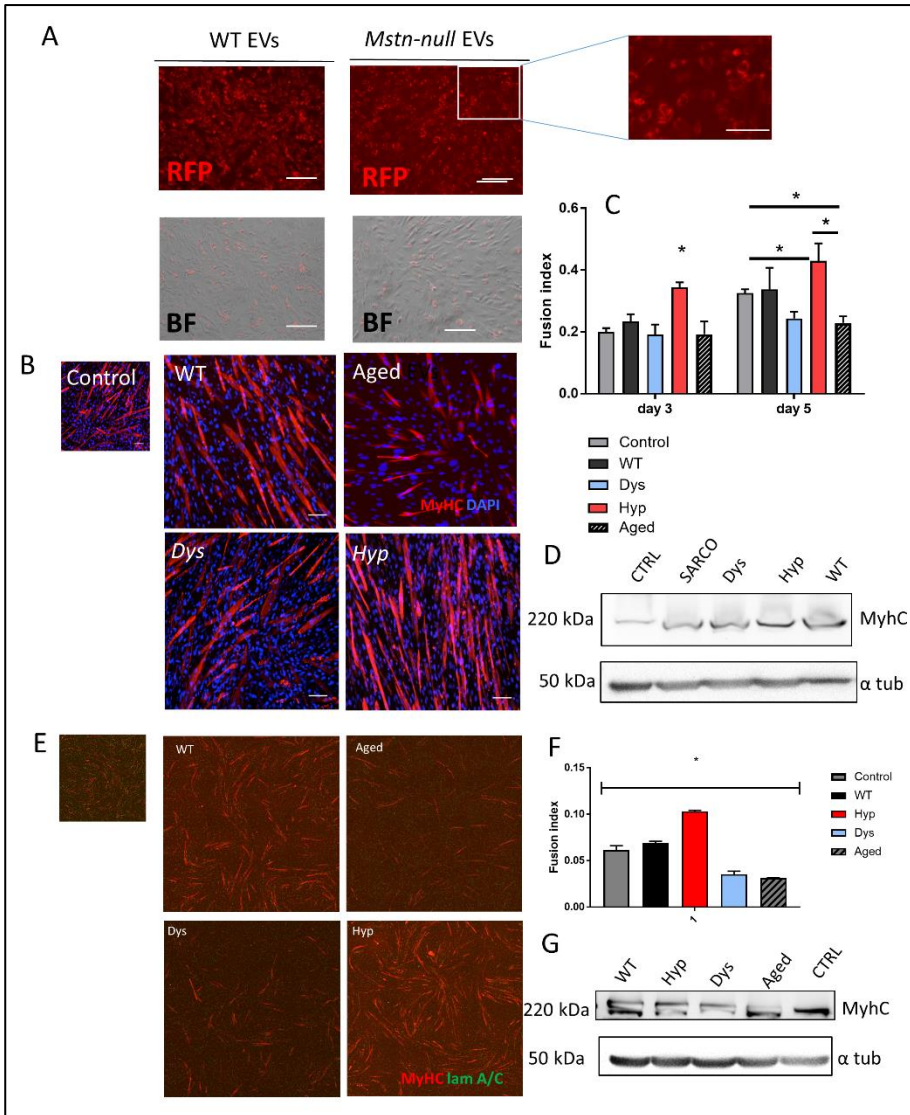


Figure 4.2 Effects of EVs treatment on myogenic differentiation of progenitor cells.

A) RFP marked EVs uptake from C2C12 after 4 hours of treatment. B) Myogenic differentiation of C2C12 incubated with EVs (MyHC red, DAPI blue). C) Fusion index of differentiated C2C12 at day 3 and at day 5. D) Western blot for MyHC protein level at day 5. E) Myogenic differentiation of human hMABs treated EVs (MyHC red, Lamin A/C green). F) Fusion index of differentiated hMABs at day 12. G) Western blot for MyHC protein level at day 12 ($n=5$ * $p < 0.05$ One way Anova).

Messenger RNAs appear randomly integrated in circulating extracellular vesicles

After unraveling the effects of hypertrophic-derived EVs we next asked which factors might be responsible for the observed phenotype. Hence, we performed in depth analysis of the content of the EVs in terms of mRNAs, microRNAs and protein. Bulk RNA sequencing revealed that mRNAs loaded into EVs from different conditions was not discriminative, suggesting that mRNA is not likely driving the enhanced differentiation. Our results show that the EVs are rather low in content of mRNA, with about 2000 to 6000 uniquely aligned transcripts. Moreover hypertrophic-derived EVs contained more than double mRNA than controls and dystrophic and wild type-derived (Supplementary Figure 4.1 A). PC analysis revealed a rather contingent clustering of the samples, suggesting that the RNA profile was very variable within each condition (Supplementary Figure 4.1 B). Based on this observation, a differentially expressed analysis of the transcript would not lead to any solid conclusions, therefore we opted for deeply profiling the content of each conditions. Analysis of the 30 most abundant transcripts in each condition revealed that all samples expressed middle –high levels of mitochondrial RNA such as mt – Rnr2 and hemoglobin Hb-bbs (Supplementary Figure 4.1 C- E). In order to understand better the specific content of our samples we selected a cut off of >50 reads and analyzed the expressed genes. Notably, only 2.3% of the genes were shared between all conditions and while dystrophic and wild type derived EVs shared about 25% of genes, hypertrophic-derived EVs only had 1.3% and 3.9% of genes in common with wild type and dystrophic EVs respectively (Supplementary Figure 1 F).

Our findings and current analysis suggest that the presence of mRNA in the EVs cargo is a stochastic event that might depend on multiple factors and might not be necessarily related to the underlying phenotype.

Characterization of the protein content of extracellular vesicles.

Preliminary mass spectrometry analysis on EVs from all conditions allowed overall detection of 197 proteins in total (Supplementary Figure 4.2) . From the total detected proteins, 122 were present in all conditions, while 4 were specific for *Mstn*-

null EVs, 13 for wt EVs, 10 were only found in EVs from aged mice and 9 in *Sgcb-null* EVs. Surprisingly, we detected a common marker in all preparations CD5, and a high number of immunoglobulin in all conditions. Additionally, our first analysis allowed also identification of myosin 9 and 7 peptides in EVs from *Mstn-null* mice, and high levels of adiponectin in EVs derived from aged mice.

MicroRNAs derived from extracellular vesicles influence myogenic propensity of target cells.

In order to identify the factors that drive myogenic differentiation in hypertrophic EVs we deeply profiled the microRNAs content performing a SYBR GREEN based analysis of > 700 miRNAs in EVs (Supplementary Figure 4.3). Among the differentially expressed miRNAs we investigated selected miRNAs that were enriched in hypertrophic-derived EVs and downregulated in dystrophic or aged- derived EVs compared to wild type, or that were downregulated in hypertrophic- derived EVs compared to wildtype. Our high throughout analysis appointed at a set of miRNAs that could be responsible for the enhanced myogenic differentiation. Among the candidates we selected a group of miRNAs that were either highly enriched and /or relevant for myogenesis . mir150*, mir30e* were highly enriched in hypertrophic samples, while mir574-5p was downregulated in hypertrophic samples (Supplementary Figure 4.4). Upon testing inhibitors and mimics of these miRNAs on the differentiation of human MABs *in vitro* we did not detect any myogenic effect (Supplementary Figure 4.4). We continued our analysis of the differentially expressed miRNAs investigating mir208a, mir1, highly expressed in hypertrophic samples and mir206, downregulated in hypertrophic samples. Additionally, these miRNAs are implicated in myogenesis and myogenic differentiation (Figure 4.3). We have validated the expression levels of these miRNAs by means of Taqman-based qpcr, and we have confirmed high levels of mir1, mir133a and mir208a in the plasma of hypertrophic- derived EVs, while high levels of mir206 could be found in dystrophic-derived EVs (Figure 4.3 A). Furthermore, we have checked the expression of such miRNAs in both skeletal and cardiac muscle tissues to elucidate whether the

presence of determined miRNAs in the plasma could be tissue specific (Supplementary Figure 4.5). These results suggest that the content of miRNAs loaded into the EVs is directly correlated to the content of muscular miRNAs, and further suggest that the origin of the EVs enriched with the selected miRNAs could be the skeletal or cardiac muscle. Nonetheless further investigation in this direction is needed. Interestingly, when analyzing the miRNA content in plasma-derived EVs of a different mouse model of muscle hypertrophy¹⁸⁸, we have identified the very same miRNA signature, namely and upregulation of mir1 and mir208a, and a downregulation of mir206 compared to control (Supplementary Figure 4.6).

We next tested the effects of this set of miRNAs on human MABs: combining mimics and inhibitors oligonucleotides we upregulated and downregulated mir1, mir133a and mir208a in different combination (Figure 4.3). As shown in Figure 3D the simultaneous upregulation of mir1 and mir208a increased the myogenic differentiation of human MABs resulting in a 2-fold upregulation of fusion index. Immunofluorescence analysis and protein analysis further confirmed this result (Figure 4.3 D, E and G). Furthermore, upregulation of mir1 and mir208a resulted in a significant increase in Myogenic and Myf5 (Figure 4.3 F).

Taken together our results indicate that enhanced myogenic differentiation of myogenic progenitors observed *in vitro* is driven by miRNAs with mir1 and mir208a representing the main factors.

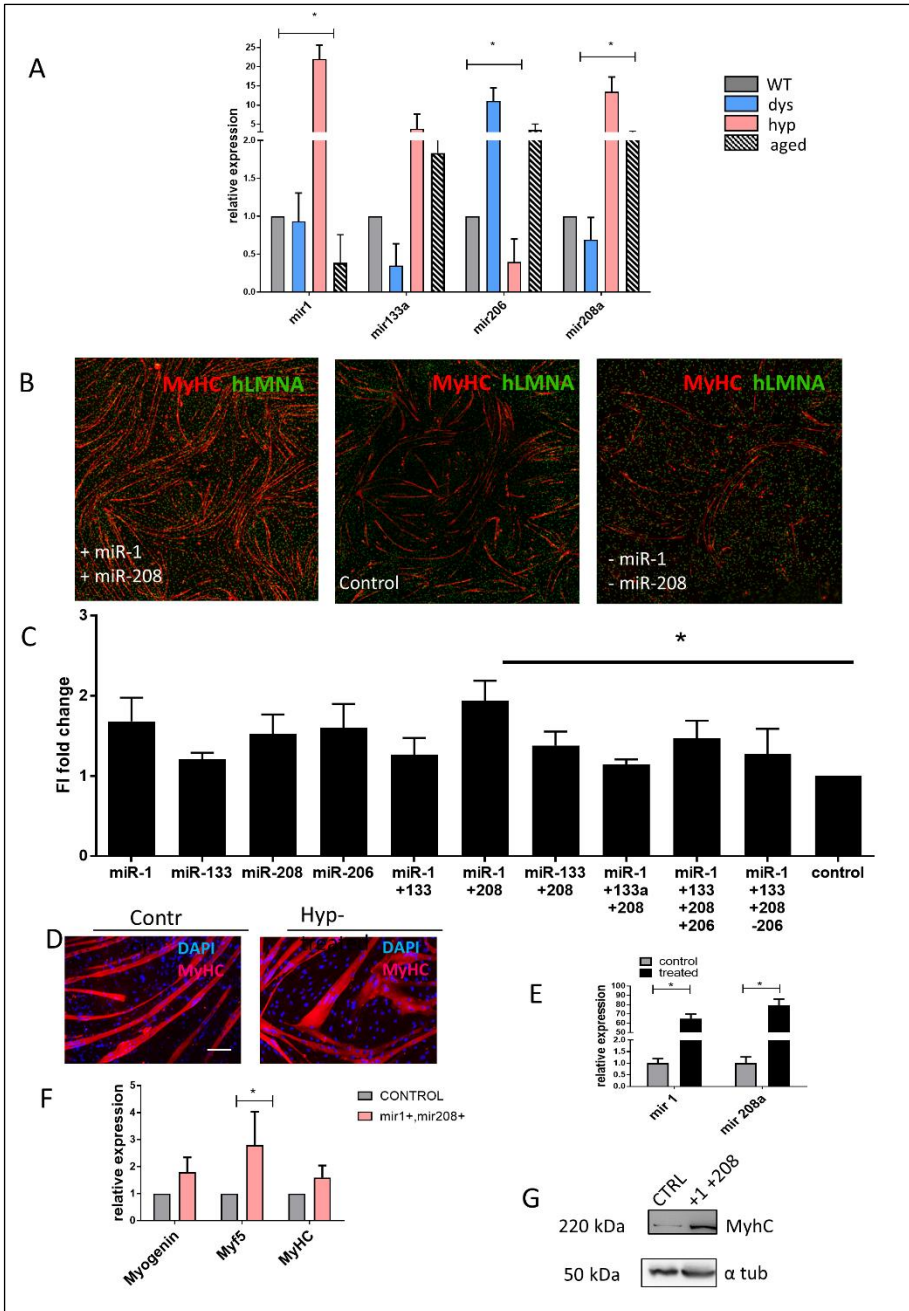


Figure 4.3 Mir1 and mir208a increased myogenic differentiation on hMABs *in vitro*.

A) Taqman qPCR validation for a set of selected miRNAs B) Myogenic differentiation of hMABs treated with combinations of mir mimics and inhibitors. (MyHC red, lamin A/C green). C) Fusion index of

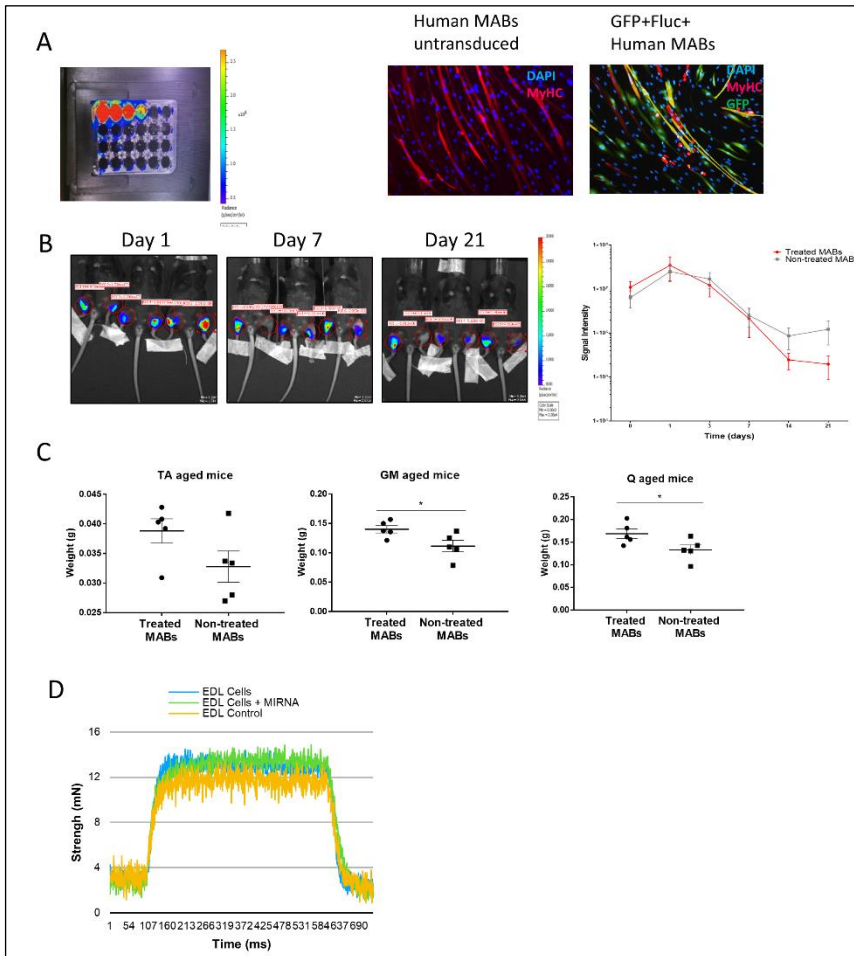
differentiated hMABs after miRNA treatments. D-G) Differentiation of hMABs treated with mir1 and mir208 mimic (E) give the highest increase in fusion index, RNA level (F), protein level (G) (n=5 * p< 0.05 One way Anova).

EVs-derived microRNAs modulation of human mesoangioblasts is beneficial for muscle regeneration *in vivo* in aged mice.

Next, we wanted to elucidate whether the miRNAs we have selected were able to enhance myogenic contribution of human MABs *in vivo*. Recent evidence has shown that human MABs derived from young donor engraft and regenerate skeletal muscle when injected in dystrophic mice ⁶³. Additionally, the enhanced myogenic performance of human MABs from young donors, with respect to human MABs from older donors can also be observed in presence of an acute injury.

Thus, as a proof of principle that the identified miRNAs are able to increase hypertrophy of the skeletal muscle *in vivo*, we injected intramuscularly miRNA-treated and untreated MABs in immunodeficient aged mice (≥ 18 months old) after an acute muscle injury induced by cardiotoxin (Figure 4.4). In order to be able to visualize the biodistribution and the survival of the injected MABs we equipped them with GFP and LUCIFERASE reporter genes. As shown in Figure 4.4 A GFP+ Luc+ transduced MABs were still capable to differentiate to fully formed chimeric myotubes. After viral transduction MABs were treated with mir1 and mir208a mimics 48 hours before injections. At the same time cardiotoxin damage was induced in aged mice. 48 hours after damage miRNA-treated MABs and untreated MABs were injected intramuscularly in hindlimb muscles (*tibialis anterior*, *gastrocnemius*, *quadriceps*) of aged mice. We were able to visualize the cells distribution and survival by means of bioluminescence, up to day 21 (Figure 4.4 B). We did not detect any significant difference in the survival of treated and untreated MABs at this point, however we observed a peak of the signal in both conditions at day 3 (Figure 4.4 B). At day 21 aged mice were euthanized and we noticed a significant upregulation of the weight of all hindlimbs muscle injected with miRNA-treated MABs (Figure 4.4 C). Notably, we observed that EDL injected with miRNA-

treated MABs show a stronger tetanic force trend (Figure 4.4 D). MABs localization and presence in the injected muscle was visualized by immunofluorescence analysis for human laminin A/C (hLMNA) and laminin. Both miRNA-treated and untreated MABs were mainly detected in the interstitial space among fibres (Figure 4.4 E). Interestingly, morphometric analysis of the injected muscle revealed that treated MABs-injected TA showed higher frequency of fibres with larger cross-sectional areas in comparison to control muscle but also to muscle injected with untreated MABs (Figure 4.4 F). Finally, fibrosis, as shown by Masson's staining, was reduced in muscle injected with untreated MABs, and a further reduction was observed in muscle injected with miRNA-treated MABs (Figure 4.4 G).



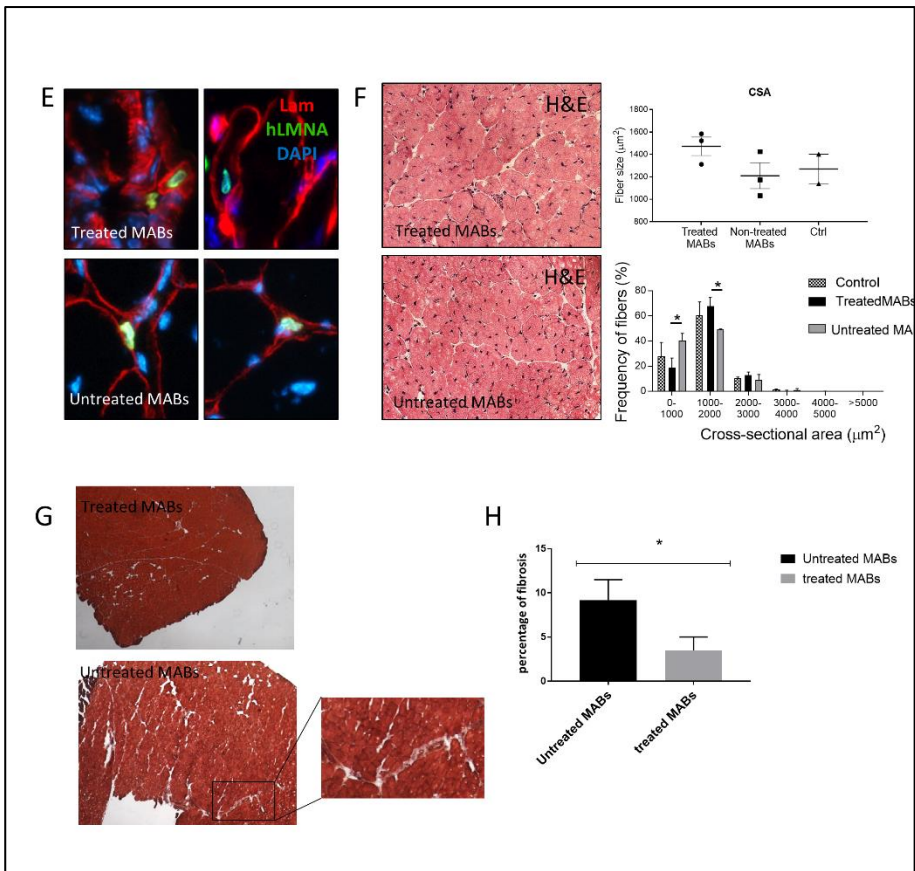


Figure 4.4 Injections of miRNA treated and non-treated hMABs in aged mice after acute injury.

A) In vitro proof of bioluminescence of hMABs transduced with LUC+ GFP+ vector (left) and myogenic differentiation before and after transduction B) BLI at day 7, 14, and 21 of injected mice (left) and signal quantification. Left leg received non-treated MABs, right leg received miRNA treated MABs C) Weight of hindlimb muscles after mice were sacrificed at day 21. TA *tibialis anterior*, Q *quadriceps*, GM *gastrocnemius*. D) Functional analysis of EDL (*Extensor digitorum longus*) via evaluation of tetanic force. E) Localization of hMABs in the injected skeletal muscle (laminin red, lamin A/C green, DAPI blue) F) H&E and quantification of regenerating fibres size after treatment. G-H) Massons' staining of injected hindlimb muscle and quantification of area of fibrosis. * p < 0.05, animals injected N=5).

4.5 Discussion

The balance between pathways inducing hypertrophy and atrophy in striated muscle is a crucial aspect to consider when approaching therapeutic strategies for skeletal muscle wasting. In our work we have made use of information derived by animal models displaying on one side muscle hypertrophy, and on the other side muscle wasting both disease- and aged-associated. The rationale behind our analysis was to identify common dysregulated signatures with the final goal to identify players that could be tuned to enhance muscle regeneration. Given the growing evidence implicating circulating EVs as paracrine mediators in tissues regeneration ¹⁸⁹, we performed in depth screening the content of EVs derived from serum of mice. Our analysis of the EVs cargo has encompassed both RNAs species (mRNAs and miRNAs) and proteins, resulting in the identification of two main miRNAs, mir1 and mir208a able to impact on the muscle phenotype.

MiRNAs are largely implicated in myogenesis and muscle regeneration, with several evidence reporting that miRNAs can be detected in EVs ¹⁹⁰. It is therefore not surprising that in our system EVs- derived miRNAs appear to drive the modulating effect on myogenic progenitors. Mir1 is a known modulator of hypertrophy, in skeletal and cardiac muscles, where its overexpression is beneficial for reducing cardiac hypertrophy ¹⁹¹. Supporting this evidence, we have identified target miRNAs in two different models of skeletal muscle hypertrophy (*Mstn-null* and MAGIC-F1 mice), where cardiac hypertrophy is only mildly observed. *Mstn-null* do not display cardiac hypertrophy at all, while MAGIC-F1 animals have a attenuated cardiac phenotype ¹⁸⁸. Similarly, mir208a was along the highest detected circulating EV-miRNA in both models. Albeit considered a specific cardiac miRNA, mir208a is also a known regulator of *myostatin*, together with miR-208b and miR-499 ¹⁹², implying a potential role in driving skeletal muscle hypertrophy that thus far remains unravelled. Our work proposes mir208a as an additional modulator of myogenic

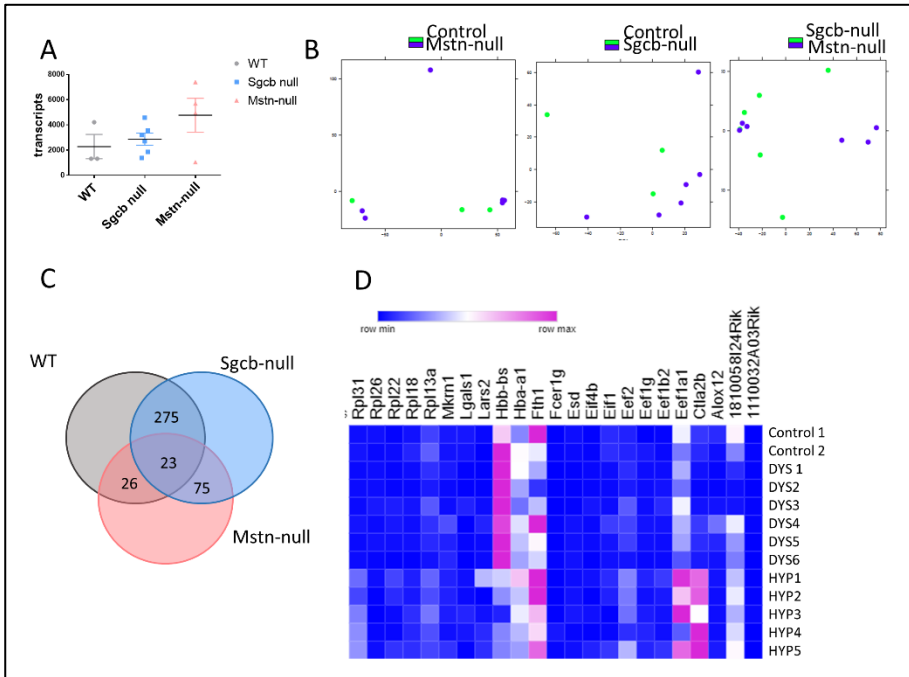
commitment of progenitor cells. The identification of the same EVs-derived signature in two diverse murine models of skeletal muscle hypertrophy is compelling and further suggests that these miRNAs are crucial players in maintaining the phenotype. Although this latter information is still speculative, we have provided evidence that both miRNAs represent the best combination out of all the EVs-detected miRNAs to increase myogenic commitment of human MABs. Further experiments need to be designed to address in detail questions regarding the mode of action of these miRNAs, sorting out their specific targets. However, we can hypothesize that both miRNAs regulate common pathways, based on several shared predicted targets, such as members of the TGF β pathway (TGFB2, TAB2), SMAD4/6, and common epigenetic modulators (HDAC3).

When screening the mRNA content of EVs we have not detected any differentially expressed genes and we have thus concluded that mRNAs are stochastically entrapped in EVs in our setting and it is not likely to be responsible for the enhanced myogenic effect we have observed. This might be due to many reasons, first of which the low number of transcripts detected. This data is consistent with other reports reporting deep sequencing of EV-derived mRNAs^{193, 194}. Despite our analysis was statistically robust, we shall note that increasing the number of samples might be beneficial to unravel mRNAs possibly involved in the observed phenotype. Finally, although preliminary, our mass spectrometry analysis has resulted in two important observations: first, there is high number of immunoglobulins present in all preparations, and second all preparations share expression of CD5- antigen like, which has been recently described as a novel marker for plasma-derived EVs¹⁸⁷. Analysis of additional samples will provide more insight on the protein content and allow a comprehensive understanding of the EVs cargo. We have conducted a large scale analysis of the EV cargo, nonetheless, it must be noted that we have not investigated other RNA species that have been implicated in EV- mediated mode of action and intercellular communication such as long- non coding RNAs¹⁹⁵.

The myogenic effect of the identified miRNA signature *in vitro* on human MABs was striking; we observed a strong increase in myogenic differentiation. When transplanting miRNA-treated MABs *in vivo* in aged mice after acute muscle injury, we had less discriminative results. Muscle functionality was not improved *per se*, however we detected a clear hypertrophic remodelling as shown by both increase in fibre size and increase in muscle weight. We also showed a significant reduction in fibrosis, that is associated with a poor recovery after injury in aged individuals ¹⁹⁶. We acknowledge that additional strategies can be implemented to refine our approach, for instance stronger modulation of miRNAs by creating a stable cell line. Furthermore, given our *in vitro* results, mir1 and mir208a might show a direct effect in modulating resident myogenic stem cells. Novel methods to activate stem cells *in loco* is particularly demanding, if moving towards a cell-free method of tissue-specific regeneration is desired. In this scenario, EVs holds an ideal advantage, since they are less immunogenic than stem cells, readily deliverable, and can be designed to carry tailored messages to target cells. Recent evidence has shown that EVs loaded with a specific cargo were successfully delivered to skeletal muscle by adding modified, dystrophin splice-correcting phosphorodiamidate morpholino oligomer (EXOPMO) ¹⁹⁷. In light of this result, a follow up of our work would comprise the production of engineered EVs that could deliver directly mir1 and mir208a to target myogenic cells, granting a cell-free approach to target muscle wasting.

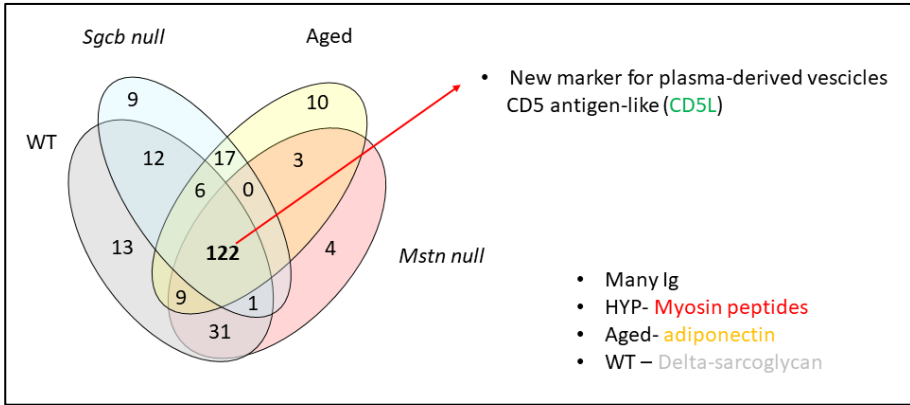
4.6 Supplementary data

Supplementary Figure 4.1 RNA-sequencing analysis of EVs

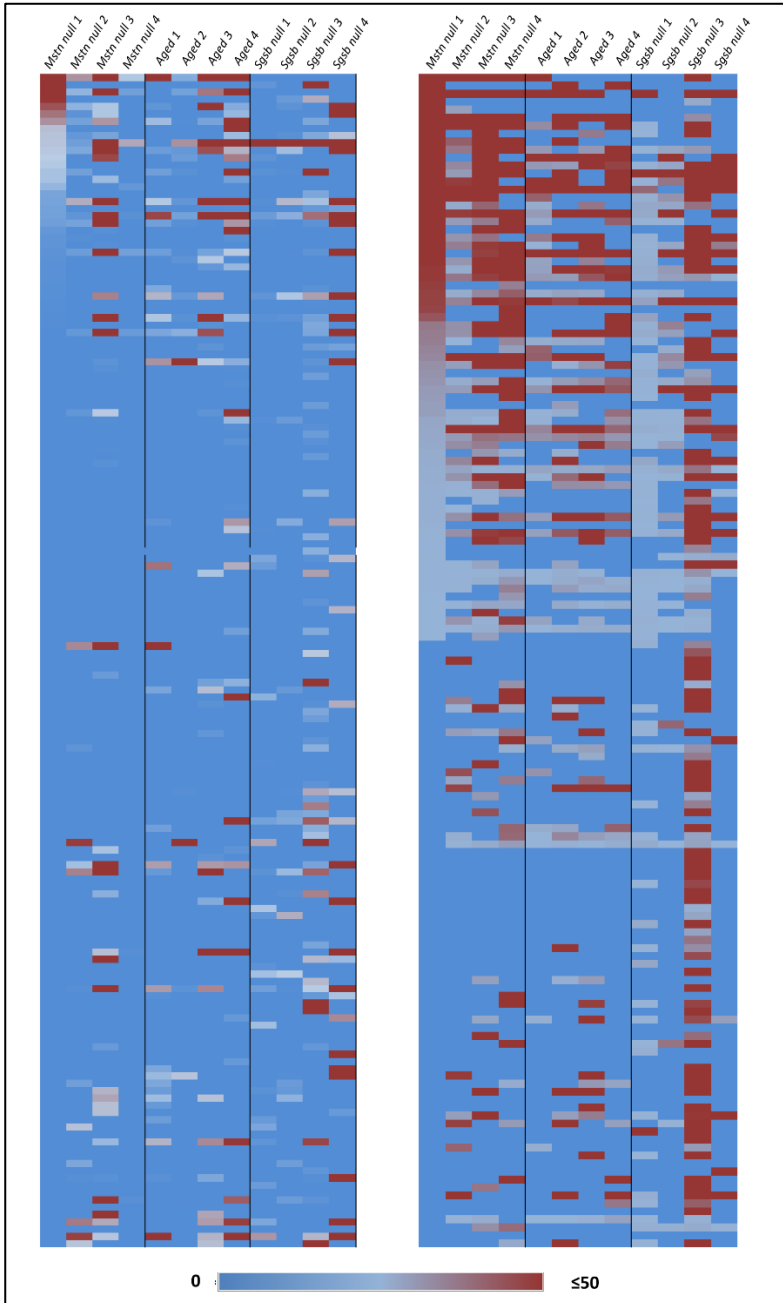


A) Transcripts content in EVs from different conditions. **B)** PCA plot show stochastic distribution of different sample. **C)** Venn diagram of shared genes in three different conditions. WT and dystrophic EVs share a much higher number of genes. **D)** Heatmap representing the 23 shared genes among all conditions.

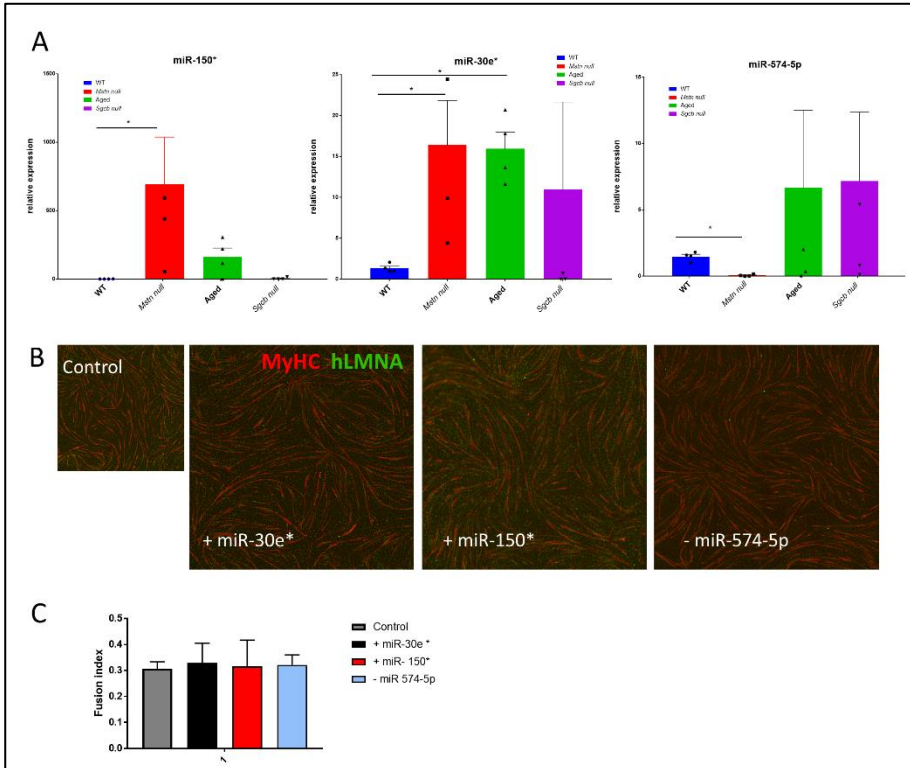
Supplementary Figure 4.2 Preliminary proteomics analysis of EVs.



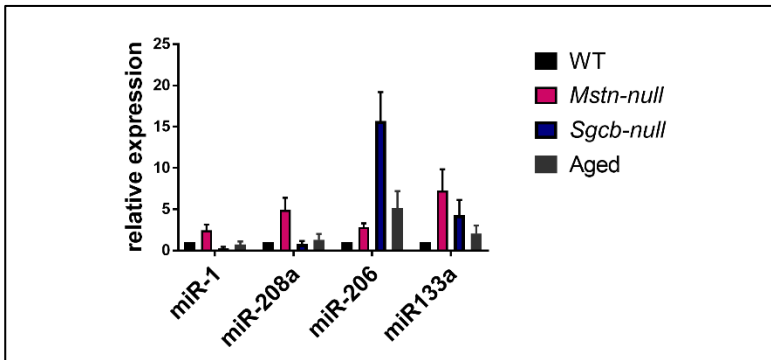
Venn diagram showing preliminary data obtained from proteomics analysis of EVs (N=1).

Supplementary Figure 4.3 Heatmap of the differentially expressed EVs-derived miRNAs.

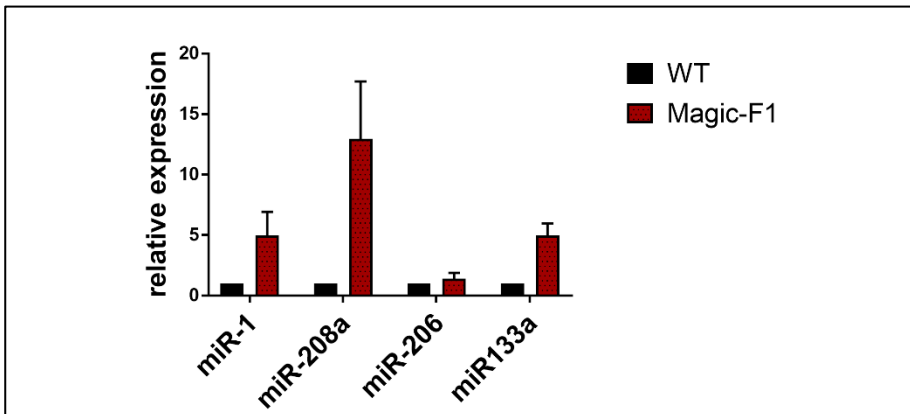
Supplementary figure 4.4. Modulation of some of the top differentially expressed miRNAs did not lead to any myogenic differentiation improvement.



A) Expression level of some of the highest differentially expressed miRNAs in EVs from different conditions. **B-C)** Modulation of miR 30e*, miR-150* and miR-574-5p did not show a significant increase in hMABs myogenic differentiation, as shown by IF and fusion index analysis. N=3

Supplementary figure 4.5. miRNAs content in hindlimb muscles of mice.

miRNAs content in the hindlimb of *Mstn*- null (red) and *Sgcb*-null (blue) and aged (gray) animals compared to WT (black bar) n=3.

Supplementary figure 4.6. Analysis of selected miRNAs in EVs derived from MAGIC-F1 animals.



Chapter 5- General discussion

The emerging field of miRNAs technology combined with stem cells differentiation potential is gaining momentum in regenerative medicine. Our results are embedded in such scenario, as we explore possible applications of miRNAs technology in targeting muscle decay and loss of function.

In the first part of the manuscript we have shown that human MiPs, iPSCs derivatives, injected intraarterially in the hindlimb muscles of dystrophic mice are able to engraft and contribute to regeneration of the skeletal muscle. We have further attributed this potential to intrinsic features depending on the cell type of origin. Our data illustrate that some epigenetic signatures can be conserved during differentiation of iPSCs derivatives, thus influencing the *in vivo* regenerative capabilities of stem cell derived approaches. In light of epigenetic regulators being involved in lineage retention processes, we asked whether miRNAs might drive this process. Our analysis disclosed a number of miRNAs that were conserved in MAB-MiPs vs f-MiPs, and by overlaying the two datasets we narrowed our list down to 5 miRNAs upregulated in MABs- derived progenitors and 5 miRNAs downregulated. By delivering mimics and inhibitors we were able to increase myogenic potential of the MiPs both *in vitro* and *in vivo*.

Our work comprises the combination of the use of PSCs derivatives and finding new approaches to enhance their *in vivo* performance for stem cell-based therapies. PSCs derived therapeutic potential has indeed been explored for decades. Ever since the first successful applications of stem cell therapy to treat bone marrow disorders¹⁹⁸, growing expectations in stem cell biology have led to a significant increase in scientific investment in the field. Preclinical studies have demonstrated that adult stem cells can achieve therapeutic efficacy in a number of chronic diseases including neuromuscular diseases such as multiple sclerosis, spinal cord injury and MD. However, albeit further phase I/II clinical studies proving adult stem cell therapy safety, there is an unmet need for improving effectiveness^{42, 199, 200}. Notably, skin regeneration can be considered an exception, since striking results have been achieved in the field. Stem cell therapy for skin lesion and wound healing has

reached significant efficacy in generating a functional epidermis, leading to permanent corrections of skin injuries in patient suffering from Junctional epidermolysis bullosa (JEB) ²⁰¹. More recently, it has been shown that the use of autologous transgenic keratinocyte regenerated an entire, upon proper mutation correction fully functional epidermis in a 7 years old patient affected by a life threatening form of JEB ²⁰². This impressive study highlights the relevance of gene editing in the context of stem cell therapy, while ultimately underlining the importance of defining which components of the heterogenous stem cell pool are really driving the tissue regeneration.

Despite such an impressive study, tissues regeneration mediated via adult stem cells has been challenging and has encountered problems such as progressively exhausted renewal capacity of adult stem cells and low regeneration efficiency. In light of these compelling issues, PSC derivatives constitute an even more promising and innovative candidate for cell therapy in degenerative diseases, although still associated with complexity of technical features. In the last 5 years a considerable number of PSC- based trials are currently conducted or are recruiting patients ²⁰³. This trend has started with the very first patients suffering from macular degeneration being enrolled in Japan, be treated with iPSC-derived retinal pigment epithelium, using both autologous and human leukocyte antigen (HLA)-matched allogeneic cells ²⁰⁴. With regards to clinical applicability iPSCs technology has reached important milestones in the past years, including highly efficient technologies for the transgene-free reprogramming ²⁰⁵, targeted and safe site- specific genetic engineering of iPSCs ²⁰⁶, and technical progresses for the expansion and differentiation of iPSCs at clinical scale ²⁰⁷. To begin with, intense research has led to an improvement in the protocols for footprint free site-specific integration of transgene, utilizing Zinc finger- and TALE (transcription activator-like effector)-nucleases as well as the CRISPR/Cas9 (clustered regularly interspaced short palindromic repeats; CRISPR-associated proteins) technology. Secondly, researchers have notably improved the differentiation protocols of PSC derivatives, inhibiting

and activating specific molecular differentiation pathways and adding small molecules to obtain a more robust achievement of specific lineages²⁰⁸. Thirdly, the development of iPSC- based transplants and clinical applications faces the paramount requirement of safety. Hence, standardized procedures are required to routinely check for abnormalities potentially leading to tumour related risk. At the same time, risk assessment has to be evaluated for specific hazards, related to the PSC-derived cells themselves or, more generally, the tissues of engraftment. In our work, we have considered the safety related to clinical translation on PSC technology and thus we have equipped the MiPs with a inducible suicidal gene²⁰⁹. Suicide genes are widely used for instance in cancer cell therapy, as they induce either toxin-related cell death or apoptosis. For PSC derivatives, the integration of suicidal genes moves in the direction of providing a safeguarding control in transplanted cells for preclinical trials.

A last aspect, crucial to consider when approaching PSC derivatives therapeutic applications, is the importance of epigenetic remodeling. As discussed earlier, if “*bona fide*” iPSC wished to be derived, epigenetic signatures ought to be wiped out. However, results obtained in the first part of the manuscript have provided evidence that incomplete wash out of epigenetic traits is amenable for enhancing commitment of MiPs derived from fibroblasts. Studies enforcing this feature have shown that transcriptional divergence can influence the outcome of iPSC- derived progenitor cells, and further suggested that intrinsic epigenetic traits might depend not only of cell type of origin, but also on the stage of reprogramming²¹⁰.

Among epigenetic modulators, miRNAs have been implicated in the reprogramming of somatic cells to iPSCs. Recent evidence has unravelled a family of miRNAs which markedly reduces generation of iPSC by modulating the chromatin remodeling process²¹¹. Similarly, miRNAs have been credited with governing the differentiation of PSC and their lineage specification, as it is the case of miR-375, which regulates pancreatic islet formation, or myomir mir-206, that induces muscle differentiation. Therefore, miRNAs are well equipped to serve as fate determinants. To this regard,

recent data coming from interlineage analysis of iPSCs differentiated to three germ layers has disclosed a number of key miRNAs holding cardinal regulatory roles in early lineage specification²¹². Among the identified miRNAs, miR-372-3p was found implicated in mesodermal lineages specification, in accordance with our results that have reported such miRNAs in the mesodermal progenitors. This line of research substantiates the rising role of miRNA to enhance differentiation of stem cells for tissue regeneration. Furthermore, miRNAs are suitable candidates for resident stem cell modulation in their specific niche, as for instance SC or MABs in skeletal muscle wasting conditions.

In the second part of the manuscript we have focused on EVs that appear to be a rich source of miRNAs. Screening of the content of EVs from animal models of muscle hypertrophy and muscle wasting associated with a chronic disease and aging has allowed us to identify a key miRNAs signature, applicable for targeting muscle wasting. In light of the potential role of miRNAs in modulating resident stem cells, we have tested this signature *in vitro* on MABs, adult stem cells, known for contributing to muscle regeneration. Our approach has shown that EV-derived miRNAs improve MABs differentiation potential *in vitro* and also when injected *in vivo* in the hindlimb muscles of aged mice following acute muscle injury. Future studies will be needed to evaluate whether the hypertrophic miRNAs will be effective in directing eliciting a myogenic response in resident stem cells, when delivered in a cell-free method. Indeed, our second study paves the way for a cell-free approach to treat muscle wasting disorders.

Our results combined provide evidence that miRNAs might constitute a feasible, efficacious mean to positively impact tissue regeneration. To this regard, the issue of delivering is crucial in regenerative medicine, i.e. not only delivering the right information but also delivering the messages to the right target. EV might ultimately embody the ideal delivery method. Integrating artificial messages with natural cells is, indeed, a well-known concept in tissues engineering^{189, 213}. Since chemical communications between cells relies on carriers such as EVs and other vesicles

among others, these can be engineered *ad hoc* to hand over a specific message in a specific target cell or tissue. For instance, a study has shown that systemic administration of EVs loaded with a modified, dystrophin splice-correcting phosphorodiamidate morpholino oligomer (EXOPMO) was able to direct uptake of the EVs from the skeletal muscle itself¹⁹⁷. The addition of this anchor peptide ultimately increased delivery of dystrophin in quadriceps of dystrophin-deficient mdx mice, resulting in a functional improvement.

As alternative to cell therapy, EVs hold an advantage in terms of safety and delivery, in fact tissue engineering and tissue regeneration technologies would largely benefit from the employment of cell-free delivery methods in forms of EVs. To this regard, there are EV specific characteristics that are of paramount importance when approaching the design of EV-based therapies. Firstly, the cells of origin, and how similar they have to be to the recipient cells, in terms of surface markers and any additional intracellular information that might be loaded into the EVs. EVs are bound to elicit a stronger response in the delivery cells, bypassing the issue of compatibility. Secondly, the interaction with biomaterials, often used to stabilize engineered tissues, and lastly the mode of delivery, whether local or systemic. Finally, immunogenicity is an important feature of PSC-derived therapeutic applications that might be outflanked using of EVs. In fact, EVs show very little immunogenic activity when administered in vivo in preclinical studies. At the same time, EVs have been implicated in the regulation of immunity, since they can carry engineered antigens that can modulate the immune system. As a matter of fact, EVs are being explored as immunomodulators for engineering tailored strategies for cancer immunotherapy²¹⁴.

While certainly EVs represent an attractive alternative to stem cell therapies, they can also be added value in a more comprehensive vision that encompasses the use of stem cells combined with EVs, in order to improve cell-based therapeutic regeneration. In this vision, EV are adjuvants in delivering crucial message mediating tissue regeneration. This role of EVs has been explored in several preclinical studies,

that have implicated EVs derived from stem cells in cardiac ¹²⁷, liver ²¹⁵ and brain tissue ²¹⁶ regeneration and wound healing ²¹⁷. An ongoing clinical trial conducted on patients with cardiomyopathy receiving sheets of cardiac progenitor cells derived from PSC (ESCORT) has given signs of an initial beneficial effect. Although not directly observed or supported by evidence, authors speculate that such effect might be likely mediated by miRNA cargos of EVs released by cardiac progenitors' cells. The possibility of combining stem cell therapies and miRNAs technology in the form of EV delivery is surely intriguing and our work belongs tightly in this scenario.

To conclude, stem cell therapy for degenerative diseases has been explored for more than 60 years, with the first successful allogenic transplantation taking place in 1956 and performed by Dr E Donnall Thomas in New York ²¹⁸. Ever since the first patient, affected by leukemia, was treated with healthy bone marrow from an identical twin, intensive scientific effort has been devoted to improve and move forward this approach with regards to other pathologies. On the other side, EVs- based therapeutics is a budding idea of the last 10-15 years, that is gaining more and more importance, but that will certainly require further work especially in the direction of improving targeted delivery. Therapeutics for degenerative disease should therefore be designed as a comprehensive, multi approach effectively taking into consideration cell-based regenerative capabilities, EVs vehicle properties and tissue modulators, such as miRNAs.



1. Henningsen, J. *et al.* Dynamics of the skeletal muscle secretome during myoblast differentiation. *mcp. M110. 002113* (2010).
2. Meriggioli, M.N. & Roubenoff, R.J.C.t.i. Prospect for pharmacological therapies to treat skeletal muscle dysfunction. **96**, 234-242 (2015).
3. Egerman, M.A., Glass, D.J.J.C.r.i.b. & biology, m. Signaling pathways controlling skeletal muscle mass. **49**, 59-68 (2014).
4. Sandri, M. *et al.* Foxo transcription factors induce the atrophy-related ubiquitin ligase atrogin-1 and cause skeletal muscle atrophy. **117**, 399-412 (2004).
5. Zanou, N., Gailly, P.J.C. & Sciences, M.L. Skeletal muscle hypertrophy and regeneration: interplay between the myogenic regulatory factors (MRFs) and insulin-like growth factors (IGFs) pathways. **70**, 4117-4130 (2013).
6. Rosenthal, S.M. & Cheng, Z.-Q.J.P.o.t.N.A.o.S. Opposing early and late effects of insulin-like growth factor I on differentiation and the cell cycle regulatory retinoblastoma protein in skeletal myoblasts. **92**, 10307-10311 (1995).
7. Musarò, A. *et al.* Localized Igf-1 transgene expression sustains hypertrophy and regeneration in senescent skeletal muscle. **27**, 195 (2001).
8. Tatsumi, R., Anderson, J.E., Nevoret, C.J., Halevy, O. & Allen, R.E.J.D.b. HGF/SF is present in normal adult skeletal muscle and is capable of activating satellite cells. **194**, 114-128 (1998).
9. Dominique, J.-E. & Gérard, C.J.E.c.r. Myostatin regulation of muscle development: molecular basis, natural mutations, physiopathological aspects. **312**, 2401-2414 (2006).
10. Trendelenburg, A.U., Meyer, A., Jacobi, C., Feige, J.N. & Glass, D.J.J.S.M. TAK-1/p38/nNFκB signaling inhibits myoblast differentiation by increasing levels of Activin A. **2**, 3 (2012).
11. Minetti, G.C. *et al.* Gai2 signaling is required for skeletal muscle growth, regeneration and satellite cell proliferation and differentiation. *MCB. 00957-00913* (2013).
12. Mercuri, E. & Muntoni, F.J.T.L. Muscular dystrophies. **381**, 845-860 (2013).
13. Emery, A.E.J.T.L. The muscular dystrophies. **359**, 687-695 (2002).
14. Bushby, K. *et al.* Diagnosis and management of Duchenne muscular dystrophy, part 1: diagnosis, and pharmacological and psychosocial management. **9**, 77-93 (2010).

15. Moreira, E.S. *et al.* Limb-girdle muscular dystrophy type 2G is caused by mutations in the gene encoding the sarcomeric protein telethonin. **24**, 163 (2000).
16. Manzur, A.Y., Kuntzer, T., Pike, M. & Swan, A. (2008).
17. Quattrocelli, M. *et al.* Intermittent glucocorticoid steroid dosing enhances muscle repair without eliciting muscle atrophy. **127**, 2418-2432 (2017).
18. Quattrocelli, M. *et al.* Intermittent glucocorticoid dosing improves muscle repair and function in mice with limb-girdle muscular dystrophy. **187**, 2520-2535 (2017).
19. Wang, B., Li, J. & Xiao, X.J.P.o.t.N.A.o.S. Adeno-associated virus vector carrying human minidystrophin genes effectively ameliorates muscular dystrophy in mdx mouse model. **97**, 13714-13719 (2000).
20. Niks, E.H. & Aartsma-Rus, A.J.E.o.o.b.t. Exon skipping: a first in class strategy for Duchenne muscular dystrophy. **17**, 225-236 (2017).
21. Sakuma, K. & Yamaguchi, A.J.I.j.o.e. Sarcopenia and age-related endocrine function. **2012** (2012).
22. Zembroń-Łacny, A., Dziubek, W., Rogowski, Ł., Skorupka, E. & Dąbrowska, G.J.P.r. Sarcopenia: monitoring, molecular mechanisms, and physical intervention. **63** (2014).
23. Sousa-Victor, P. & Munoz-Canoves, P.J.M.a.o.m. Regenerative decline of stem cells in sarcopenia. **50**, 109-117 (2016).
24. Taaffe, D.R. *et al.* Alterations in muscle attenuation following detraining and retraining in resistance-trained older adults. **55**, 217-223 (2009).
25. Burton, L.A. & Sumukadas, D.J.C.i.i.a. Optimal management of sarcopenia. **5**, 217 (2010).
26. Barns, M. *et al.* Molecular analyses provide insight into mechanisms underlying sarcopenia and myofibre denervation in old skeletal muscles of mice. **53**, 174-185 (2014).
27. Tezze, C. *et al.* Age-associated loss of OPA1 in muscle impacts muscle mass, metabolic homeostasis, systemic inflammation, and epithelial senescence. **25**, 1374-1389. e1376 (2017).
28. Brioché, T., Pagano, A.F., Py, G. & Chopard, A.J.M.a.o.m. Muscle wasting and aging: experimental models, fatty infiltrations, and prevention. **50**, 56-87 (2016).
29. Wakabayashi, H. & Sakuma, K.J.C.c.p. Comprehensive approach to sarcopenia treatment. **9**, 171-180 (2014).

30. Partridge, T., Morgan, J., Coulton, G., Hoffman, E. & Kunkel, L.J.N. Conversion of mdx myofibres from dystrophin-negative to-positive by injection of normal myoblasts. **337**, 176 (1989).
31. Cossu, G. & Biressi, S. in *Seminars in cell & developmental biology*, Vol. 16 623-631 (Elsevier, 2005).
32. Biressi, S., Molinaro, M. & Cossu, G. Cellular heterogeneity during vertebrate skeletal muscle development. *Developmental biology* **308**, 281-293 (2007).
33. Kuang, S., Gillespie, M.A. & Rudnicki, M.A.J.C.s.c. Niche regulation of muscle satellite cell self-renewal and differentiation. **2**, 22-31 (2008).
34. Cerletti, M. *et al.* Highly efficient, functional engraftment of skeletal muscle stem cells in dystrophic muscles. **134**, 37-47 (2008).
35. Sacco, A., Doyonnas, R., Kraft, P., Vitorovic, S. & Blau, H.M.J.N. Self-renewal and expansion of single transplanted muscle stem cells. **456**, 502 (2008).
36. Montarras, D. *et al.* Direct isolation of satellite cells for skeletal muscle regeneration. *Science* **309**, 2064-2067 (2005).
37. Minasi, M.G. *et al.* The meso-angioblast: a multipotent, self-renewing cell that originates from the dorsal aorta and differentiates into most mesodermal tissues. *Development* **129**, 2773-2783 (2002).
38. Dellavalle, A. *et al.* Pericytes of human skeletal muscle are myogenic precursors distinct from satellite cells. *Nature cell biology* **9**, 255-267 (2007).
39. Sampaolesi, M. *et al.* Cell therapy of α -sarcoglycan null dystrophic mice through intra-arterial delivery of mesoangioblasts. *Science* **301**, 487-492 (2003).
40. Sampaolesi, M. *et al.* Mesoangioblast stem cells ameliorate muscle function in dystrophic dogs. *Nature* **444**, 574 (2006).
41. Tedesco, F.S. *et al.* Stem cell-mediated transfer of a human artificial chromosome ameliorates muscular dystrophy. **3**, 96ra78-96ra78 (2011).
42. Cossu, G. *et al.* Intra-arterial transplantation of HLA-matched donor mesoangioblasts in Duchenne muscular dystrophy. e201505636 (2015).
43. Barberi, T. *et al.* Derivation of engraftable skeletal myoblasts from human embryonic stem cells. **13**, 642 (2007).
44. Darabi, R. *et al.* Functional skeletal muscle regeneration from differentiating embryonic stem cells. **14**, 134 (2008).

45. Takahashi, K. & Yamanaka, S.J.c. Induction of pluripotent stem cells from mouse embryonic and adult fibroblast cultures by defined factors. **126**, 663-676 (2006).
46. Park, I.-H. *et al.* Reprogramming of human somatic cells to pluripotency with defined factors. **451**, 141 (2008).
47. Kodaka, Y., Rabu, G. & Asakura, A.J.S.c.i. Skeletal muscle cell induction from pluripotent stem cells. **2017** (2017).
48. Darabi, R. *et al.* Human ES-and iPSc-derived myogenic progenitors restore DYSTROPHIN and improve contractility upon transplantation in dystrophic mice. **10**, 610-619 (2012).
49. Jiwwat, N., Lynch, E., Jeffrey, J., Van Dyke, J.M. & Suzuki, M.J.S.c.i. Current Progress and Challenges for Skeletal Muscle Differentiation from Human Pluripotent Stem Cells Using Transgene-Free Approaches. **2018** (2018).
50. Hosoyama, T., McGivern, J.V., Van Dyke, J.M., Ebert, A.D. & Suzuki, M.J.S.c.t.m. Derivation of myogenic progenitors directly from human pluripotent stem cells using a sphere-based culture. **3**, 564-574 (2014).
51. Chal, J. *et al.* Generation of human muscle fibers and satellite-like cells from human pluripotent stem cells in vitro. **11**, 1833 (2016).
52. Caron, L. *et al.* A Human Pluripotent Stem Cell Model of Facioscapulohumeral Muscular Dystrophy-Affected Skeletal Muscles. **5**, 1145-1161 (2016).
53. Borchin, B., Chen, J. & Barberi, T.J.S.c.r. Derivation and FACS-mediated purification of PAX3+/PAX7+ skeletal muscle precursors from human pluripotent stem cells. **1**, 620-631 (2013).
54. Chal, J. *et al.* Differentiation of pluripotent stem cells to muscle fiber to model Duchenne muscular dystrophy. **33**, 962 (2015).
55. Boularaoui, S.M. *et al.* Efficient transdifferentiation of human dermal fibroblasts into skeletal muscle. **12**, e918-e936 (2018).
56. Bar-Nur, O. *et al.* Direct Reprogramming of Mouse Fibroblasts into Functional Skeletal Muscle Progenitors. **10**, 1505-1521 (2018).
57. Sousa-Victor, P. *et al.* Muscle stem cell aging: regulation and rejuvenation. **26**, 287-296 (2015).
58. Shea, K.L. *et al.* Sprouty1 regulates reversible quiescence of a self-renewing adult muscle stem cell pool during regeneration. **6**, 117-129 (2010).
59. García-Prat, L., Muñoz-Cánoves, P.J.M. & endocrinology, c. Aging, metabolism and stem cells: Spotlight on muscle stem cells. **445**, 109-117 (2017).

60. Sperka, T., Wang, J. & Rudolph, K.L.J.N.r.M.c.b. DNA damage checkpoints in stem cells, ageing and cancer. **13**, 579 (2012).
61. García-Prat, L., Muñoz-Cánoves, P. & Martínez-Vicente, M.J.A. Dysfunctional autophagy is a driver of muscle stem cell functional decline with aging. **12**, 612-613 (2016).
62. Beerman, I. *et al.* Proliferation-dependent alterations of the DNA methylation landscape underlie hematopoietic stem cell aging. **12**, 413-425 (2013).
63. Rotini, A. *et al.* Aging affects the in vivo regenerative potential of human mesoangioblasts. **17**, e12714 (2018).
64. Brix, J., Zhou, Y., Luo, Y.J.J.o.G. & Genomics The epigenetic reprogramming roadmap in generation of iPSCs from somatic cells. **42**, 661-670 (2015).
65. Kim, K. *et al.* Epigenetic memory in induced pluripotent stem cells. **467**, 285 (2010).
66. Polo, J.M. *et al.* Cell type of origin influences the molecular and functional properties of mouse induced pluripotent stem cells. **28**, 848 (2010).
67. Bar-Nur, O., Russ, H.A., Efrat, S. & Benvenisty, N. Epigenetic memory and preferential lineage-specific differentiation in induced pluripotent stem cells derived from human pancreatic islet beta cells. *Cell Stem Cell* **9**, 17-23 (2011).
68. Ohi, Y. *et al.* Incomplete DNA methylation underlies a transcriptional memory of somatic cells in human iPS cells. **13**, 541 (2011).
69. Quattrocelli, M. *et al.* Intrinsic cell memory reinforces myogenic commitment of pericyte-derived iPSCs. **223**, 593-603 (2011).
70. Quattrocelli, M. *et al.* Mesodermal iPSC-derived progenitor cells functionally regenerate cardiac and skeletal muscle. *The Journal of clinical investigation* **125**, 4463-4482 (2015).
71. Giacomazzi, G., Sampaolesi, M., Quattrocelli, M.J.C.s.c.r. & therapy Unconventional players on the striated muscle field: microRNAs, signaling pathways and epigenetic regulators. **11**, 554-560 (2016).
72. Westholm, J.O. & Lai, E.C.J.B. Mirtrons: microRNA biogenesis via splicing. **93**, 1897-1904 (2011).
73. Shenoy, A. & Blelloch, R.H.J.N.R.M.C.B. Regulation of microRNA function in somatic stem cell proliferation and differentiation. **15**, 565 (2014).
74. Ha, M. & Kim, V.N.J.N.r.M.c.b. Regulation of microRNA biogenesis. **15**, 509 (2014).

75. Gregory, R.I., Chendrimada, T.P., Cooch, N. & Shiekhattar, R.J.C. Human RISC couples microRNA biogenesis and posttranscriptional gene silencing. **123**, 631-640 (2005).
76. Quattrocelli, M. & Sampaolesi, M. The mesmiRizing complexity of microRNAs for striated muscle tissue engineering. *Advanced drug delivery reviews* **88**, 37-52 (2015).
77. Djuranovic, S., Nahvi, A. & Green, R.J.S. miRNA-mediated gene silencing by translational repression followed by mRNA deadenylation and decay. **336**, 237-240 (2012).
78. Chen, J.-F. *et al.* The role of microRNA-1 and microRNA-133 in skeletal muscle proliferation and differentiation. **38**, 228 (2006).
79. Liu, N. *et al.* An intragenic MEF2-dependent enhancer directs muscle-specific expression of microRNAs 1 and 133. **104**, 20844-20849 (2007).
80. Kim, H.K., Lee, Y.S., Sivaprasad, U., Malhotra, A. & Dutta, A.J.T.J.o.c.b. Muscle-specific microRNA miR-206 promotes muscle differentiation. **174**, 677-687 (2006).
81. Eisenberg, I., Alexander, M.S., Kunkel, L.M.J.J.o.c. & medicine, m. miRNAs in normal and diseased skeletal muscle. **13**, 2-11 (2009).
82. Naguibneva, I. *et al.* The microRNA miR-181 targets the homeobox protein Hox-A11 during mammalian myoblast differentiation. **8**, 278 (2006).
83. Sun, Q. *et al.* Transforming growth factor- β -regulated miR-24 promotes skeletal muscle differentiation. **36**, 2690-2699 (2008).
84. Crist, C.G. *et al.* Muscle stem cell behavior is modified by microRNA-27 regulation of Pax3 expression. **106**, 13383-13387 (2009).
85. Wong, C.F. & Tellam, R.L.J.J.o.B.C. MicroRNA-26a targets the histone methyltransferase Enhancer of Zeste homolog 2 during myogenesis. **283**, 9836-9843 (2008).
86. Feng, Y., Cao, J.H., Li, X.Y., Zhao, S.H.J.C.b. & function Inhibition of miR-214 expression represses proliferation and differentiation of C2C12 myoblasts. **29**, 378-383 (2011).
87. Greco, S. *et al.* Common micro-RNA signature in skeletal muscle damage and regeneration induced by Duchenne muscular dystrophy and acute ischemia. **23**, 3335-3346 (2009).
88. Feng, Y. *et al.* A feedback circuit between miR-133 and the ERK1/2 pathway involving an exquisite mechanism for regulating myoblast proliferation and differentiation. **4**, e934 (2013).

89. Saccone, V. *et al.* HDAC-regulated myomiRs control BAF60 variant exchange and direct the functional phenotype of fibro-adipogenic progenitors in dystrophic muscles. (2014).
90. Nakasa, T. *et al.* Acceleration of muscle regeneration by local injection of muscle-specific microRNAs in rat skeletal muscle injury model. **14**, 2495-2505 (2010).
91. Liu, N. *et al.* microRNA-206 promotes skeletal muscle regeneration and delays progression of Duchenne muscular dystrophy in mice. *J Clin Invest* **122**, 2054-2065 (2012).
92. Alexander, M.S. *et al.* MicroRNA-486–dependent modulation of DOCK3/PTEN/AKT signaling pathways improves muscular dystrophy–associated symptoms. **124**, 2651-2667 (2014).
93. Meadows, E. *et al.* MicroRNA-29 Overexpression Delivered By Adeno-Associated Virus Suppresses Fibrosis in mdx: utrn+/-Mice (S61. 003). **82**, S61. 003 (2014).
94. Ardite, E. *et al.* PAI-1–regulated miR-21 defines a novel age-associated fibrogenic pathway in muscular dystrophy. **196**, 163-175 (2012).
95. Seok, H.Y. *et al.* miR-155 inhibits the expression of MEF2A to repress skeletal muscle differentiation. *jbc.* M111. 273276 (2011).
96. Cacchiarelli, D. *et al.* MicroRNAs involved in molecular circuitries relevant for the Duchenne muscular dystrophy pathogenesis are controlled by the dystrophin/nNOS pathway. **12**, 341-351 (2010).
97. Giacomazzi, G. *et al.* MicroRNAs promote skeletal muscle differentiation of mesodermal iPSC-derived progenitors. *Nature Communications* **8**, 1249 (2017).
98. Osella, M., Riba, A., Testori, A., Corà, D. & Caselle, M.J.F.i.g. Interplay of microRNA and epigenetic regulation in the human regulatory network. **5**, 345 (2014).
99. O'Rourke, J.R. *et al.* Essential role for Dicer during skeletal muscle development. **311**, 359-368 (2007).
100. Ge, Y. & Chen, J.J.C.C. MicroRNAs in skeletal myogenesis. **10**, 441-448 (2011).
101. Beh-Pajooh, A., Cantz, T.J.J.o.s.c. & medicine, r. The Role of microRNAs in Embryonic and Induced Pluripotency. **14**, 3 (2018).
102. Rosa, A., Spagnoli, F.M. & Brivanlou, A.H.J.D.c. The miR-430/427/302 family controls mesendodermal fate specification via species-specific target selection. **16**, 517-527 (2009).

103. Zhao, Y., Samal, E. & Srivastava, D.J.N. Serum response factor regulates a muscle-specific microRNA that targets Hand2 during cardiogenesis. **436**, 214 (2005).
104. Ivey, K.N. & Srivastava, D.J.C.s.c. MicroRNAs as regulators of differentiation and cell fate decisions. **7**, 36-41 (2010).
105. Crippa, S. *et al.* miR669a and miR669q prevent skeletal muscle differentiation in postnatal cardiac progenitors. *The Journal of cell biology* **193**, 1197-1212 (2011).
106. Rupaimoole, R. & Slack, F.J.J.N.r.D.d. MicroRNA therapeutics: towards a new era for the management of cancer and other diseases. **16**, 203 (2017).
107. Yang, N.J.I.j.o.p.i. An overview of viral and nonviral delivery systems for microRNA. **5**, 179 (2015).
108. Eulalio, A. *et al.* Functional screening identifies miRNAs inducing cardiac regeneration. **492**, 376 (2012).
109. Davis, M.E.J.C.o.i.b. Non-viral gene delivery systems. **13**, 128-131 (2002).
110. Janssen, H.L. *et al.* Treatment of HCV infection by targeting microRNA. **368**, 1685-1694 (2013).
111. Hong, D.S. *et al.* (American Society of Clinical Oncology, 2016).
112. Raposo, G. & Stoorvogel, W.J.J.C.B. Extracellular vesicles: exosomes, microvesicles, and friends. **200**, 373-383 (2013).
113. Harding, C., Heuser, J. & Stahl, P.J.E.j.o.c.b. Endocytosis and intracellular processing of transferrin and colloidal gold-transferrin in rat reticulocytes: demonstration of a pathway for receptor shedding. **35**, 256-263 (1984).
114. Deregibus, M.C. *et al.* Endothelial progenitor cell-derived microvesicles activate an angiogenic program in endothelial cells by a horizontal transfer of mRNA. **110**, 2440-2448 (2007).
115. Ostrowski, M. *et al.* Rab27a and Rab27b control different steps of the exosome secretion pathway. **12**, 19 (2010).
116. Batagov, A.O., Kuznetsov, V.A. & Kurochkin, I.V. in *BMC genomics*, Vol. 12 S18 (BioMed Central, 2011).
117. Buschow, S.I. *et al.* MHC II in dendritic cells is targeted to lysosomes or T cell-induced exosomes via distinct multivesicular body pathways. **10**, 1528-1542 (2009).
118. Rak, J. in *Seminars in thrombosis and hemostasis*, Vol. 36 888-906 (© Thieme Medical Publishers, 2010).
119. Vlassov, A.V., Magdaleno, S., Setterquist, R. & Conrad, R.J.B.e.B.A.-G.S. Exosomes: current knowledge of their composition, biological

- functions, and diagnostic and therapeutic potentials. **1820**, 940-948 (2012).
120. Le Bihan, M.-C. *et al.* In-depth analysis of the secretome identifies three major independent secretory pathways in differentiating human myoblasts. **77**, 344-356 (2012).
 121. Murphy, C. *et al.* Emerging role of extracellular vesicles in musculoskeletal diseases. (2017).
 122. Forterre, A. *et al.* Proteomic analysis of C2C12 myoblast and myotube exosome-like vesicles: a new paradigm for myoblast-myotube cross talk? **9**, e84153 (2014).
 123. Guescini, M. *et al.* Muscle releases alpha-sarcoglycan positive extracellular vesicles carrying miRNAs in the bloodstream. **10**, e0125094 (2015).
 124. Ibrahim, A.G.-E., Cheng, K. & Marbán, E.J.S.c.r. Exosomes as critical agents of cardiac regeneration triggered by cell therapy. **2**, 606-619 (2014).
 125. Lai, R.C., Chen, T.S. & Lim, S.K.J.R.m. Mesenchymal stem cell exosome: a novel stem cell-based therapy for cardiovascular disease. **6**, 481-492 (2011).
 126. Choi, J.S. *et al.* Exosomes from differentiating human skeletal muscle cells trigger myogenesis of stem cells and provide biochemical cues for skeletal muscle regeneration. **222**, 107-115 (2016).
 127. Yu, B. *et al.* Exosomes secreted from GATA-4 overexpressing mesenchymal stem cells serve as a reservoir of anti-apoptotic microRNAs for cardioprotection. **182**, 349-360 (2015).
 128. Aminzadeh, M.A. *et al.* Exosome-mediated benefits of cell therapy in mouse and human models of Duchenne muscular dystrophy. **10**, 942-955 (2018).
 129. McCullagh, K.J. & Perlingeiro, R.C. Coaxing stem cells for skeletal muscle repair. *Adv Drug Deliv Rev* **84**, 198-207 (2015).
 130. Fox, I.J. *et al.* Stem cell therapy. Use of differentiated pluripotent stem cells as replacement therapy for treating disease. *Science* **345**, 1247391 (2014).
 131. Costamagna, D. *et al.* Fate choice of post-natal mesoderm progenitors: skeletal versus cardiac muscle plasticity. *Cell Mol Life Sci* **71**, 615-627 (2014).
 132. Quattrocelli, M., Cassano, M., Crippa, S., Perini, I. & Sampaolesi, M. Cell therapy strategies and improvements for muscular dystrophy. *Cell Death Differ* **17**, 1222-1229 (2010).

133. Emery, A.E. The muscular dystrophies. *Lancet* **359**, 687-695 (2002).
134. Takahashi, K. & Yamanaka, S. A developmental framework for induced pluripotency. *Development* **142**, 3274-3285 (2015).
135. Liang, G. & Zhang, Y. Genetic and epigenetic variations in iPSCs: potential causes and implications for application. *Cell Stem Cell* **13**, 149-159 (2013).
136. Sanchez-Freire, V. *et al.* Effect of human donor cell source on differentiation and function of cardiac induced pluripotent stem cells. *J Am Coll Cardiol* **64**, 436-448 (2014).
137. Quattrocelli, M. & Sampaolesi, M. The mesmiRizing complexity of microRNAs for striated muscle tissue engineering. *Adv Drug Deliv Rev* **88**, 37-52 (2015).
138. Vitaloni, M. *et al.* MicroRNAs contribute to induced pluripotent stem cell somatic donor memory. *J Biol Chem* **289**, 2084-2098 (2014).
139. Quattrocelli, M. *et al.* Mesodermal iPSC-derived progenitor cells functionally regenerate cardiac and skeletal muscle. *J Clin Invest* **125**, 4463-4482 (2015).
140. Sandri, M. Memory or amnesia: the dilemma of stem cell therapy in muscular dystrophies. *J Clin Invest* **125**, 4331-4333 (2015).
141. Straathof, K.C. *et al.* An inducible caspase 9 safety switch for T-cell therapy. *Blood* **105**, 4247-4254 (2005).
142. Holvoet, B. *et al.* Sodium Iodide Symporter PET and BLI Noninvasively Reveal Mesoangioblast Survival in Dystrophic Mice. *Stem Cell Reports* (2015).
143. Carey, M.F., Peterson, C.L. & Smale, S.T. Chromatin immunoprecipitation (ChIP). *Cold Spring Harb Protoc* **2009**, pdb prot5279 (2009).
144. Trapnell, C. *et al.* Differential gene and transcript expression analysis of RNA-seq experiments with TopHat and Cufflinks. *Nat Protoc* **7**, 562-578 (2012).
145. Anders, S. *et al.* Count-based differential expression analysis of RNA sequencing data using R and Bioconductor. *Nat Protoc* **8**, 1765-1786 (2013).
146. Perez-Llamas, C. & Lopez-Bigas, N. Gitoools: analysis and visualisation of genomic data using interactive heat-maps. *PLoS One* **6**, e19541 (2011).
147. Betel, D., Wilson, M., Gabow, A., Marks, D.S. & Sander, C. The microRNA.org resource: targets and expression. *Nucleic Acids Res* **36**, D149-153 (2008).

148. Betel, D., Koppal, A., Agius, P., Sander, C. & Leslie, C. Comprehensive modeling of microRNA targets predicts functional non-conserved and non-canonical sites. *Genome Biol* **11**, R90 (2010).
149. Xie, X. *et al.* Adenovirus-mediated tissue-targeted expression of a caspase-9-based artificial death switch for the treatment of prostate cancer. *Cancer Res* **61**, 6795-6804 (2001).
150. Townsend, D., Yasuda, S., Li, S., Chamberlain, J.S. & Metzger, J.M. Emergent dilated cardiomyopathy caused by targeted repair of dystrophic skeletal muscle. *Mol Ther* **16**, 832-835 (2008).
151. Jin, L. *et al.* In vivo selection using a cell-growth switch. *Nat Genet* **26**, 64-66 (2000).
152. Zhang, B.G. *et al.* Combination of agrin and laminin increase acetylcholine receptor clustering and enhance functional neuromuscular junction formation In vitro. *Dev Neurobiol* (2015).
153. Adams, M.E., Anderson, K.N. & Froehner, S.C. The alpha-syntrophin PH and PDZ domains scaffold acetylcholine receptors, utrophin, and neuronal nitric oxide synthase at the neuromuscular junction. *J Neurosci* **30**, 11004-11010 (2010).
154. Heydemann, A. *et al.* Latent TGF-beta-binding protein 4 modifies muscular dystrophy in mice. *J Clin Invest* **119**, 3703-3712 (2009).
155. Swaggart, K.A. *et al.* Annexin A6 modifies muscular dystrophy by mediating sarcolemmal repair. *Proc Natl Acad Sci U S A* **111**, 6004-6009 (2014).
156. Li, Z. & Rana, T.M. Therapeutic targeting of microRNAs: current status and future challenges. *Nat Rev Drug Discov* **13**, 622-638 (2014).
157. Roberts, T.C. *et al.* Expression analysis in multiple muscle groups and serum reveals complexity in the microRNA transcriptome of the mdx mouse with implications for therapy. *Mol Ther Nucleic Acids* **1**, e39 (2012).
158. Dmitriev, P. *et al.* Defective regulation of microRNA target genes in myoblasts from facioscapulohumeral dystrophy patients. *J Biol Chem* **288**, 34989-35002 (2013).
159. Endo, K. *et al.* MicroRNA 210 as a biomarker for congestive heart failure. *Biol Pharm Bull* **36**, 48-54 (2013).
160. Liu, T. *et al.* MicroRNA-590 is an EMT-suppressive microRNA involved in the TGFbeta signaling pathway. *Mol Med Rep* **12**, 7403-7411 (2015).

161. Wang, Y. *et al.* Identification and profiling of microRNAs and their target genes from developing caprine skeletal Muscle. *PLoS One* **9**, e96857 (2014).
162. Fiorillo, A.A. *et al.* TNF-alpha-Induced microRNAs Control Dystrophin Expression in Becker Muscular Dystrophy. *Cell Rep* **12**, 1678-1690 (2015).
163. Naguibneva, I. *et al.* The microRNA miR-181 targets the homeobox protein Hox-A11 during mammalian myoblast differentiation. *Nat Cell Biol* **8**, 278-284 (2006).
164. Mayer, S.C. *et al.* Adrenergic Repression of the Epigenetic Reader MeCP2 Facilitates Cardiac Adaptation in Chronic Heart Failure. *Circ Res* **117**, 622-633 (2015).
165. Conti, V. *et al.* MeCP2 Affects Skeletal Muscle Growth and Morphology through Non Cell-Autonomous Mechanisms. *PLoS One* **10**, e0130183 (2015).
166. Patel, M.S. *et al.* Growth differentiation factor-15 is associated with muscle mass in chronic obstructive pulmonary disease and promotes muscle wasting in vivo. *Journal of cachexia, sarcopenia and muscle* **7**, 436-448 (2016).
167. Hernández-Hernández, J.M., Mallappa, C., Nasipak, B.T., Oesterreich, S. & Imbalzano, A.N. The Scaffold attachment factor b1 (Safb1) regulates myogenic differentiation by facilitating the transition of myogenic gene chromatin from a repressed to an activated state. *Nucleic acids research* **41**, 5704-5716 (2013).
168. Rusmini, P. *et al.* Aberrant autophagic response in the muscle of a knock-in mouse model of spinal and bulbar muscular atrophy. *Scientific reports* **5**, 15174 (2015).
169. Braun, T. & Gautel, M.J.N.r.M.c.b. Transcriptional mechanisms regulating skeletal muscle differentiation, growth and homeostasis. **12**, 349 (2011).
170. Sousa-Victor, P. *et al.* Geriatric muscle stem cells switch reversible quiescence into senescence. **506**, 316 (2014).
171. Blau, H.M., Cosgrove, B.D. & Ho, A.T. The central role of muscle stem cells in regenerative failure with aging. *Nature medicine* **21**, 854 (2015).
172. Fukada, S.-i.J.T.J.o.B. The roles of muscle stem cells in muscle injury, atrophy and hypertrophy. **163**, 353-358 (2018).
173. Sampaolesi, M. *et al.* Mesoangioblast stem cells ameliorate muscle function in dystrophic dogs. **444**, 574 (2006).

174. Costamagna, D. *et al.* Smad1/5/8 are myogenic regulators of murine and human mesoangioblasts. **8**, 73-87 (2015).
175. Pedersen, B.K. & Febbraio, M.A.J.N.R.E. Muscles, exercise and obesity: skeletal muscle as a secretory organ. **8**, 457 (2012).
176. Wang, H. & Wang, B.J.B.r. Extracellular vesicle microRNAs mediate skeletal muscle myogenesis and disease. **5**, 296-300 (2016).
177. Fry, C.S., Kirby, T.J., Kosmac, K., McCarthy, J.J. & Peterson, C.A.J.C.s.c. Myogenic progenitor cells control extracellular matrix production by fibroblasts during skeletal muscle hypertrophy. **20**, 56-69 (2017).
178. Frattini, P. *et al.* Autologous intramuscular transplantation of engineered satellite cells induces exosome-mediated systemic expression of Fukutin-related protein and rescues disease phenotype in a murine model of limb-girdle muscular dystrophy type 2I. **26**, 3682-3698 (2017).
179. He, W.A. *et al.* Microvesicles containing miRNAs promote muscle cell death in cancer cachexia via TLR7. **111**, 4525-4529 (2014).
180. Wang, J. *et al.* Effects of microRNAs on skeletal muscle development. **668**, 107-113 (2018).
181. Kamekar, S. *et al.* Exosomes facilitate therapeutic targeting of oncogenic KRAS in pancreatic cancer. **546**, 498 (2017).
182. Tian, Y. *et al.* A doxorubicin delivery platform using engineered natural membrane vesicle exosomes for targeted tumor therapy. **35**, 2383-2390 (2014).
183. Ohno, S.-i. *et al.* Systemically injected exosomes targeted to EGFR deliver antitumor microRNA to breast cancer cells. **21**, 185-191 (2013).
184. Li, L. *et al.* Extracellular vesicles carry microRNA-195 to intrahepatic cholangiocarcinoma and improve survival in a rat model. **65**, 501-514 (2017).
185. Giovannelli, G., Giacomazzi, G., Grosemans, H., Sampaolesi, M.J.M. & nerve Morphological and functional analyses of skeletal muscles from an immunodeficient animal model of limb-girdle muscular dystrophy type 2E. (2018).
186. Greening, D.W., Xu, R., Ji, H., Tauro, B.J. & Simpson, R.J. A protocol for exosome isolation and characterization: evaluation of ultracentrifugation, density-gradient separation, and immunoaffinity capture methods, in *Proteomic Profiling* 179-209 (Springer, 2015).

187. de Menezes-Neto, A. *et al.* Size-exclusion chromatography as a stand-alone methodology identifies novel markers in mass spectrometry analyses of plasma-derived vesicles from healthy individuals. **4**, 27378 (2015).
188. Cassano, M. *et al.* Magic-factor 1, a partial agonist of Met, induces muscle hypertrophy by protecting myogenic progenitors from apoptosis. **3**, e3223 (2008).
189. Lamichhane, T.N. *et al.* Emerging roles for extracellular vesicles in tissue engineering and regenerative medicine. **21**, 45-54 (2014).
190. Zhang, J. *et al.* Exosome and exosomal microRNA: trafficking, sorting, and function. **13**, 17-24 (2015).
191. Wang, J., Liew, O.W., Richards, A.M. & Chen, Y.-T.J.I.j.o.m.s. Overview of microRNAs in cardiac hypertrophy, fibrosis, and apoptosis. **17**, 749 (2016).
192. Callis, T.E. *et al.* MicroRNA-208a is a regulator of cardiac hypertrophy and conduction in mice. **119**, 2772-2786 (2009).
193. Li, M. *et al.* Analysis of the RNA content of the exosomes derived from blood serum and urine and its potential as biomarkers. **369**, 20130502 (2014).
194. Huang, X. *et al.* Characterization of human plasma-derived exosomal RNAs by deep sequencing. **14**, 319 (2013).
195. Dragomir, M., Chen, B. & Calin, G.A.J.T.c.r. Exosomal lncRNAs as new players in cell-to-cell communication. **7**, S243 (2018).
196. Mann, C.J. *et al.* Aberrant repair and fibrosis development in skeletal muscle. **1**, 21 (2011).
197. Gao, X. *et al.* Anchor peptide captures, targets, and loads exosomes of diverse origins for diagnostics and therapy. **10**, eaat0195 (2018).
198. Thomas, E.D. *et al.* Bone-marrow transplantation. **292**, 895-902 (1975).
199. Uccelli, A., Laroni, A. & Freedman, M.S.J.T.L.N. Mesenchymal stem cells for the treatment of multiple sclerosis and other neurological diseases. **10**, 649-656 (2011).
200. Mothe, A.J. & Tator, C.H.J.T.J.o.c.i. Advances in stem cell therapy for spinal cord injury. **122**, 3824-3834 (2012).
201. Mavilio, F. *et al.* Correction of junctional epidermolysis bullosa by transplantation of genetically modified epidermal stem cells. **12**, 1397 (2006).
202. Hirsch, T. *et al.* Regeneration of the entire human epidermis using transgenic stem cells. **551**, 327 (2017).

203. Martin, U.J.F.i.m. Therapeutic application of pluripotent stem cells: challenges and risks. **4**, 229 (2017).
204. Mandai, M. *et al.* Autologous induced stem-cell–derived retinal cells for macular degeneration. **376**, 1038-1046 (2017).
205. Haase, A., Göhring, G. & Martin, U.J.S.c.r. Generation of non-transgenic iPS cells from human cord blood CD34+ cells under animal component-free conditions. **21**, 71-73 (2017).
206. Li, H.L. *et al.* Precise correction of the dystrophin gene in duchenne muscular dystrophy patient induced pluripotent stem cells by TALEN and CRISPR-Cas9. **4**, 143-154 (2015).
207. Zweigerdt, R., Olmer, R., Singh, H., Haverich, A. & Martin, U.J.N.p. Scalable expansion of human pluripotent stem cells in suspension culture. **6**, 689 (2011).
208. Qi, Y. *et al.* Combined small-molecule inhibition accelerates the derivation of functional cortical neurons from human pluripotent stem cells. **35**, 154 (2017).
209. Yagyu, S., Hoyos, V., Del Bufalo, F. & Brenner, M.K.J.M.T. An inducible caspase-9 suicide gene to improve the safety of therapy using human induced pluripotent stem cells. **23**, 1475-1485 (2015).
210. Bhere, D. *et al.* Stem Cells Engineered During Different Stages of Reprogramming Reveal Varying Therapeutic Efficacies. (2018).
211. Pfaff, N. *et al.* Inhibition of miRNA-212/132 improves the reprogramming of fibroblasts into induced pluripotent stem cells by de-repressing important epigenetic remodelling factors. **20**, 70-75 (2017).
212. Li, L., Miu, K.-K., Gu, S., Cheung, H.-H. & Chan, W.-Y.J.S.r. Comparison of multi-lineage differentiation of hiPSCs reveals novel miRNAs that regulate lineage specification. **8** (2018).
213. Lentini, R. *et al.* Integrating artificial with natural cells to translate chemical messages that direct E. coli behaviour. **5**, 4012 (2014).
214. Gehrmann, U., Näslund, T.I., Hiltbrunner, S., Larssen, P. & Gabrielsson, S. in *Seminars in cancer biology*, Vol. 28 58-67 (Elsevier, 2014).
215. Lou, G., Chen, Z., Zheng, M., Liu, Y.J.E. & medicine, m. Mesenchymal stem cell-derived exosomes as a new therapeutic strategy for liver diseases. **49**, e346 (2017).
216. Zhang, Y. *et al.* Exosomes derived from mesenchymal stromal cells promote axonal growth of cortical neurons. **54**, 2659-2673 (2017).

217. Hu, L. *et al.* Exosomes derived from human adipose mesenchymal stem cells accelerates cutaneous wound healing via optimizing the characteristics of fibroblasts. **6**, 32993 (2016).
218. Thomas, E.D., Lochte Jr, H.L., Lu, W.C. & Ferrebee, J.W.J.N.E.J.o.M. Intravenous infusion of bone marrow in patients receiving radiation and chemotherapy. **257**, 491-496 (1957).



Scientific acknowledgment

The work published in chapter 3 has been supported by FWO (#G060612N, #G0A8813N, #G088715N), Opening the Future Campaign EJJ-OPTFUT-02010, Excellentiefinanciering KUL Project grant and Rondoufonds voor Duchenne Onderzoek to M.S., to E.M., and AFM#18373, FWO#1263314 to M.Q. S.H. receives support by a grant from the German Research Foundation (HA 3309/1-3) and the Interdisciplinary Center for Clinical Research Erlangen (E17). M.S. and D.H. are supported by KU Leuven Research Council funding (OT-09/053) and GOA-11/012), the Belgian Agency for Science Policy (Belspo) network IUAPVII-07 DevRepair. G.G. and M.Q. are grateful to Andy Vo for critically reviewing the ms, and to Ruben Dries for valuable suggestions about RNA-seq data analysis.

Personal contribution

For chapter 3: G.G. M.Q. research and drafted the ms; G.G. M.Q., B.H., S.T., I.B. E.C. and H.G performed experiments; G.G. M.Q., C.D., D.H., S.H., S.J., S.B., A.C.C, and E.M. analysed data, contributed to critical experiments/insights; M.Q., E.M., and M.S. provided funding.

For chapter 4: G.G and E.M. S designed the research and the experiments G.G. and E.M.S. S.Q. H.G performed experiments and analysed data, G.G drafted the manuscript.

Conflict of interest

The authors declare no conflicts of interest.



Curriculum Vitae

Personal information

Name:	Giacomazzi, Giorgia	Date of birth:	16/05/1989
Address:	Tiensestraat 17, 3000 Leuven, Belgium	Place of birth:	Voghera (Italy)
E-mail:	giorgia.giacomazzi@kuleuven.be	Nationality:	Italian
Cell phone	+32 468151765		

Education

2014 to present **PhD student training**
Translational Cardiology Lab, KU Leuven, Leuven, Belgium
Research project
MicroRNAs modulate skeletal muscle remodeling and regeneration

2012 to 2014 **Master of Science in Biomedical Sciences**
KU Leuven, Leuven (Belgium)

One academic year of master thesis, at Translational Cardiology Lab, KU Leuven.

Master thesis title "Effects of epigenetic memory on myogenic commitment of induced pluripotent stem cells"
Grade: *Magna cum Laude*

2008 to 2012 **Bachelor degree in Biotechnology**
Università degli Studi di Pavia, Pavia (Italy)

Bachelor thesis title: "Plasmid and viral vectors for genetic integration"
Grade: *107/110*
January-June 2011: Erasmus placement at Translational Cardiology lab, KU Leuven, Belgium

Publications

Monteiro Carvalho Mori da Cunha G; **Giacomazzi G**; et al. "Fate of mesoangioblasts in a vaginal birth injury model: influence of the route of administration" *Sci Rep*. 2018 Jul 13;8(1):10604.

Rotini A., Martinez-Sarrà E., Duellen R., Costamagna D., **Giacomazzi G**., Di Filippo ES., Fulle S., Sampaolesi M. "Aging affects the in vivo regenerative potential of human mesoangioblasts". *Aging cell* 2018 Feb 4. doi: 10.1111/ace1.12714

Giacomazzi G et al "MicroRNAs promote skeletal muscle differentiation of mesodermal iPSC-derived progenitors." *Nat Commun*. 2017 Nov 1;8(1):1249.

Rotini A, **Giacomazzi G**, Di Filippo E. "MicroRNA in muscle gene therapy " in press in *Muscle Gene Therapy* (book chapter).

Giovannelli G, **Giacomazzi G**, Grosemans H, Sampaolesi M. "Morphological and functional analyses of skeletal muscles from an immunodeficient animal model of limb girdle muscular dystrophy type 2E" *Under revision in Muscle and Nerve*.

Giacomazzi G., Giovannelli G., Rotini A., Costamagna D., Quattrocelli M. and Sampaolesi M. "Isolation of mesoangioblasts, a subset of pericytes with strong myogenic potential, from mammals". In press in *Methods Mol Biol* (book chapter).

Quattrocelli M, **Giacomazzi G**, Broeckx SY, Ceelen L, Bolca S, Spaas JH, Sampaolesi M. "Equine-Induced Pluripotent Stem Cells Retain Lineage Commitment Toward Myogenic and Chondrogenic Fates". *Stem Cell Reports*. 2016 Jan 12;6(1):55-63.

Quattrocelli M, Swinnen M, **Giacomazzi G**, Camps J, Barthélemy I, Ceccarelli G, Caluwé E, Grosemans H, Thorrez L, Pelizzo G, Muijtjens M, Verfaillie CM, Blot S, Janssens S, Sampaolesi M "Mesodermal iPSC-derived progenitor cells functionally regenerate cardiac and skeletal muscle" *J Clin Invest*. 2015 Dec;125(12):4463-82.

Giacomazzi G, Sampaolesi M, Quattrocelli M. "Unconventional Players on the Striated Muscle Field: microRNAs, Signaling Pathways and Epigenetic Regulators". *Curr Stem Cell Res Ther*. 2016;11(7):554-60.

Quattrocelli M, Costamagna D, **Giacomazzi G**, Camps J, Sampaolesi M. "Notch signaling regulates myogenic regenerative capacity of murine and human mesoangioblasts". *Cell Death Dis*. 2014 Oct 9;5:e1448

Conferences contributions

- International society for stem cell research (ISSCR) Melbourne, Australia 20-23 June 2018.

Poster presentation: "MicroRNAs promote skeletal muscle differentiation of mesodermal iPSC-derived progenitors".

- Inter-University Institute of Myology (IIM) Meeting, Assisi (Italy), Oct. 13-16 2016.

Oral presentation: "Exosome-borne microRNAs as modulator for enhancing striated muscle regeneration".

- BeSSCR/BSCDB spring meeting: Stem Cells as Disease Model and for Gene Therapy, Brussels, May 27, 2016

Poster presentation: "Exosome-derived microRNAs in dystrophic and hypertrophic striated muscles".

- Inter-University Institute of Myology (IIM) Meeting, Reggio Emilia (Italy), Oct. 1-4 2015.

Oral presentation: "Exosome-derived microRNAs in muscle hypertrophic and dystrophic conditions".

- Interuniversity Stem Cell Meeting , Leuven, April 20, 2015

Poster presentation: "The exosome network as potential modulator of striated muscles in dystrophic and hypertrophic conditions".